Diana Ferreira Franco

Licenciada em Ciências de Engenharia Mecânica

Wobbling laser beam welding of copper

Dissertação para a obtenção do Grau de Mestre em
Mestrado Integrado em Engenharia Mecânica

Orientador: Professora Doutora Rosa Maria Mendes Miranda,
Professora Associada com Agregação aposentada da FCT-UNL

FACULDADE DE CIÊNCIAS E TECNOLOGIA
UNIVERSIDADE NOVA DE LISBOA

Setembro 2017

Diana Ferreira Franco

Licenciada em Ciências de Engenharia Mecânica

Wobbling laser beam welding of copper

Dissertação para a obtenção do Grau de Mestre em

Mestrado Integrado em Engenharia Mecânica

Orientador:

Professora Doutora Rosa Maria Mendes Miranda,
Professora Associada com Agregação aposentada da FCT-UNL

Lisboa

2017

Wobbling laser beam welding of copper

To my family

AGRADECIMENTOS

Em primeiro lugar, gostaria de agradecer à minha orientadora, Professora Rosa Miranda, por quem nutro a mais profunda admiração. Agradeço imenso a oportunidade que me proporcionou e, sobretudo, o apoio e orientação constantes.

Ao engenheiro Phil Carr quero agradecer por me ter aceite na sua empresa, Carrs Welding Technologies, e por me ter proporcionado esta fantástica experiência. Quero deixar um especial agradecimento ao engenheiro João Silva, que me apoiou durante o meu estágio. Deixo, ainda, um obrigado à Alison Holland e à Evelina Guduke por toda a simpatia e amabilidade com que sempre me trataram. Por fim, gostaria ainda de agradecer à Pat Gibson pela forma calorosa com que me acolheu durante a minha estadia em Inglaterra.

Agradeço também ao IPG Photonics por me permitirem desenvolver todo o conteúdo experimental nas suas instalações. Ao Nil Reinermann agradeço a partilha constante de conhecimento e disponibilidade.

Os meus sinceros agradecimentos ao Doutor João Oliveira pela contribuição ao nível das análises de XRD e pelo constante aconselhamento.

Ao Professor Rui Silva pelo apoio nas análises SEM bem como ao Professor Alexandre Velhinho na metalografia um sincero obrigado.

O meu obrigada ao Professor Telmo Santos pelo apoio e orientação no desenvolvimento das análises de condutividade eléctrica.

À minha família agradeço o apoio incondicional e a oportunidade que me deram de delinear o meu futuro. Quero agradecer em especial à minha mãe, o meu porto de abrigo, ao meu pai, cujos olhos transbordam de orgulho sempre que fala de mim, e à minha prima, que tanto carinho me dá.

Ao meu namorado, Pedro Ramos, agradeço todo o apoio, palavras de encorajamento, dedicação e amor. Obrigada por estares e teres estado sempre ao meu lado. Não há consultor financeiro que perceba mais de soldadura laser de cobre que tu.

Quero deixar um agradecimento muito especial à minha afilhada, Catarina Brites, que, para além de ser uma amiga importantíssima foi, também, uma das pessoas que mais me ajudou e apoio ao longo desta etapa.

Por fim, aos meus grandes amigos, Bruno Duarte, Gonçalo Garcia e João Bentes, um muito obrigada por todas as horas de estudo, riso e companheirismo que vivemos ao longo destes últimos anos. É com enorme carinho que irei guardar todos esses momentos. Muito além de amigos, uma verdadeira família.

ACKNOWLEDGEMENTS

First, I would like to thank my thesis supervisor, Professor Rosa Miranda, whom I deeply admire. I would never had accomplished my goal if it wasn´t for her providing me a chance to develop and carry a research in this field, believing in me, for her counselling and support.

To Eng. Phill Carr, I would like to thank for welcoming me at his company, Carrs Welding Technologies. He provided me with an amazing experience and opportunity. A special thanks to Eng. João Silva who supported me through the whole process and during my stay at the company. I also leave a big thanks to Alison Holland and Evelina Guduke for the sympathy and kindness they shown me every day. Finally, to Pat Gibson for the kindness of welcoming me at her house during the time I was in England.

I thank to IPG Photonics for supplying the facilities for my experiments and to Nil Reinermann for all the time and availability during the process.

My heartfelt thanks to Doctor João Oliveira for his contribution to the XRD analysis and for the constant advisory.

To Professor Rui Silva I thank for the helping with SEM analysis and to Alexandre Velhinho in metallography.

To Professor Telmo Santos thank him for all the guidance and support during the development of the electrical conductivity analysis.

To my family, a special and unique thanks to the unconditional support and the opportunity of choosing and tracing my own future. To my mum, my every day shelter, to my dad which the eyes overflow pride every time someone mentions my name and to my cousin for all the love and affection.

To my boyfriend, Pedro Ramos, I thank him for all the support, encouraging me during the rough times, dedication and love. Thank you for being always available for me and at my side. There is no financial consultant that knows more about laser welding than you!

I leave a very special thanks to my University goddaughter, Catarina Brites. On top of being a very important friend, she had a major contribution during this thesis.

Lastly, to my special friends, Bruno Duarte, Gonçalo Garcia e João Bentes, a huge and special thanks for all the long hours studying, for all the laughs and the unique companionship throughout these past 5 years. It is more than friendship, we are a true family.

RESUMO

O aumento de componentes eletrónicos na indústria automóvel e a expansão das energias renováveis conduziram à necessidade de um processo fiável e produtivo de soldadura de cobre. A soldadura laser satisfaz estes requisitos, mas é um desafio devido à elevada condutividade térmica do cobre e à sua baixa absortividade da radiação. Contudo, desenvolvimentos recentes sugerem que estes problemas podem ser ultrapassados através da modulação espacial da distribuição de intensidade de potência do laser.

O presente trabalho, desenvolvido na empresa Carrs Welding Technologies, visou estudar a viabilidade da soldadura laser de componentes a baterias em cobre. O principal objectivo foi determinar a combinação de parâmetros que permitiam obter um cordão de soldadura sem defeitos, sem perda de condutividade eléctrica e com uma profundidade de 1,5 mm.

Foram produzidas soldaduras com laser de fibras em diferentes combinações de parâmetros e com diferentes modulações que foram analisadas por metalografia e com ensaios de condutividade eléctrica, de forma a determinar a influência de cada parâmetro na geometria e propriedades dos cordões. Posteriormente, realizaram-se soldaduras com lasers diferentes de modo a comparar fibras simples e multimodo.

Verificou-se que a modulação do feixe permite suprimir porosidades e defeitos de forma do cordão. Uma penetração igual ou superior a 1,5 mm foi observada para potências acima de 4 kW, velocidades de soldadura entre 3,5 e 4 m/min, diâmetros de rotação entre 0,6 a 1 mm para uma frequência de rotação de 100 Hz com uma modulação circular. Os valores de dureza sugerem que não existe uma variação significativa na resistência mecânica da zona soldada quando comparada com o material base. Os ensaios de Correntes de Eddy mostraram que a soldadura não afecta a condutividade eléctrica do material.

Finalmente, o laser de fibras em modo simples permite produzir soldaduras mais estreitas e profundas do que em multimodo.

ABSTRACT

The increase of electrical components in automotive industry and the expansion of renewable energy generation lead to a rising need of a reliable and highly productive welding process for copper. Laser beam welding of copper has been a challenge due to the high thermal conductivity of Cu and its low absorptivity of laser radiation. However, recent developments suggest that these problems can be overcome by power spatial modulation of the beam.

This research work was developed at Carrs Welding Technologies, UK, aiming to study the feasibility of fiber laser to weld electrolytic copper components to batteries. The main goal was to determine the parameter combination that allows to obtain a welded seam free of porosity and other weld defects with a penetration of 1.5 mm without losing electrical conductivity which was a mandatory requirement.

In a first stage, multiple weld beads with different welding parameter combinations were produced in order to determine the influence of each parameter in the process. In the second stage, single-mode and multimode fiber lasers were compared. The outcome of these two stages were examined using metallography and electrical conductivity tests, namely, Eddy Currents.

The results have shown that power spatial modulation can supress porosities, weld shape defects and spatter. A penetration of 1.5 mm can be achieved for a multimode beam power above 4 kW, welding speed between 3.5 and 4 m/min with a circular spatial modulation with a beam rotation of 0.6 to 1 mm diameter at 100 Hz frequency. The hardness measured suggest that there is no significant variation of mechanical resistance of the joins compared to the base material. Electrical conductivity measurements showed there is no variation in the welds.

Finally, single-mode fiber laser produced narrow and deeper welds than when multimode fibers were tested, as expected.

PALAVRAS-CHAVE

Soldadura de cobre electrolítico

Soldadura laser

Modulação laser

Laser *Wobbling*

Condutividade eléctrica

KEYWORDS

Electrolytic Copper welding

Laser beam welding

Laser modulation

Laser Wobbling

Electrical conductivity

LIST OF CONTENTS

LIST OF FIGURES

LIST OF TABLES

ABBREVIATIONS

BM – Base material

Cu-ETP – Electrolytic tough pitch copper

FZ – Fusion zone

HAZ – Heat affected zone

LBW – Laser beam welding

Nd:YAG – Neodymium-doped yttrium aluminium garnet

SYMBOLS

a – Rotation diameter [mm]

f – Rotation frequency [Hz]

P – Laser power [W]

v – Welding speed [m/min]

CHAPTER 1

INTRODUCTION

1.1. Motivation

Nowadays, copper is frequently used for the current-carrying components of batteries, power modules, industrial motors, etc. Due to the increasing demand of electrical components in the automotive industry and the expansion of renewable energy generation, the consumption of copper for fabrication of electrical components increases.

In modern industrial production, automatic and highly productive manufacturing processes are required. Laser welding meets these requirements and is now commonly used. A laser light beam with high intensity is focused into a small spot size and this concentrated heat source enables fine, deep welding at high welding speeds.

A notable progress in high-power and high-brightness lasers has been seen in recent years. At the same time applications have been developed in difficult-to-weld materials, like copper. When welding copper, it is difficult to form a melt pool because copper has not only a high thermal conductivity, but also a high reflectivity to solid state lasers emitting at 1 μm wavelength.

Thus, beam scanning has been tried to overcome these drawbacks. Different techniques have been experimentally tested, namely rapid rotation of the beam around its axis while it travels along the joint at a very high speed. The results reported, so far, show this may be a technique to overcome welding problems, as porosities, spatter, increasing the beam/material coupling.

1.2. Objectives

This thesis was developed at Carrs Welding Technologies in the UK aiming to study the feasibility of fiber laser to weld electrolytic copper plates. The laser welding of copper plates for join electrical connections on batteries has been a challenge due to the high thermal conductivity and low absorptivity of the material. Carrs Welding Technologies has been welding copper plates with Nd:YAG pulsed lasers which produce irregular and inconstant weld seams with a large amount of spatter and occasional drilling. Additionally, Nd:YAG lasers have lower efficiency when compared to fiber lasers.

The company was seeking to access the feasibility of multimode fiber laser for this particular application where sound welds with no loss of electrical conductivity were mandatory.

Therefore, the main objective was to investigate the influence of major process parameters (laser power, welding speed, focal point position, rotation diameter, rotation frequency and beam trajectory) on the weld geometry (weld width and penetration) and soundness. So, metallographic analysis and electrical conductivity testing were performed to assess the welds. Additionally, single-mode and multimode fibers have been also tested for comparison.

1.3. Structure

This thesis was structured in five chapters.

Chapter 2 provides an overview of the state of the art which is divided in two main sections. The first one concerns the material studied, while the most relevant findings and breakthroughs reported in literature are summarized in the second section. This chapter aims to establish both a theoretical basis and a framework for result analysis and discussion throughout this thesis.

Chapter 3 describes the experimental methodology and characterization techniques adopted. A description of the base material and the welding equipment characteristics are included. The tested range of process parameters is presented.

Chapter 4 presents and discusses the results achieved in light of the literature reports. This chapter was organized according to the characterization techniques performed.

Main conclusions are described in Chapter 5 as well as proposals for future developments.

CHAPTER 2

LITERATURE REVIEW

2.1. Copper and its properties

Copper was first used to fabricate tools and weapons since about 3500 years BC. Nowadays, it is one of the most used materials for electrical current-carrying components in batteries, power modules, industrial motors, etc., because of its excellent electrical and thermal conductivities and high formability.

Pure copper is soft, ductile and easily worked but can only be strengthened by cold working. It does not undergo phase changes in solid state, so it cannot be hardened by heat treatment. Pure copper contains more than 99.3% and has the highest electrical and thermal conductivity. Impurities like phosphorus, tin, selenium, tellurium, and arsenic are detrimental to properties such as electrical conductivity and recrystallization temperature [2].

At all temperatures below the melting point, copper exhibits the face-centered cubic (FCC) structure. In FCC metals, the {111} octahedral planes and the <110> directions are the most packed atomic systems and, therefore, constitute the most active slip systems. Copper lattice has 12 possible slip systems which ensure an excellent deformation and formability. Due to its FCC structure, copper tends to easily form twins, to accommodate deformation arising from recrystallization following cold work. Thus, the presence of twins in the microstructure is evidence that the metal has been mechanically deformed prior to annealing [1]. Typical microstructures of cold worked pure copper are shown in Figure 2.1.

Twinning is an important process to strengthen copper, once twinning causes an effective decrease in slip barrier spacing, which reduces the linear dimensions over which internal stress concentrations may accumulate: an increased applied stress is required to initiate further plastic flow. Additionally, twinning brings into play auxiliary deformation systems that work harden the material to prevent the accumulation of stress concentrations. The interfaces of deformation twins represent effective obstacles to slip [3].

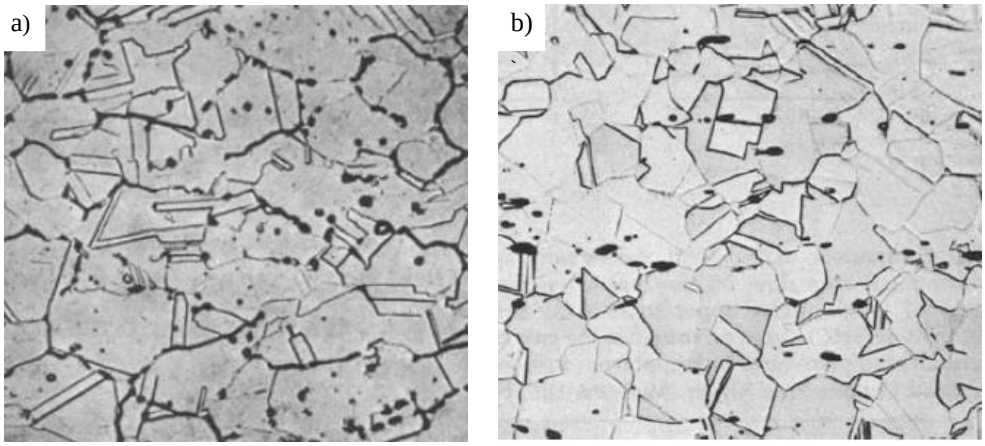

Figure 2.1 - Grain structure of Cu-ETP containing several annealing twins [1]. a) Microstructure of a wrought tough pitch copper sample heated in hydrogen (300x); b) Microstructure of wrought and annealed tough pitch copper (250x).

Copper density is about 8.90-8.95 g/cm^3, depending on its thermomechanical history. Density initially decreases with increasing degrees of cold work owing to the generation of vacancies and dislocations. Therefore, it increases to a value higher than that of a recrystallized copper, which has been explained by the presence of subgrain boundaries [1].

Electrical Conductivity

As shown in Table 2.1, just silver has a higher electrical conductivity than copper. The electrical conductivity scale established in 1913 was based on a copper standard defined as 100%, and the electrical conductivity of any material is still expressed as a percentage of IACS (International Annealed Copper Standard), equal to 100 times the ratio of the volume resistivity of the annealed copper standard (0.017241 μΩ·m) at 293 K to the value measured for the material concerned. The highest purity copper produced today (99.999% Cu) has been found to be 103 % IACS [1].

Table 2.1 – Electrical conductivity values for various metals [1].

Material	**% IACS**
Pure silver	106
Pure copper (99.999% Cu)	103.06
C10100 (oxygen-free electronic, OFE)	101
C11000 (electrolytic tough pitch, ETP)	101
C12000 (phosphorus deoxidised, DLP)	98
Pure gold	73.4
Pure aluminium	65
Pure iron	17.6

Electrical conductivity is sensitive to temperature: for copper, it drops from 800% IACS at –33 K to 38% IACS at 698 K. However, it is independent of its crystal orientation and does not vary significantly with grain size. Cold working an annealed copper to about 90% reduction can cause a drop of 2 to 3% IACS. Copper composition is also important since all additives reduce its electrical conductivity [1]. Although decreasing the electrical conductivity, oxygen and hydrogen are used in small and controlled amounts because they remove from solution impurities such as iron that are far more detrimental [2].

Thermal Conductivity

Copper is a good conductor of heat as well. Thermal conductivity is the rate at which heat flows through a material. Materials with high thermal conductivity dissipate heat rapidly resulting in a relatively uniform temperature profile in the material. Changes in thermal conductivity generally follow those in electrical conductivity in accordance with the Wiedemann-Franz relationship, which states that thermal conductivity is proportional to the product of electrical conductivity and temperature [1]. Figure 2.2 shows the influence of temperature on the thermal conductivity of pure copper.

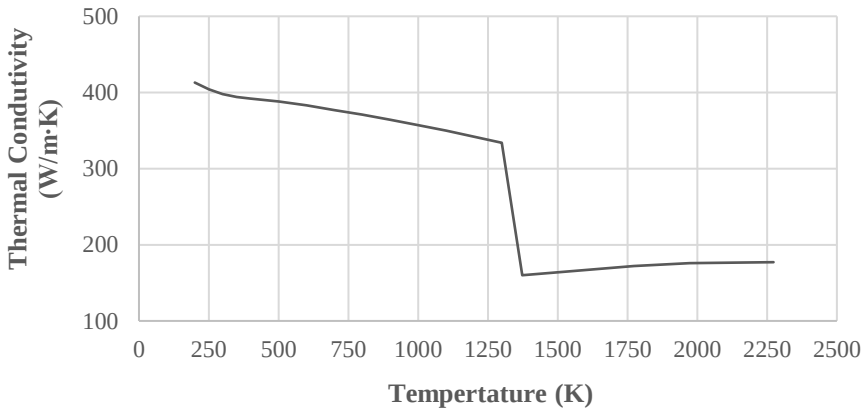

Figure 2.2 - Thermal conductivity of pure copper.

Absorptivity

Figure 2.3 shows the absorption behaviour of copper and gold compared to other two important groups of metals, aluminium and iron based materials. As it can be seen, the absorptivity of copper is very low for the typical wavelength of solid-state lasers and diode lasers compared to frequency doubled lasers [5]. At a wavelength of 1070 μm the absorptivity is approximately 3%, whereas at a wavelength of 532 μm the absorptivity is nearly 40%.

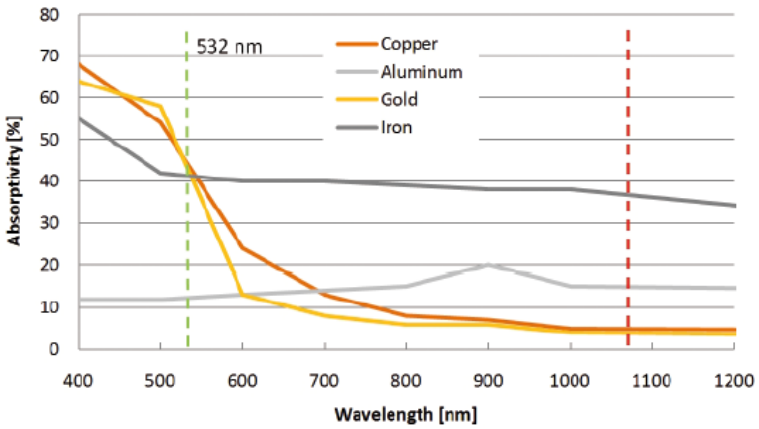

Figure 2.3 - Absorptivity of different metal groups at room temperature as a function of wavelength [5].

Absorptivity of copper also depends on the temperature. Figure 2.4 shows the relation between absorption and temperature at a wavelength of 1070 µm. It is possible to identify an abrupt increase of the absorptivity in copper during the phase change from solid to liquid. As soon as the threshold for the welding of copper material is overcome and liquid melt is available, the absorptivity of copper increases [6].

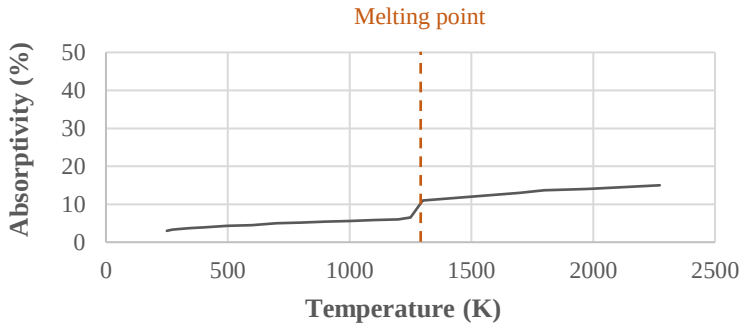

Figure 2.4 - Thermal conductivity and absorptivity as a function of temperature for copper at a wavelength of 1070 µm [6].

Mechanical properties

Copper is considered a soft and ductile metal. Tensile properties for both annealed and cold-drawn coper are listed in Table 2.2.

Table 2.2 – Tensile properties of pure copper [1].

	Tensile strength (MPa)	**Yield strength at 0.5% extension (MPa)**	**Elongation (%)**	**Reduction in area (%)**
Annealed condition	209	33	60	92
Cold-drawn condition	344	333.4	14	88

Unlike ferrous materials, the relationship between hardness and tensile strength is not constant. Table 2.3 shows typical hardness values for a range of tempers.

Table 2.3 – Hardness properties of pure copper [7].

	Hardness (HV)
Annealed	60 max.
Half-hard	70-95
Hard	90 in.

2.1.1. Electrolytic tough pitch copper

There are three separate grades of pure copper: oxygen-free copper (with less than 0.02% oxygen); tough pitch copper (that contains <0.1% of oxygen) and phosphorous deoxidised copper (with 0.05% P up to 0.05% arsenic). The influence of oxygen content on the microstructure of copper-oxygen alloys are shown in Figure 2.5.

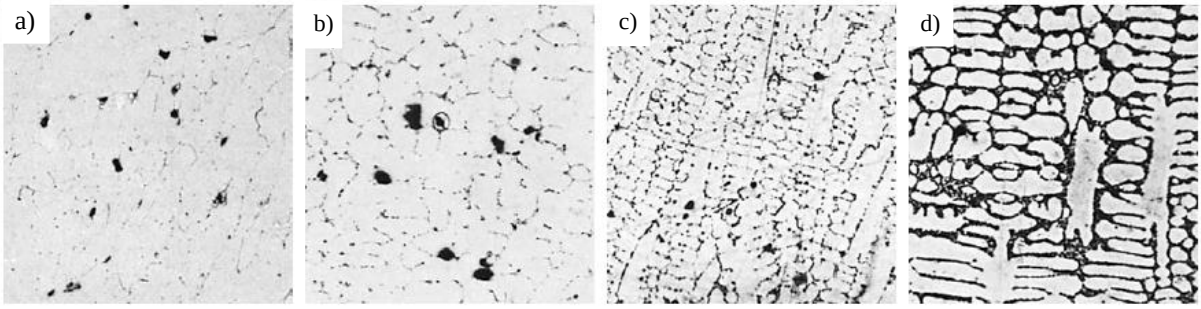

Figure 2.5 - The effect of oxygen content on the microstructure of copper-oxygen alloys [1]. Oxygen content: a) 0.024%; b) 0.05%; c) 0.09%; d) 0.18%. (100x).

Electrolytic tough pitch copper (Cu-ETP) is a commercially pure high-conductivity copper of any origin that has been refined by electrolytic deposition, then melted, oxidized, and brought to tough pitch or controlled low oxygen content, and finally cast into cakes, billets, wire bars, and so on, suitable for hot or cold working, or both [2].

The typical grain boundaries of pure copper are sharply defined due to twinning, as shown in Figure 2.6 a). In Figure 2.6 b) it is possible to identify columnar grains resulting of the welding process. Columnar grains are usually developed with a preferred crystal orientation in the direction of heat flow and with the grain boundaries parallel to this direction [1].

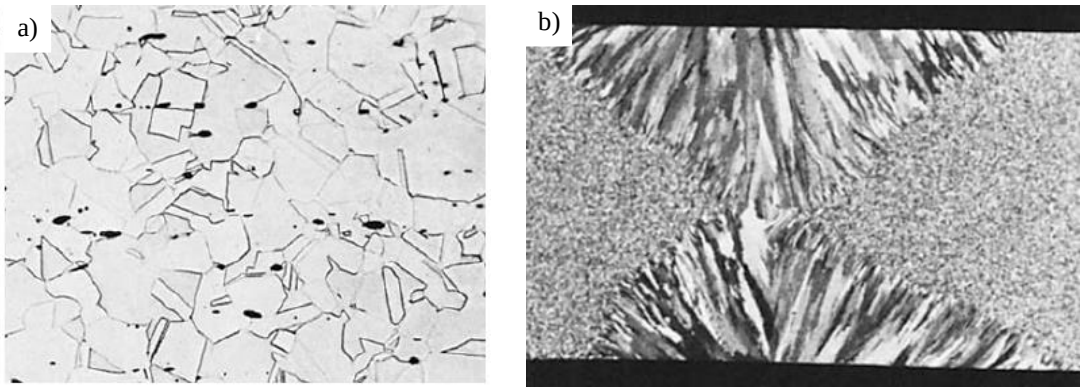

Figure 2.6 – Samples of Cu-ETP [1]. a) Longitudinal section shows equiaxed grains and well-dispersed, slightly elongated Cu_2O particles (dark dots) (250x); b) Copper cold-rolled bar, annealed and then tungsten arc welded in two passes (2x).

The copper oxides in tough pitch copper can result in embrittlement of the heat affected zones due to oxide films forming on the grain boundaries. Weld metal porosity, even when using fully deoxidised filler metals, is also a major problem caused by the dissociation of the copper oxide, particularly when hydrogen is present [4]. If oxygen-bearing copper is heated above approximately 400 °C in a hydrogen containing atmosphere (or in some cases other reducing gases), the hydrogen dissolves readily in the copper and then diffuses rapidly. On encountering the Cu_2O particles, the following reaction occurs:

$$2\,H + Cu_2O \leftrightarrow 2\,Cu + H_2O$$

The H_2O molecules formed combine readily into gas (steam) pockets, as these molecules are insoluble in the copper. This gas pockets evolve to voids during solidification [1]. The influence of hydrogen content on the microstructure of electrolytic tough pitch copper are shown in Figure 2.7.

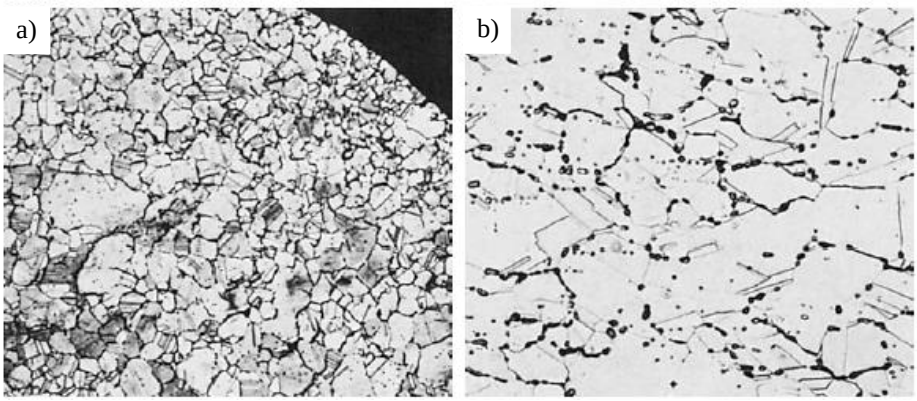

Figure 2.7 – Effect of the copper oxides in Cu-ETP [1]. a) The hydrogen diffused into copper reacted with Cu_2O at the grain boundaries, formed steam and force grains apart, causing embrittlement and porosity (75x); b) Voids caused by hydrogen presence (250x).

2.2. Laser beam welding

2.2.1. Basic laser fundamentals

Laser is one of the greatest innovations of the second half of the 20 century. The initial foundation of laser theory was laid by Einstein, in 1916, with the theory of light emission. Years later, Schawlow and Townes invented the maser, a device that produced consistent electromagnetic waves through amplification by stimulated emission. In 1960, Mainman developed the first working laser, a ruby laser [8, 9].

Light amplification by stimulated emission of radiation (laser) is a coherent, convergent and monochromatic beam of electromagnetic radiation. Laser can deliver very low (~mW) to extremely high (1–100 kW) focused beam power with a precise spot size/dimension and interaction/pulse time (10^{-3} to 10^{-15} s) onto any kind of substrate through any medium. As a result, laser has wide applications in engineering as automotive, aeronautics or aerospace but also in other fields such as communication, metrology, reprography, military, chemical, medical, etc. [9].

Laser beam welding

Laser beam welding (LBW) is a process in which joining is achieved by heating the parts with a laser beam and let them rapidly solidify. Figure 2.8 compares laser beam intensity with other heat sources and the fusion zone profile for several fusion welding processes. The laser beam can be produced either by a solid-state laser or a gas laser. In either case, the laser beam can be focused and directed by optical means to achieve high power densities [10]. The focused laser beam is one of the highest power density sources available to industry today [8].

Process	Heat source intensity ($W\ m^{-2}$)	Fusion zone profile
Flux-shielded arc welding	5×10^6–10^8	
Gas-shielded arc welding	5×10^6–10^8	low high
Plasma	5×10^6–10^{10}	low high
Laser or electron beam	10^{10}–10^{12}	defocus focus

Figure 2.8 - Comparison of the power density of various welding processes [8].

In a solid-state laser, a single crystal is doped with small concentrations of transition or rare earth elements. The electrons of the dopant element can be selectively excited to higher energy levels upon exposure to high-intensity flash lamps. Lasing occurs when these excited electrons return to their normal energy state. In gas laser, a gas mixture is continuously excited by electrodes connected to the power supply and lasers. Besides solid-state and gas lasers, semiconductor-based diode lasers are also used in engineering [8].

Each type of laser has a characteristic wavelength which is determined by the energy difference between excited and fundamental energy levels [8]. There are several types of laser with different excited species but, for material processing, CO_2, Nd:YAG and fiber lasers are the most popular systems. Table 2.4 summarizes the typical beam quality and wavelength of several commercial lasers.

Table 2.4 - Beam quality and wavelength for several commercial lasers [11].

Laser type	**Typical beam quality BPP (mm·mrad)**	**Wavelength (μm)**
CO_2	3.7	10600
Lamp pumped Nd:YAG	25	1060
Diode pumped Nd:YAG	12	1060
Yb fiber laser (IPG YLR7000)	18.5	1070
Yb fiber laser (IPG YLR10000)	11.6	1070
Yb fiber laser (IPG YLR17000)	11.7	1070

2.2.2. Fiber laser beam welding

Fiber lasers are solid-state lasers, with high power efficiency and beam quality. The first use of fiber lasers dates from the early 1960s, when low power lasers were used in optical amplifiers. In 2000, a fiber laser with 100 W was produced for materials processing [11] and a rapid increase in output power was seen since then.

The basic structure of a fiber laser is shown in Figure 2.9. In fiber laser, the active medium (most commonly, silica) is doped with a rare-earth element. The beam pump is launched longitudinally along the fiber length and it may be guided by the core itself. The active medium doped with erbium (1540-1560 μm), ytterbium (1070-1080 μm) or thallium (1800-2000 μm), is excited by battery of diode lasers [8, 9]. Two Bragg gratings (thin layers of different refractive index), which reflect a predetermined narrow or broad range of wavelengths of light incident on the grating while passing all other wavelengths of the light, are written into the fiber generating the laser emission and resulting in an efficient, compact laser source with high beam quality. The outer cladding is made of glass or polymeric material, with low refraction coefficient, to prevent signal attenuation [11].

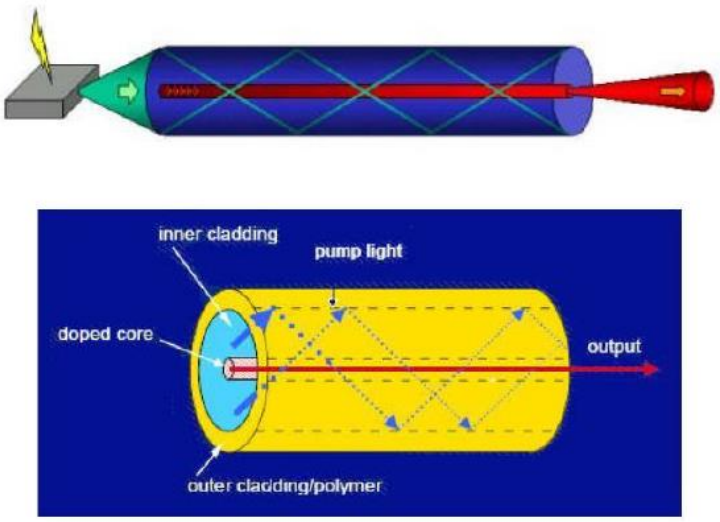

Figure 2.9 - Schematic of a high-power, double-clad fiber laser [21].

The high power fiber lasers present several advantages, including: high efficiency, compared to lamp or diode pumped rod lasers; compact design, which simplifies installation; good beam quality, due to the use of small diameter fibers, and consequently a small beam focus diameter; and a robust setup for mobile applications [11]. Additionally, maintenance costs are virtually zero. The lifetime of the pumping diodes exceeds the lifetime of other diode pumped lasers [2], which leads to low long-term costs.

High power fiber lasers can be used for deep penetration welding in a vast diversity of materials since the low wavelength that characterizes these lasers allows its absorption by almost all metals and alloys, and the fiber delivery system provides the necessary flexibility for positioning the beam [11].

Single-mode and multimode fiber lasers

When a ray travels down a fiber, it can follow many paths or modes. For example, it can follow the axis of the core or it can reflect off the core-cladding interface. Fiber cables can be divided in two categories: single-mode and multimode. Figure 2.10 illustrates the differences between single-mode and multimode fibers.

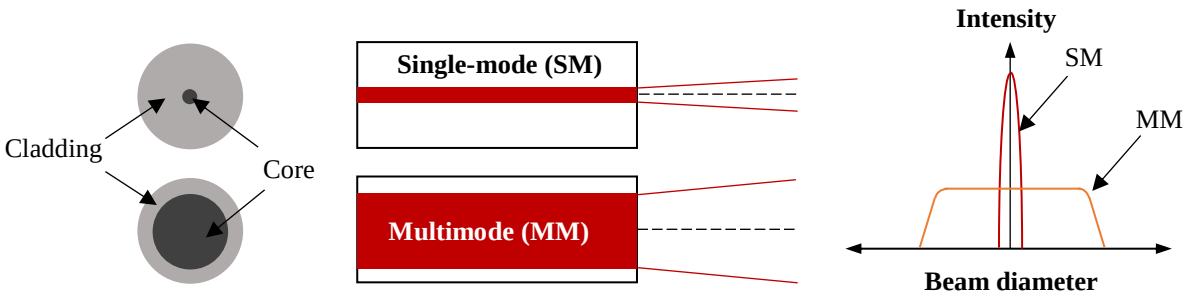

Figure 2.10 - Single-mode and multimode fibers, laser intensity and beam diameter.

Single-mode fiber is an optical glass fiber with a core diameter so small it has only one mode for light to travel. It usually has a core size between 8 and 9 μm and, because of this straight path, dispersion is negligible [13]. Sigle-mode cables are used in long-distance and extremely high bandwidth applications. This type of fiber produces a narrow and high intensity beam that can be focused down to a very small spot size.

Multimode fiber has a core with a relatively large diameter (50 to 200 μm) and light rays can travel along many modes and paths. This causes dispersion and limits the distances and bandwidth of multimode cable. The dispersion can be considerably reduced using a graded-index multimode where the core-cladding boundary is gradual rather than a sharp transition [13]. The resulting beam of multimode fibers has lower intensity and larger focused spot sizes.

Multimode fibers are commonly used for welding purposes. Multimode fiber laser beam more equally distributes its intensity across the weld, resulting in more stable welding conditions. It is less sensitive to gaps between welding surfaces, and its larger flat top intensity profile melts more base material volume, effectively bridging gaps as needed. However, there are some cases where single-mode fiber lasers can be implemented effectively in welding applications; high speed lap welding, for example, or very close-fitting joints that can be welded with significantly lower laser power, but still achieve a certain penetration over multimode lasers [14].

Beam quality

In high-power beam laser, the ability to focus the beam is critical, because good focusability means a smaller spot size, higher power density and larger depth of field. When focusability is good, focusing optics with a longer focal length can be used, which in turn leads to a large work clearance. The focusability of a laser beam is often referred to as the beam quality, and can be measured in various ways [8]. According to ISO standard 111146:1999, the parameters to quantify the beam quality of a laser beam are:

- The beam parameter product (BPP), i.e., the product of the beam radius at the beam waist ($d_{waist}/2$) with the far field beam divergence angle (Θ) and is defined by equation 1:

$$BPP = \frac{d_{waist} \cdot \Theta}{4} \tag{1}$$

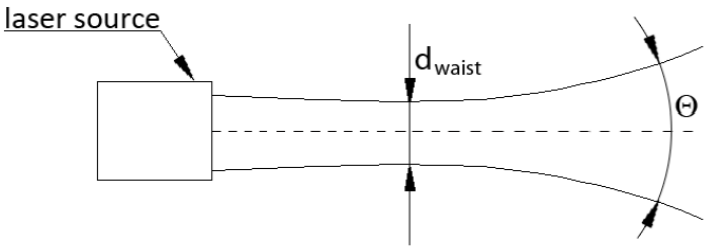

Figure 2.11 – Beam divergence [16].

- The M^2 factor, that represents the degree of variation of a beam intensity from the ideal Gaussian beam. It is defined as the beam parameter product dived by the corresponding product for a diffraction-limited Gaussian beam with the same wavelength (λ) as defined in equation 2. Gaussian beams have the highest possible beam quality, which is associated to lower beam parameter products and corresponds to M^2=1.

$$M^2 = BPP \cdot \frac{\pi}{\lambda} \tag{2}$$

- The K factor, defined by equation 3, is the inverse of M^2 factor and is high (ideally 1) for high quality beams.

$$K = \frac{1}{M^2} \tag{3}$$

The fundamental propagation modes of fibers are generally not exactly Gaussian, but also not too far from that shape. Therefore, a Gaussian beam can usually be launched into a single-mode fiber with high efficiency (80% or larger), provided that suitable optics are used [15].

2.2.3. Welding process

There are three welding modes with a laser: conduction, transition and keyhole as shown in Figure 2.12. The first occurs when the power density is insufficient to cause metal vaporization at a given welding speed. The weld pool has strong stirring forces driven by Marangoni currents resulting from the variation in surface tension and density with the temperature. The Marangoni forces are related to surface-tension-temperature-gradient-driven fluid flow, where the flow at the weld pool surface progresses from regions of low surface tension to regions of high surface tension [8].

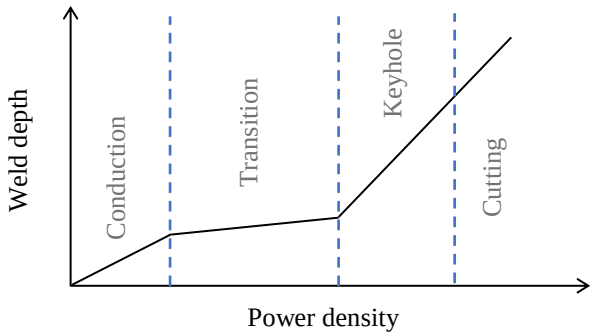

Figure 2.12 - Influence of the power density on the welding mode.

Opposite to this is keyhole welding mode, in which there is sufficient energy per unit length to cause vaporization and hence a capillary of vaporized metal forms in the melt pool. This capillary is stabilised by the balance of pressures from the vapour being generated. In some high-power plasma welds, there is an apparent hole, but this is mainly due to gas pressures from the plasma or cathode jet rather than from evaporation. The 'keyhole' behaves like an optical black body in that the radiation enters the hole and is subjected to multiple reflections before being able to escape [8, 9].

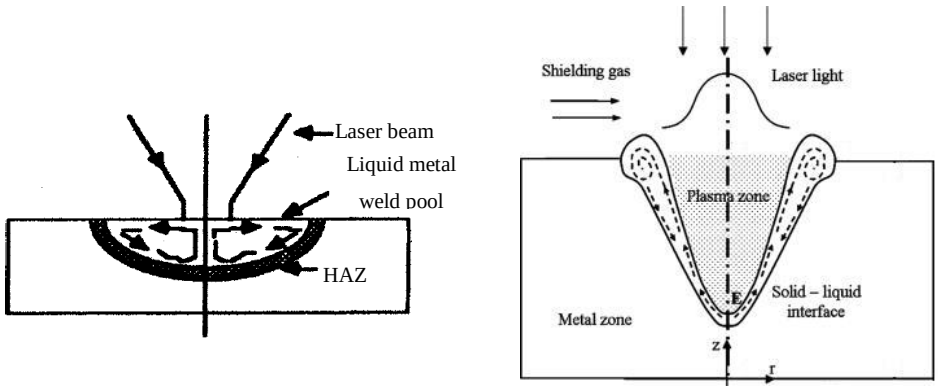

Figure 2.13 - Conduction-limited welding (on the left) [8] and keyhole welding (on the right) [18].

For the keyhole to remain open continually, to permit the transfer of energy necessary for welding to take place, various forces must interact. The vapour presses from inside onto the wall of the keyhole, and thus also acts against the hydrostatic pressure and surface tension of the molten envelope. The upward and downward flowing vapour applies a force to the inner wall of the molten envelope by friction against which the weight of the molten material reacts, these forces thus support the weight of the molten metal. In addition, there is a considerable amount of movement of the molten metal generated within the keyhole once the laser beam begins to move through the workpiece in the welding direction [19].

The mixed mode regime or the transition mode between conduction and keyhole occurs when the power density is enough to heat the material and just above the vaporization threshold the keyhole is not stable and does not extend beyond the melt front.

The weld bead geometry, such as the width and the penetration depth, are key factors when assessing the weld quality. Indeed, insufficient penetration reduces weld strength resulting in a poor weld quality. Moreover, the instability and eventual collapse of the keyhole is considered as a possible cause of porosity in laser welding due to the entrapment of vaporized alloying elements or shielding gas [20]. The advantages and disadvantages of conduction and keyhole in LBW are presented in Table 2.5.

Table 2.5 – Advantages and disadvantages of conduction and keyhole LBW [17].

Process	**Advantages**	**Disadvantages**
Conduction laser welding	- No porosity, no cracking and no undercut on the welds; - No spatter; - Stable process; - Control of the heat input; - Applicable to laser systems with any beam quality; - Good gap bridging ability due to the large beams used.	- High energy; - Slow process; - Low productivity; - Low coupling efficiency.
Keyhole laser welding	- High productivity; - Deep penetration welds with a high aspect ratio; - Low distortion; - Narrow HAZ.	- High amount of spatter; - Unstable process; - High levels of porosity; - Degradation of mechanical properties; - Loss of alloying elements.

2.2.4. Operating parameters

To obtain a good weld, several process parameters must be controlled. Parameters such as wavelength and beam quality depend on the selected laser source and cannot be changed. Others, like laser power, welding speed, focusability, material properties and focus spot should be adjusted to improve the weld quality. Laser beam parameters are resumed in Figure 2.14.

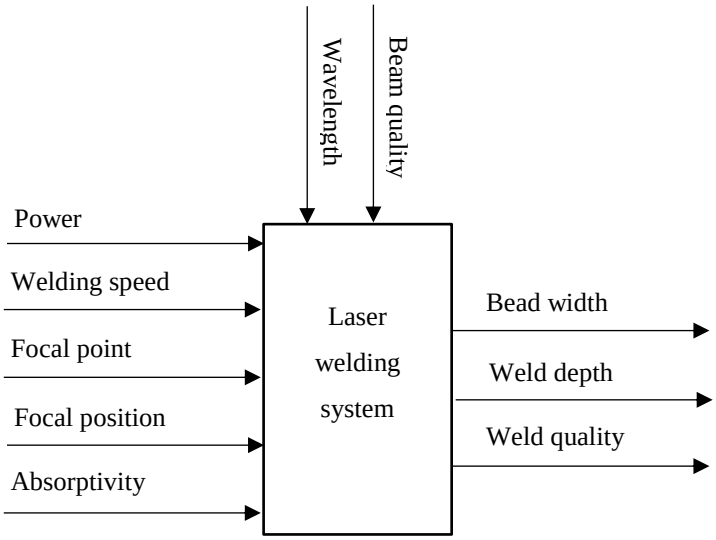

Figure 2.14 - Laser welding system. Horizontal input variables, vertical fixed input parameters and process output parameters.

Laser power: The depth of penetration with laser welding is directly related to the power density of the laser beam and is a function of incident laser power and beam diameter. For a constant beam diameter, penetration typically increases as the laser power is increased [28].

Welding speed: As the welding speed increases the pool flow pattern and size change. At slow welding speeds, the pool is large and wide and may result in dropout. In this case the surface tension is not enough to keep the pool in place and so it drops out of the weld, leaving a hole or depression. At higher welding speeds, the strong flow towards the centre of the weld in the wake of the keyhole has no time to redistribute and is hence frozen as a central ridge and an undercut at the sides of the weld [8].

Focal point: The focal point, which is the active width of the laser beam in touch with the workpiece, can be adjusted by changing either the collimation lens length or the focal lens length. The focal point size and laser power determines the power density and hence the penetration ability [8].

The fiber laser can be more finely focused than the more traditional lasers and hence the penetration for a given power is better and the welding speed can be 50–100% faster with a fiber laser than with a Nd:YAG laser [8].

Focal position: The focal point positioning distance is the distance between the focal point and the workpiece surface. Negative values for focal point positioning means positioning of laser beam focal plane below the workpiece surface and positive values means positioning of laser beam focal plane above the workpiece surface [24], as can be seen in Figure 2.15.

Changing the focal position leads to a variation on the power density which affect the weld geometry. As positive focal point positioning increases or negative focal point positioning decreases, the beam power density decreases. However, positive and negative focal point positioning doesn't affect equally the power density.

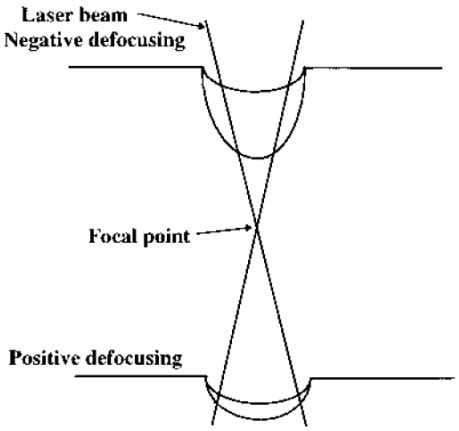

Figure 2.15 – Difference between positive and negative focal point positioning [26].

Absorptivity: The efficiency of LBW depends on the absorption of light energy by the workpiece. Any heat transfer calculation for laser processing is based on the energy absorbed by the workpiece.

Owing to the high absorptivity within the "keyhole" there is little operational difference when welding with long or short wavelengths. When welding with a conduction-limited weld, the surface reflectivity becomes paramount and the lower reflectivity with the shorter wavelengths gives a distinct advantage [8]. This differences are illustrated in Figure 2.16.

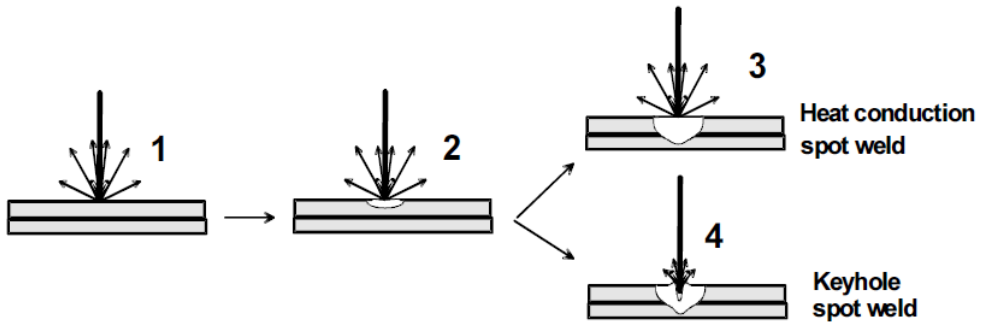

Figure 2.16 – Reflectivity during LBW for keyhole and conduction mode. [27]

However, there is another factor affecting absorption and that is the plasma formed owing to the very hot gases coming from the keyhole. The plasma will have three effects: the electrons in the plasma are free to absorb photons and hence the plasma is going to block the beam depending upon the electron density, i.e., the temperature; the hot plasma will cause density changes and hence changes in the refractive index, which will disperse the beam; and there will be condensate and particles caught up in the fast-moving plasma, which will have associated scattering effects [8].

The absorption coefficient ($\alpha_{bremm}=n^2\lambda^2T^{3/2}$, where n is the gas density, λ is the wavelength and T is the absolute temperature of the plasma) shows that for shorter wavelengths there will be less absorption and hence cooler and less absorbing plasma [8].

Shroud gas: It is also important to pay attention to the gas shroud, which is necessary for the protection of the molten and control the cooling weld. This gas can affect the formation of plasma, which may block or distort the beam and thus the absorption of the beam into the workpiece [8]. The most common gases used in LBW are listed in Table 2.6.

Table 2.6 - Chemical behaviour and physical proprieties of laser welding gases.

Laser welding gas	Molecular weight (g/mol)	Thermal conductivity at 1 bar, 15ºC (W/m·K)	Ionization energy (eV)	Density relative to air
Helium	4	0.15363	24.6	0.14
Nitrogen	28	0.02550	15.6	0.96
Argon	40	0.01732	15.8	1.38
Carbon dioxide	44	0.01615	13.8	1.52

The formation of plasma occurs through the reaction of the hot metal vapours from the keyhole with the shroud gas. If the plasma is near the workpiece surface or in the keyhole, it is beneficial. If, however, the plasma becomes thick or leave the surface, it will block or disperse the beam. Because of this plasma effect it is usual to weld with a side-blown jet to help blow the plasma away. If the shroud gas is slightly reactive with the weld metal, then a thin film of oxide may form which will enhance the optical coupling [8].

2.2.5. Wobbling LBW

There are two types of conventional lasers, continuous wave and pulsed wave lasers [17]. Recently, due to a remarkable progress in high-power lasers, research and development efforts have been devoted to materials that, like copper, are hard to weld with a conventional laser. Spatial power modulation for

laser beam welding by superposing an oscillation movement to the feed direction is gaining more and more importance for these hard to weld materials.

The technique of wobble welding influences the temperature field during welding, creating a larger molten pool and minimizing plasma formation [8]. A scan-head is used to rapidly rotate the beam position around its axis along the welding direction using specified amplitude and frequency (Figure 2.17).

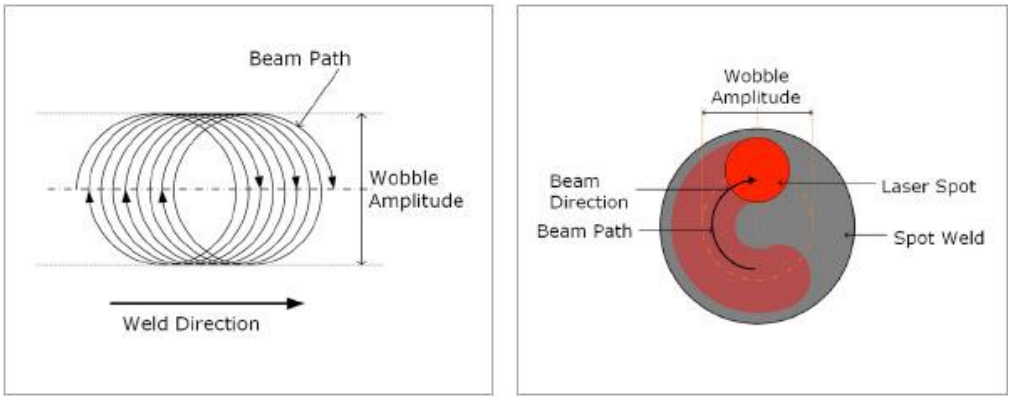

Figure 2.17 - Schematic of the wobble welding technique [28].

This relative movement between the laser beam and the workpiece results from spatial modulation that allows to superpose an oscillation movement to the weld direction [42].

According to [30] spatial modulation can affect the welding process by influencing the keyhole geometry (interface gaseous-liquid), the weld pool geometry (interface liquid-solid) and the temperature gradient in the weld pool. Different weld shapes can be produced, the most common ones are disposed in Figure 2.18. The beam shape can be circular, elliptical, linear or more complex like infinity.

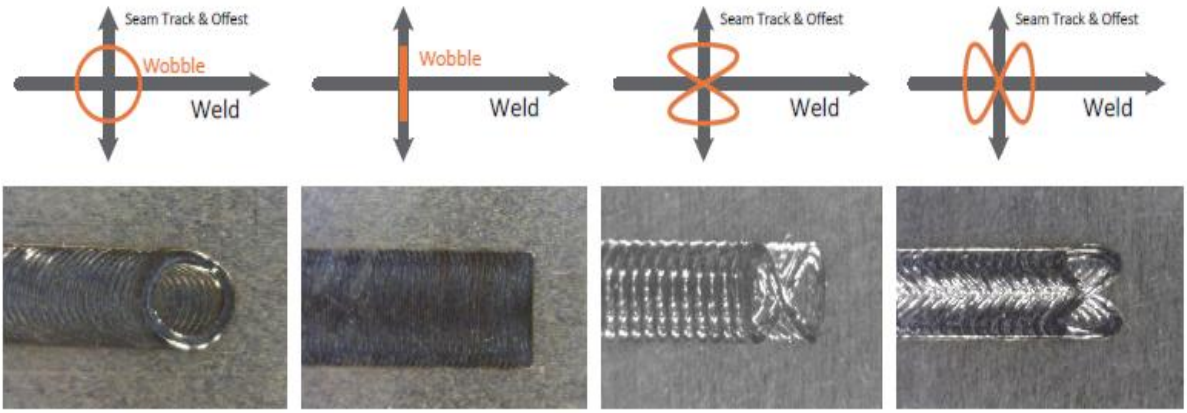

Figure 2.18 - Most common wobble shapes used [55].

The path defined by the laser beam depends on the welding speed, rotation amplitude and frequency and vary in time. The resulting path of superposing a circular oscillation can be described by the vectorial relation shown in equation 4.

$$\begin{pmatrix} x \\ y \end{pmatrix} = \begin{pmatrix} -a \cdot \cos(2 \cdot \pi \cdot f \cdot t) + v \cdot t + a \\ -a \cdot \sin(2 \cdot \pi \cdot f \cdot t) \end{pmatrix} \tag{4}$$

The degree of overlap, n, is defined as

$$n = \frac{x_{max,period1} - x_{min,period2}}{x_{max,period1} - x_{max,period1}}$$

where x_{max} and x_{min} are the local maxima and minimum of the laser movement in feed direction and

$$n = \frac{\sqrt{4a^2 - \left(\frac{v}{\pi \cdot f}\right)^2} - \left(\frac{v}{2\pi \cdot f}\right) \cdot \left(3\pi + 2 \cdot \arcsin\left(-\frac{v}{2\pi \cdot f \cdot a}\right)\right)}{\sqrt{4a^2 - \left(\frac{v}{\pi \cdot f}\right)^2} - \left(\frac{v}{2\pi \cdot f}\right) \cdot \left(\pi + 2 \cdot \arcsin\left(-\frac{v}{2\pi \cdot f \cdot a}\right)\right)} \tag{5}$$

where a is the rotation diameter, f is the rotation frequency and v is the welding speed [31]. The geometric meaning of this definition is shown in Figure 2.19.

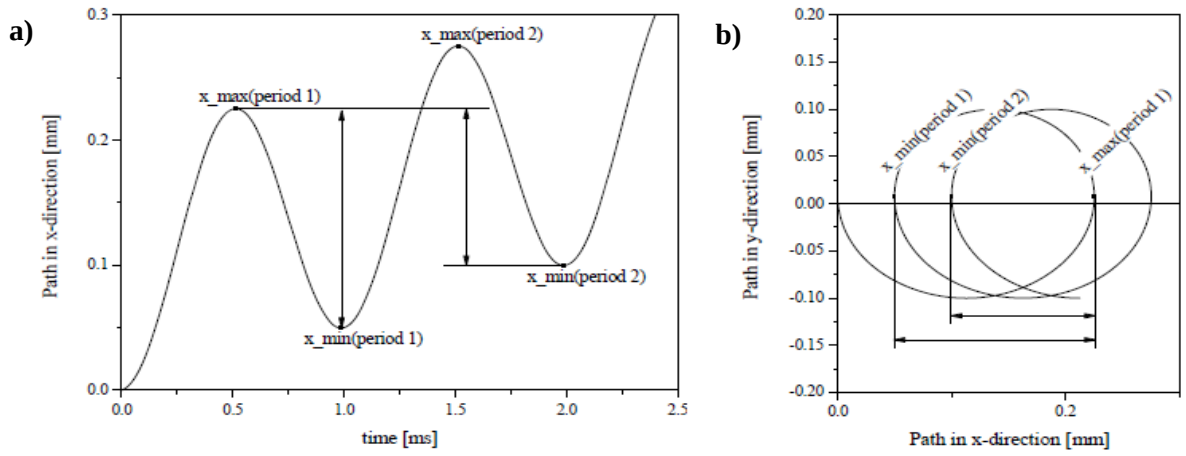

Figure 2.19 – Graphical definition of overlap (v = 50 mm/s; a = 1 mm; f = 1 kHz); a) path in feed direction over time displaying the local extrema; b) path in X and Y direction showing the same local extrema as in a) [31].

Overall, the wobble technique allows for better temperature control of the part during welding since the beam passes near any given point of the weld multiple times. The ramp in temperature and cooling rates are slower than in traditional laser welding, which minimizes weld defects including spatter [33].

2.2.6. LBW defects on pure copper

The primary difficulties with LBW of copper are the low absorptivity at 1 μm wavelength and the high thermal conductivity of copper. Figure 2.20 shows the thermal conductivity and absorptivity as a function of temperature for pure copper.

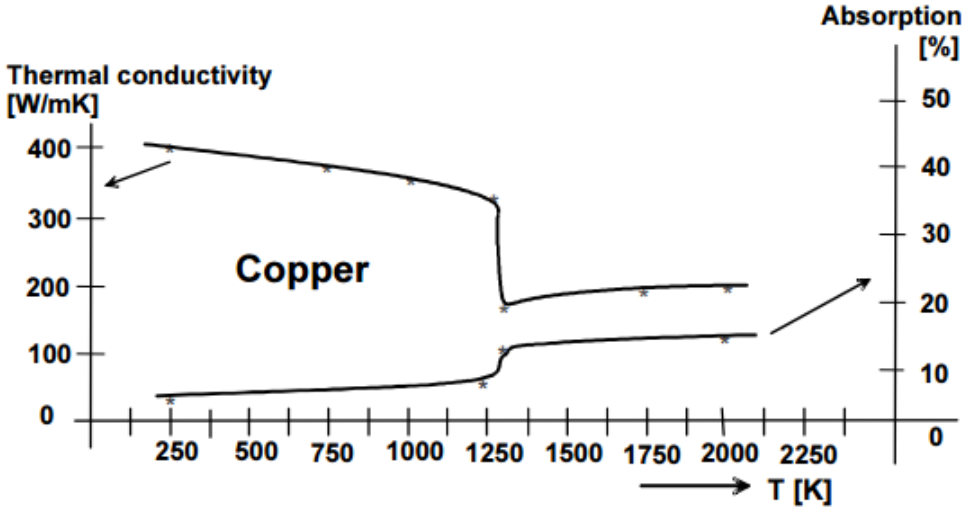

Figure 2.20 - Thermal conductivity and absorptivity as function of temperature for copper at 1064 μm [6].

Due to the high thermal conductivity, the energy input is rapidly dissipated. Therefore, to melt copper, the energy input must be high enough so that the heat losses by conduction can be overcome. The absorption coefficient of copper depends on the temperature which changes abruptly when going through the solid-liquid phase change. A similar behaviour is seen in the thermal conductivity, however with an opposite sign. This means that, when melting, the absorption of laser radiation increases, while the thermal conductivity decreases, leading to a very fast increase of the local material temperature when the input laser power remains constant. Without the right parameters, the process very quickly runs into evaporation of copper at the centre of the spot weld, and, soon afterwards, into an uncontrollable keyhole welding regime [6], where the beam is not absorbed.

Laser welding of copper materials often results in defective welds. Such weld seams suffer from many ejections and porosity [22, 47]. Also, a strong fluctuation of the penetration depth along the weld seam can often be seen. Figure 2.21 shows the top view and cross section of a laser beam welded copper sample.

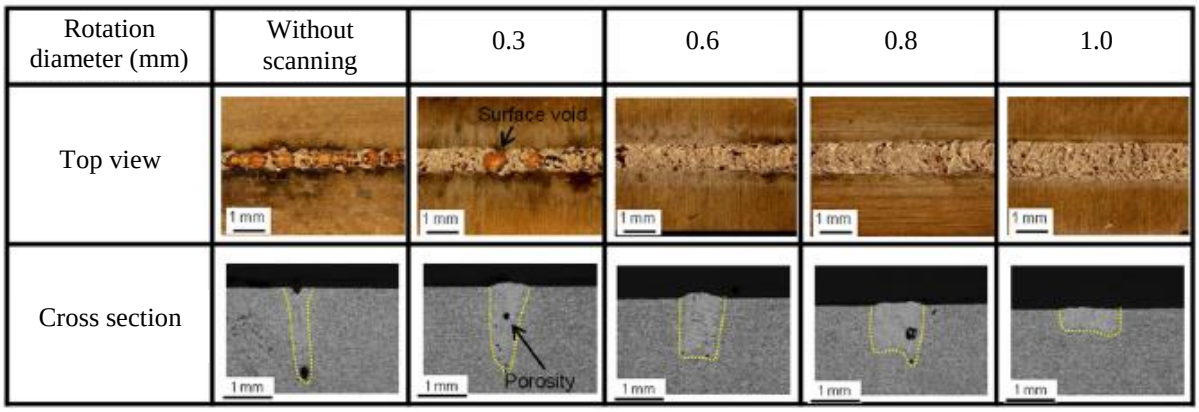

Figure 2.21 - Laser beam welded copper sample, Cu-ETP (laser power = 1500 W, welding speed = 50 mm/s, rotation frequency =200 Hz) [42].

The cause for both pores and melt ejections can be seen in a closure of the keyhole [23]. When the molten metal load based on large volume is larger than the keyhole expansion pressure, at the moment the keyhole shrinks, the porosity can be formed by separating from the bottom of the keyhole [41], as it can be seen in Figure 2.22.

On the other hand, a melt ejection might suddenly occur if the vapour pressure is higher than the closing forces. When the inside pressure of the keyhole exceeds the weld pool load, a keyhole expulsion occurs and molten metal is ejected from the weld pool as a spatter (Figure 2.23). A large void is left on the surface and a new keyhole is formed [41].

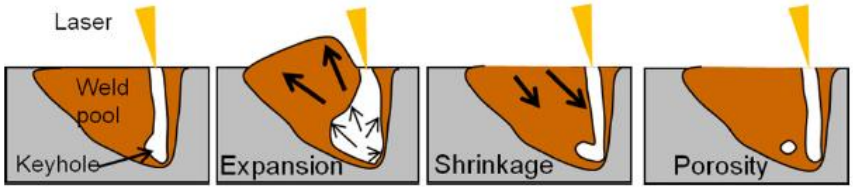

Figure 2.22 – Porosity formation [41].

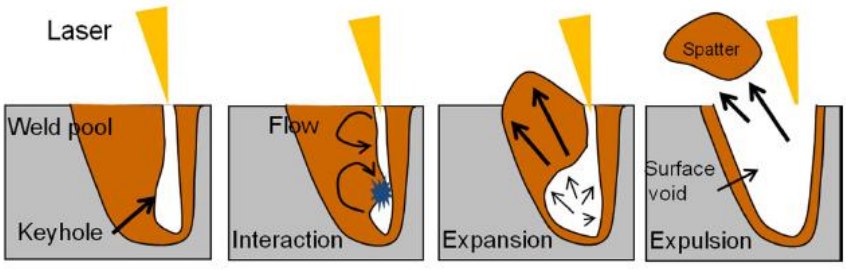

Figure 2.23 - Spatter and surface void formation [41].

2.2.7. Laser welding of Cu-ETP

As previously mentioned, with the increase use of Cu and the need to join it both in similar and dissimilar joints, several research groups have focused on LBW of copper. Table 2.7 summarizes major developments reported by those groups.

Table 2.7 – Major developments in LBW of pure copper.

Author	Year	Results and conclusions
Safdar et al.	2007	Investigated the effect of laser beam geometry on temperature distribution, heating/cooling rates and fluid flow.
Petring et al.	2011	Studied the influence of beam power, intensity and material properties on welding depth and seam width versus speed in copper welding.
Heider et al.	2011	Analysed the influence of laser power modulation during welding on weld imperfections. They reported that melt pool ejection for Cu-ETP can be reduced drastically (at 500 Hz) and the penetration depth can be increased by sinusoidal power modulation. They have also shown that the welding process becomes unstable at lower feed rates because of a small angle of the keyhole front wall and that a significantly more regular surface can be seen at the modulated welds.
Hess et al.	2011	Reported that using a combination of 1030 nm and 515 nm wavelength lasers for copper welding enables a deeper weld penetration than using the 1030 nm wavelength laser. The combined laser process also reduced the occurrence of melt pool ejection. Combining laser welding of different wavelengths is effective for avoiding dramatic changes of laser absorption based on the difference of 1 µm laser absorption in liquid and solid copper.
Kraetzsch et al.	2011	Determined that the use of brilliant fiber laser and high-speed scanning head with power modulation allows the welding of Al-Cu without cracking, compared to electron beam.
Heider et al.	2013	Utilized a high-speed X-ray imaging to analyse keyhole instabilities with respect to the formation of weld defects. They reported that laser power modulation is a method to prevent bubble growing and thereby minimizing weld defects such as spatters or melt ejection. Due to laser power modulation, at a modulation frequency of 200 Hz and welding speeds over 10 m/min, no melt ejection was observed.

Liebl et al.	2014	Conducted welding experiments using multimode fiber lasers on pure copper, and concluded that the occurrence of melt pool ejection depends on laser power and welding speed: at laser powers over 3 kW, melt pool ejection was suppressed with welding speeds over 8–9 m/min. They described that while for smaller welding velocities melt ejections and melt spatters occur, higher welding velocities produce high quality weld seams without pores visible in the cross sections. They also reported that melt pool ejections are less likely to occur with helium gas than without gas because of changes in the surface tension and in the heat dissipation. With the use of helium, the penetration depth and the cross section decrease, whereas the seam width increases.
Miyagi et al.	2015	Studied the influence of laser power, welding speed and focal point position in LBW of pure copper. They reported that the welding quality improved as the laser power increased in a range between 1000 and 5000 W. Additionally, that the welding quality improved significantly as the welding speed increased over 10 m/min. They concluded that the welding defects decreased significantly at 2 mm focal point position because the welding mode shifted to conduction.
Reisgen et al.	2016	Reported that the process stability (formation of spatter and surface voids) at a welding speed between 0.5 and 2 m/min can be increased by the reduction of the ambient pressure.
Miyagi et al.	2017	Showed that the weld depth obtained when scanning is smaller than without scanning. The rotation diameter used change from 0.3 to 1.0 mm and the rotation frequency varied from 77 to 285 Hz. The weld depth decreased as rotation frequency increases, regardless of the rotation diameter. The bead width obtained with scanning was larger than that obtained without scanning because of the larger laser radiation area. In the welding, there was an unscanned area, based on the relationship between laser scanning conditions and welding speed, that made the weld depth periodic. Spatter and surface voids decreased as rotation frequency and diameter increase. They also confirmed that, for scanning speed over 50 mm/s, large spatter and surface voids were suppressed.
Haseusler et al.	2017	Assessed the influence of the spatial power modulation on quality characteristics during laser microwelding by analysing the weld via three dimensional longitudinal cross sections and via laser measuring of the

	weld surface. The simulations produced confirmed the existence of a direct relationship between oscillatory scanning strategy and three-dimensional shape of the weld seam. The difference in path speed was identified as cause for the varying penetration depth, since locally varying scanning velocities induce different values of line energy. Consistently, the diminishing variation of the penetration depth at increasing degrees of overlap can be interpreted by the decreased difference in path speed that is combined welding speed and rotation diameter and frequency.

2.2.8. Conclusions

Due to excellent electrical performance and high formability of copper, it is one of the materials most frequently used in electrical engineering and electronics industry. To follow the modern industrial production needs, an automatic and high productive welding technology is required. Fulfilling these requirements, laser beam welding has been implemented in many industrial applications and fields. However, copper high thermal conductivity and low absorptivity makes it hard to obtain high quality laser beam welds. Dissolved oxygen from constitution also represents a limitation in Cu welding leading to porosities difficult to avoid.

Fiber laser welding of pure copper has been a recent highly debated topic of research and development. Laser power modulation combined with the use of lasers with different wavelengths and high-power laser welding is being investigated. These process variations proved to minimize weld defects; however, penetrations is still hard to control. The main goal of this research is to test these new techniques with fiber lasers to obtain high-quality welds, supressing melt ejections and spatter.

CHAPTER 3

EXPERIMENTAL PROCEDURE

This chapter presents the experimental methodology and characterization techniques to assess the quality of Cu laser welds. The set-up, the main equipment used and the base material are described.

3.1. Material characterization

The base material used on the LBW trials was Cu-ETP (pure copper) with 2 and 2.5 thick. All samples were cut to 100x50 mm in order to avoid different heat transfer conditions due to board effect since copper is a high thermal conductive material.

Tables 3.1 and 3.2 show the chemical composition and the physical and mechanical properties of Cu-ETP.

Table 3.1 - Chemical composition of the base material (material certificate available in annex A1).

Element	Cu	P	Pb	S	Fe	Ni	Te	As	Sb	Ag	Se
% wt	99.96	0.001	0.005	0.001	0.005	0.005	0.005	0.005	0.005	0.003	0.005

Table 3.2 - Physical and mechanical properties of the base material [54].

Properties	**Copper C101**
Crystal structure	Face-centered cubic
Density	8.92 g/cm^3
Melting point	1083 ºC
Thermal conductivity	391.1 W/m·K
Thermal expansion coefficient	16.9x10^6 K^{-1}
Electrical resistivity	0.0171x10^{-6} Ω·m
Yield Tensile Strength	195 MPa
Ultimate Tensile Strength	250 MPa
Modulus of elasticity	117 GPa
Hardness	89 MPa

3.2. Laser System

An IPG YLS 5000 CW Multi Axis System fiber laser with a maximum power of 5 kW was used in all experiments. The laser was available at Burbach, Germany, at IPG Photonics. In the first stage of the experiments, it was used a multimode optical fiber with 100 μm of diameter, 150 mm of collimation, 300 mm of focal length and 200 μm of spot size. In the second stage, it was used a single mode optical fiber with 50 μm of diameter, 150 mm of collimation, 300 mm of focal length and 100 μm of spot size to comparison purposes. All welding experiments were carried out with the laser beam focused on the material surface. Table 3.3 depicts the characteristics of the laser beam used.

Table 3.3 - Characteristics of the laser.

Optical Set-up		IPG FLW-D50 Wobble Head			
Set-up	**Fiber diameter (μm)**	**Collimator (mm)**	**Focal length (mm)**	**Spot size (μm)**	**Focus location**
YLS 5000 mm/ IPG Multi Axis System	100	150	300	200	On top
	50			100	

The beam profiles were measured using a PRIMES FocusMonitor FM. They are mostly top hat profiles as shown in Figure 3.1 and in Figure 3.2 for 800 and 1500 W, respectively. The properties of both laser beam fibers are shown in Table 3.4.

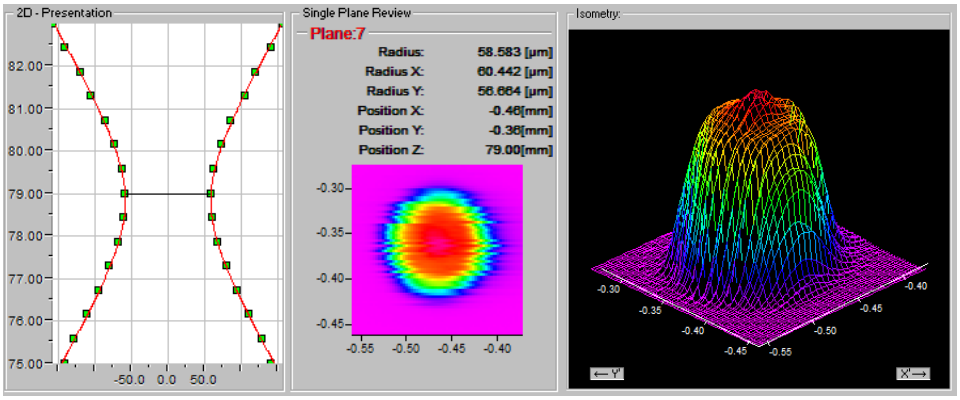

Figure 3.1 - Intensity distribution and beam profile of the fiber laser for 50 mm beam diameter (800 W).

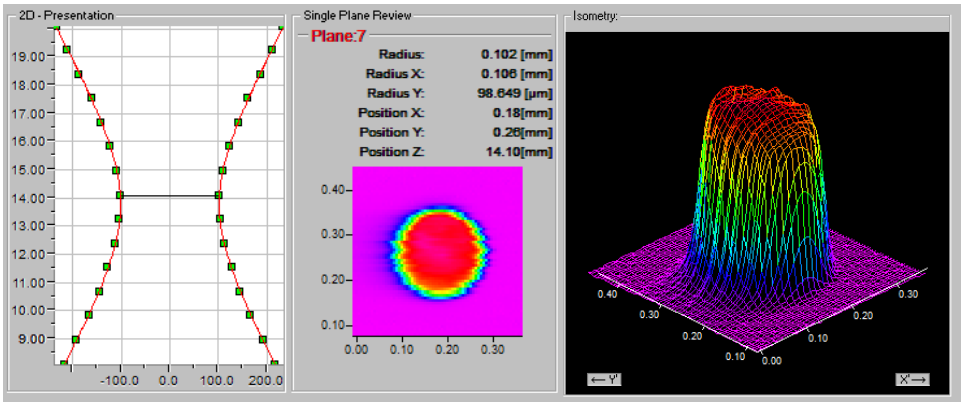

Figure 3.2 - Intensity distribution and beam profile of the fiber laser for 100 mm beam diameter (1500 W).

Table 3.4 - Beam properties of different optical fibers.

Fiber diameter (µm)	K	M^2	BPP (mm·mrad)	Rayleigh length (mm)	Divergence angle (mrad)
50	0.18	5.64	1.902	2.091	60.313
100	0.11	9.50	3.206	2.851	67.073

Figure 3.3 shows the IPG 4-axis workcell used to produce the welds. The work table travels in the X, Y and Z direction and the FLW-D30 Wobble head allows the rotation in the X axis. The tilt angle could be manually set from 0 to 90º.

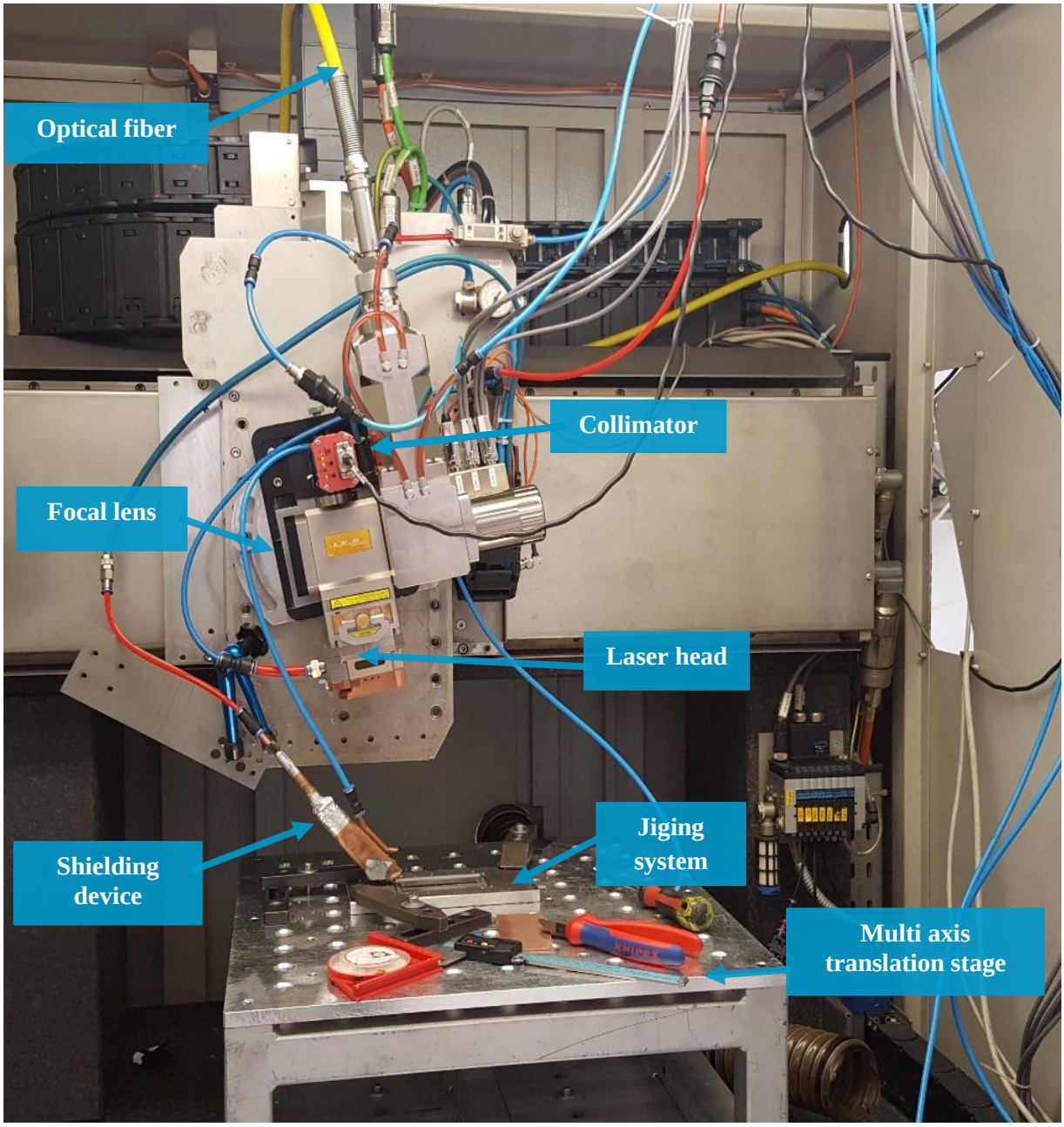

Figure 3.3 - Experimental set-up.

The welding path is predefined by an IPG program that can be changed using the control equipment shown in Figure 3.4 a). The shielding gas device and its angle in relation to the base material are displayed in Figure 3.4 b). This allows a full protection with a constant gas flow during the entire length of the weld. The flow rate used in all experiments was 35 l/min.

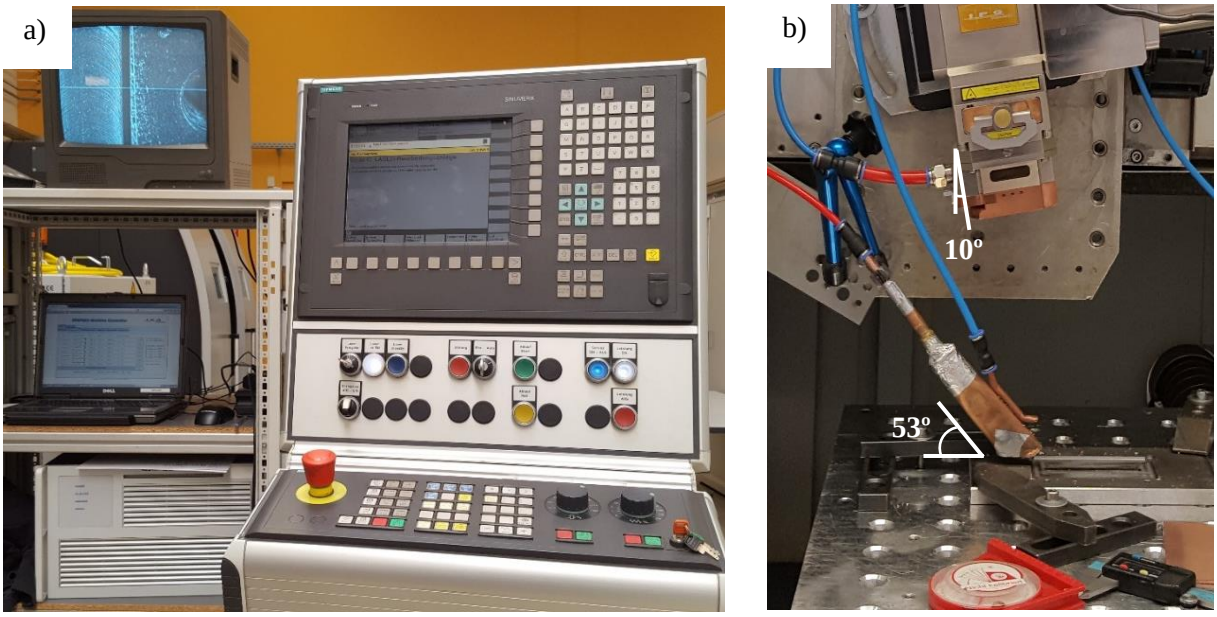

Figure 3.4 - Experimental set-up. a) Control equipment; b) Shielding device and beam angle.

3.3. Fixturing system

To ensure the repeatability, accuracy and interchangeability between all experiments, a jig was designed (drawings are shown in annex A2). It allowed to keep the working piece completely restricted, preventing any movement during the welding process and avoiding plate warping.

Figure 3.5 shows the jig used in all trials. The steel base plate has main two cavities: one to fit the welding plates, which constrain lateral movement, and other to avoid steel contaminations during the welding process for full penetration welds. This base was bolted to the work table by four screws. Vertical movement was constrained by a steel plate bolted to the base plate. The superior plate has a cavity to allow the welding process.

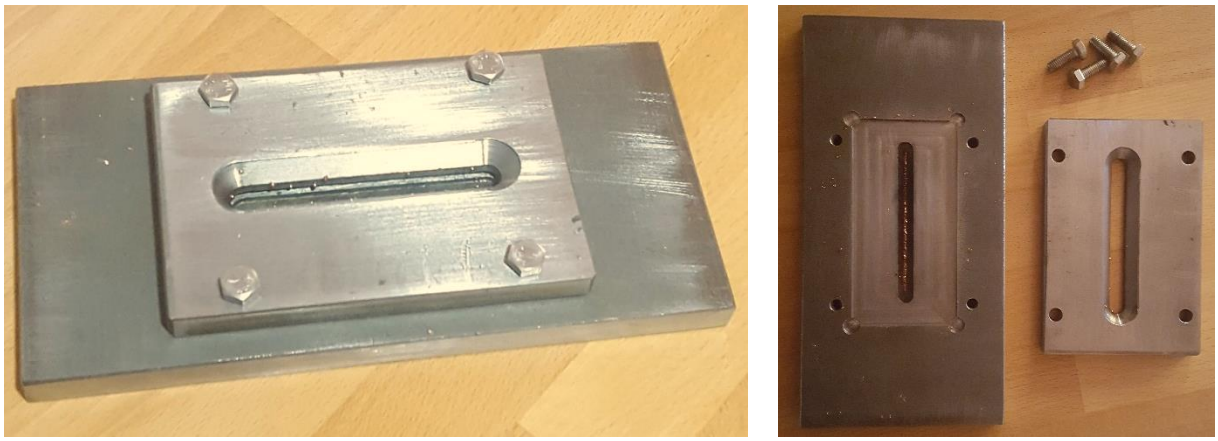

Figure 3.5 – Jig designed to the experimental trials.

3.4. Welding tests

To evaluate the effect of major welding parameters on the weld characteristics and soundness and to determine the best window of parameters to obtain a weld penetration of 1.5 mm, a set of trials was run. The welding tests were divided in 3 stages. The preliminary one enabled to identify the effect of shielding gas and tilt angle on the weld penetration and seam aspect. In the second stage, a comprehensive study about the influence of laser power, welding speed, focal point position, rotation diameter, rotation frequency and beam trajectory was performed. Finally, single-mode and multimode fiber lasers were compared. Figure 3.6 illustrates the wobbling laser welding with a circular trajectory.

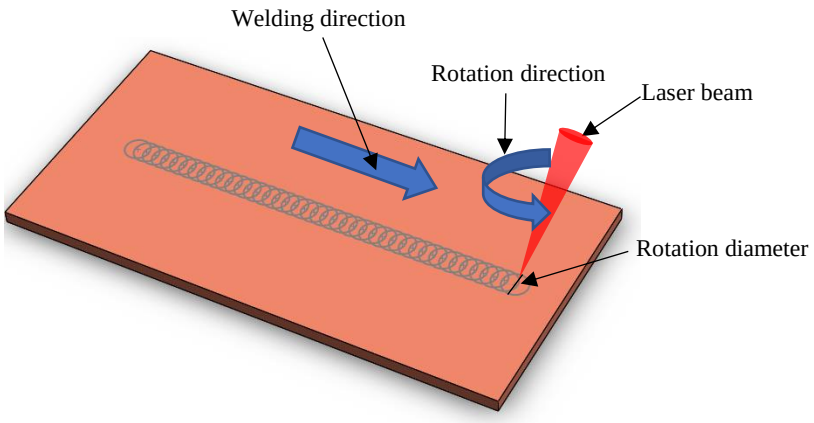

Figure 3.6 - Wobbling laser beam welding scheme.

3.4.1. Preliminary experiments

A preliminary study was conducted to assess the influence of the shielding gas and the tilt angle on the weld seam and the weld penetration. For this, a multi-mode optical fiber with 100 μm of diameter was used. The range of laser parameters tested is shown in Table 3.4. The focal point position, rotation frequency, rotation diameter and beam trajectory were kept constant and these were: focal point position= 0 mm; rotation diameter = 1 mm, rotation frequency = 100 Hz, beam trajectory = circular.

Table 3.4 - Range of laser parameters tested.

Number of trials	18
Tilt angle	0-10º
Laser power (W)	2000-5000
Welding speed (m/min)	2-5

3.4.2. Multimode fiber

A multimode optical fiber with 100 μm of diameter was used. Argon was the shielding gas and the tilt laser angle was 10º (to avoid back reflection). The welds were made on 2.5 mm thick plates. In this phase laser power, welding speed, focal point position, rotation frequency, rotation amplitude and beam trajectory were tested to predict their influence on the weld depth. The laser parameters range are displayed in Tables 3.5 to 3.10.

Table 3.5 – Laser parameters used to study the influence of laser power (welding speed = 4 m/min, focal point position = 0, rotation diameter = 1.0 mm, rotation frequency = 100 Hz, beam trajectory = circular).

Weld ref.	Laser power (W)
3B	5000
3C	2000
3D	3000
3E	4000

Table 3.6 - Laser parameters used to study the influence of welding speed (laser power = 4000 W, focal point position = 0, rotation diameter = 1.0 mm, rotation frequency = 100 Hz, beam trajectory = circular).

Weld ref.	Welding speed (m/min)
4A	2.0
4B	3.0
4C	4.0
4D	3.5
4E	4.5
4F	5.0

Table 3.7 - Laser parameters used to study the influence of focal point position (laser power = 4000 W, welding speed = 4 m/min, rotation diameter = 1.0 mm, rotation frequency = 100 Hz, beam trajectory = circular).

Weld ref.	Focal point position (mm)
5A	-2
5B	-1
5C	1
5D	2

Table 3.8 - Laser parameters used to study the influence of rotation diameter (laser power = 4000 W, focal point position = 0, rotation frequency = 100 Hz, beam trajectory = circular).

Weld ref.	Welding speed (m/min)	Rotation diameter (mm)
6A	4.0	0
6B	4.0	0.6
6C	4.0	0.8
6D	4.0	1.2
6E	4.0	1.4
6F	3.0	0.6
6G	3.0	0.8
6H	3.0	1.2

Table 3.9 - Laser parameters used to study the influence of rotation frequency (laser power = 4000 W, focal point position = 0, rotation diameter = 1.0 mm, beam trajectory = circular).

Weld ref.	Welding speed (m/min)	Rotation frequency (Hz)
7A	4.0	180
7B	4.0	240
7C	4.0	300
7D	4.0	360
7G	3.0	180
7H	3.0	240
7I	3.0	300
7J	3.0	360

Table 3.10 - Laser parameters used to study the influence of beam trajectory (laser power = 4000 W, welding speed = 4 m/min; focal point position = 0, rotation diameter = 1.0 mm, rotation frequency = 100 Hz).

Weld ref.	Beam trajectory	
8A	Linear	|
8B	Horizontal infinity	∞
8C	Vertical infinity	8
8D	Horizontal infinity	∞
8E	Vertical infinity	8

3.4.3. Single-mode fiber

The third phase aims to analyse the difference between multimode and single-mode fibers in the welding process. In this set of experiments, a single mode optical fiber with 50 μm of diameter was used. Argon was used as shielding gas and the tilt angle was 10º. The welds were made on 2 mm thick plates.

The initial values considered were based on previous knowledge at IPG Photonics. The parameters analysed were laser power, welding speed, rotation diameter and rotation frequency as shown in Table 3.11 and Table 3.12.

Table 3.11 - Laser parameters used to study the influence of laser power and rotation frequency (welding speed = 2.0 m/min, focal point position = 0, rotation diameter = 0.7 mm, beam trajectory = circular).

Weld ref.	Laser power (W)	Rotation frequency (Hz)
10A	2700	500
10B	2700	700
10C	2700	200
10D	2700	300
12A	2500	500
12B	2500	200

Table 3.12 - Laser parameters used to study the influence of rotation diameter and rotation frequency (laser power = 3100 W, welding speed = 2.5 m/min, focal point position = 0, beam trajectory = circular).

Weld ref.	Rotation diameter (mm)	Rotation frequency (Hz)
13A	0.5	500
13B	0.9	500
14A	0.7	300
14B	0.7	700

3.5. Characterization techniques

3.5.1. Visual inspection

Visual inspection was performed to identify uneven weld width, melt ejections, weld penetration and surface and root defects.

3.5.2. X-Ray inspection

The X-ray inspection was conducted as a non-destructive test to assess the occurrence of internal defects along the weld seam, such as pores. This inspection was performed at ISQ, the Portuguese Welding and Quality Institute with an Andrex CP 160kV unit with a tube voltage of 120 kV and an exposure time of 2.0 mA min.

3.5.3. Metallographic analysis

Cross sections of all welds were mechanically removed, mounted in resin, mechanically polished and etched with ferric chloride reagent.

Metallographic analysis of the welds was performed using a Leica DMI 5000 M inverted optical microscope. This analysis enabled to identify the different zones of the welds and their extension, the structural modifications in each zone, the grain morphology and size and the existence of internal defects (size and distribution).

3.5.4. SEM/EDS analysis

A deeper analysis using Scanning Electron Microscope was performed on dedicated samples to identify the solidification structure, pores or inclusions, the grain microstructure and the chemical composition of the base material, the HAZ and the FZ.

The SEM / EDS exam was performed, at CEMUP facilities, using a High resolution (Schottky) Environmental Scanning Electron Microscope with X-Ray Microanalysis and Electron Backscattered Diffraction analysis: Quanta 400 FEG ESEM / EDAX Genesis X4M. The selected samples were coated with a C thin film, by vapour deposition, using the JEOL JEE – 4X Vacuum Evaporator equipment. Facilities at CENIMAT, were also used with a ZEISS DSM 962 ESM. SEM was equipped with an energy dispersive X-ray spectrometry (EDS) from Oxford Instruments, INCA X-ACT. The selected samples were coated with an Au thin film, by vapour deposition, using a vacuum evaporator equipment.

3.5.5. X-Ray Diffraction analysis

X-Ray Diffraction was performed at DESY facilities (HEMS - High Energy Materials Science beamline) at PETRA III in Hamburg, Germany. It was used a wavelength of 0.1430 Å (87 keV). A 2D detector was used and the tests were held at room temperature (21 °C). The sample to detector distance also varied from 1.04 to 1.41 mm.

This analysis was performed to identify microstructural modifications during the weld.

3.5.6. Hardness testing

Vickers hardness measurements were performed using a Mitutoyo HM-112 under a load of 2 N. The hardness profile was evaluated on the cross section of the weld along to a horizontal line at mid thickness of the copper plate. The distance between indentations was 250 µm.

These measurements enable to evaluate changes due to thermo-mechanical cycle present in the processed material and heat affected zone (HAZ) and predict mechanical behaviour.

3.5.7. Electrical conductivity testing

Eddy current measurements were performed using an Olympus Nortec 500C equipment and a MTF905-60B probe with a frequency of 1 and 5 MHz, a gain of 50 dB and an angle of 325º. These measurements allowed to analyse the influence of the weld seam and eventual defects on the electrical conductivity. It is vital that LBW does not affect electrical conductivity for the industrial applications.

CHAPTER 4

RESULTS AND DISCUSSION

A detailed discussion of the results of this study are presented in this chapter that is organized by characterization techniques.

4.1. X-ray inspection

From the complete set of welds produced, several were considered of good quality in a visual analysis, so, these were selected for X-ray inspection to evaluate their internal integrity and the presence of porosities or other internal defects, though porosities were of major concern for the industrial application envisaged.

None of the welds inspected showed porosities as seen in Figs. 4.1 to 4.3, for samples 4E, 6E and 7I, respectively, representative of the welds produced. Figure 4.1 shows a homogeneous weld bead without noticeable defects, while small undercuts and spatter can be seen. Figure 4.3 exhibits a large amount of undercuts.

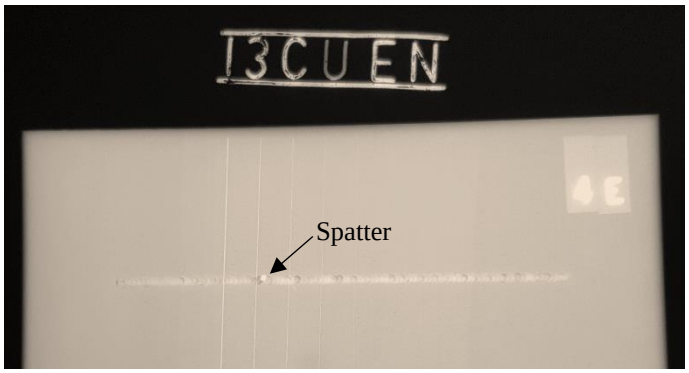

Figure 4.1 - Radiograph of sample 4E (laser power = 4000 W, welding speed = 4.5 m/min, focal point position = 0; rotation diameter = 1.0 mm; rotation frequency = 100 Hz, beam trajectory = circular).

Figure 4.2 - Radiograph of sample 6E (laser power = 4000 W, welding speed = 4.0 m/min, focal point position = 0; rotation diameter = 1.4 mm; rotation frequency = 100 Hz, beam trajectory = circular).

Figure 4.3 - Radiograph of sample 7I laser power = 4000 W, welding speed = 4.0 m/min, focal point position = 0; rotation diameter = 1.0 mm; rotation frequency = 300 Hz, beam trajectory = circular).

4.2. Visual inspection

4.2.1. Multimode fiber

The top view and cross section of the welds obtained with and without shielding gas are depicted in Table 4.1. The weld bead produced without shielding gas seems to be irregular and contain several spatters and surface voids. Additionally, without the shielding gas, it is visible a slight oxidation near the surface. With shielding gas, the number of surface voids significantly decreases and spattering is suppressed. The weld depth and the bead width is identical in both cases.

Table 4.1 – Top view and cross section obtain with and without shielding gas (laser power = 4000 W, welding speed = 4.0 m/min, focal point position = 0, rotation diameter = 1.0 mm, rotation frequency = 100 Hz, beam trajectory = circular).

Shielding gas	Without shielding gas	Argon 99.9%
Top view	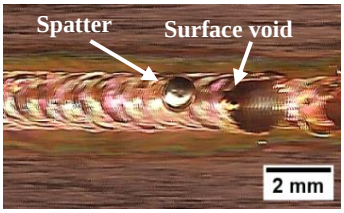	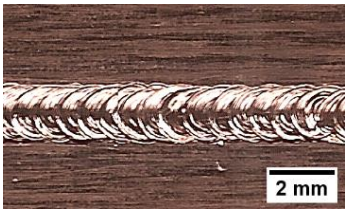
Cross section	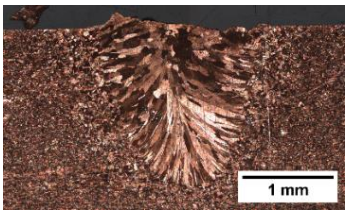	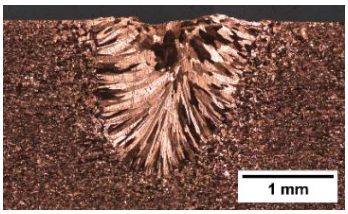

The influence of laser power in LBW of pure copper is shown in Table 4.2. It is possible to conclude that the seam weld is more uniform and regular as the laser power increased. For a laser power under 3000 W, it is not possible to weld copper using the set-up previously described since the heat input is insufficient to compensate thermal losses due to the high thermal conduction and low absorptivity of Cu. Surface voids were seen of the surface of the weld produced with 4000 W. The welding mode was keyhole for a laser power of 5000 W and conduction for the laser powers bellow, keeping constant all the other welding parameters. This weld also shows a depression at the welding centreline and undercuts characteristic of a weld with excessive power.

For a constant power (Table 4.3) very low speeds lead to irregular weld surface and keyhole mode, but the process stabilises and weld beads are more regular at speeds above 4.5 m/min. Figure 4.4 shows that surface voids decrease as welding speed increases.

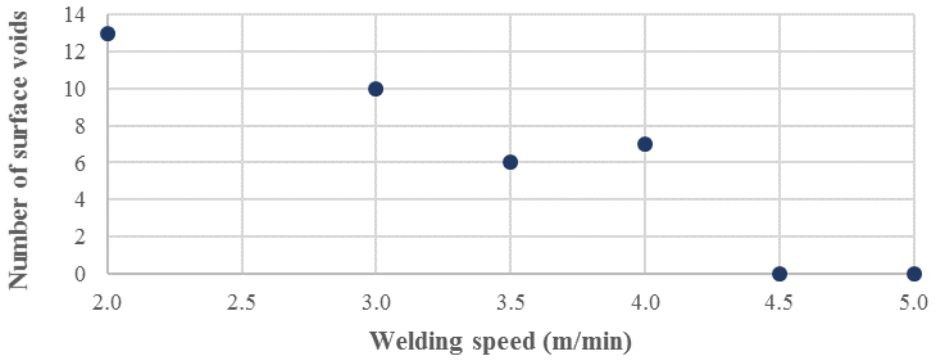

Figure 4.4 – Surface void formation tendency at different welding speeds.

Table 4.2 - Top view and cross section obtained with different laser powers (welding speed = 4.0 m/min, focal point position = 0, rotation diameter = 1.0 mm, rotation frequency = 100 Hz, beam trajectory = circular).

Laser power (w)	2000	3000	4000	5000
Top view		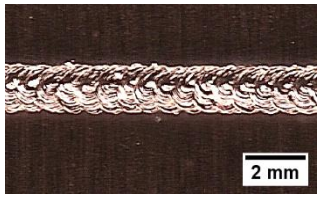	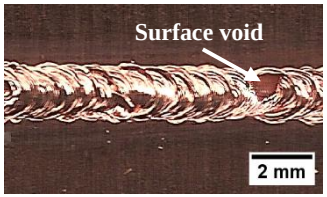	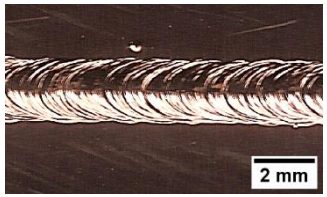
Cross section		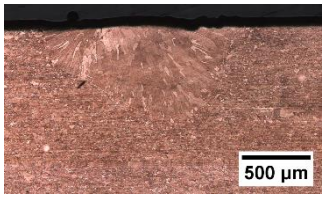	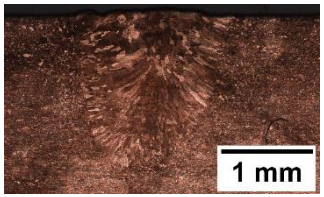	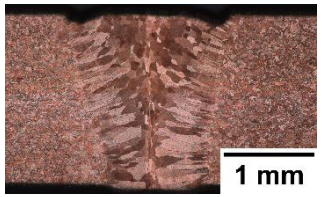

Table 4.3 - Top view and cross section obtained with different welding speeds (laser power = 4000 W, focal point position = 0, rotation diameter = 1.0 mm, rotation frequency = 100 Hz, beam trajectory = circular).

Welding speed (m/min)	2.0	3.0	3.5	4.0	4.5	5.0
Top view	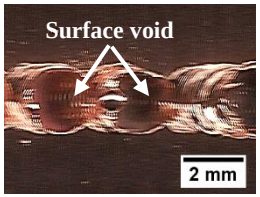	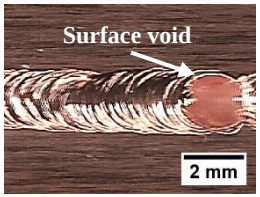	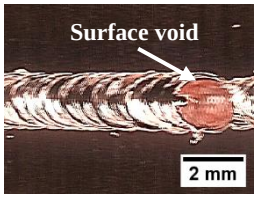	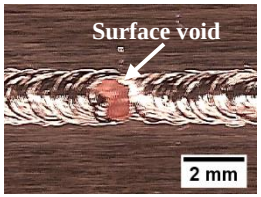	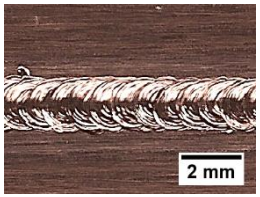	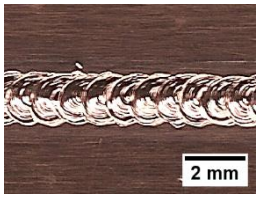
Cross section	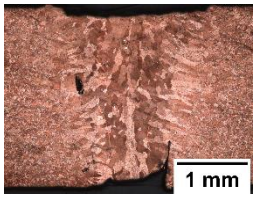	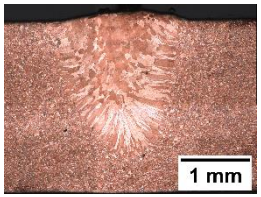	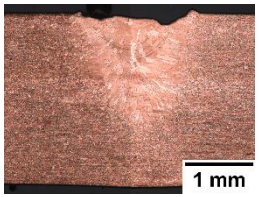	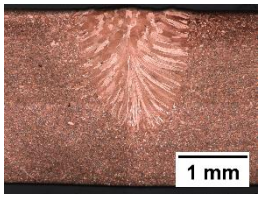	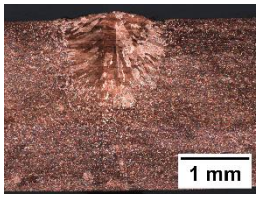	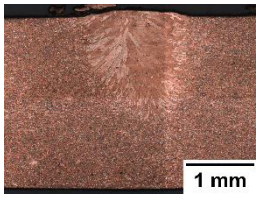

Table 4.4 – Top view and cross section obtained with different focal point positions (laser power = 4000 W, welding speed = 4.0 m/min, rotation diameter = 1.0 mm, rotation frequency = 100 Hz, beam trajectory = circular).

Focal point position (mm)	-2	-1	0	1	2
Top view	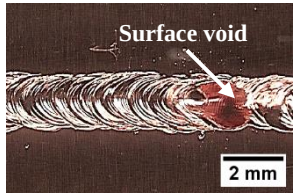	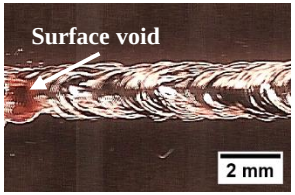	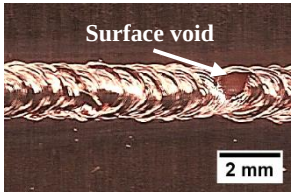	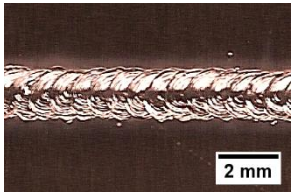	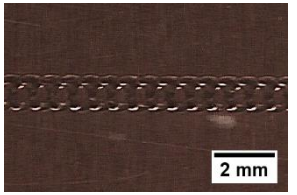
Cross section	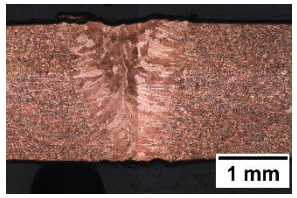	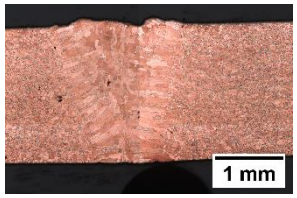	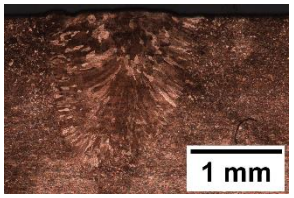	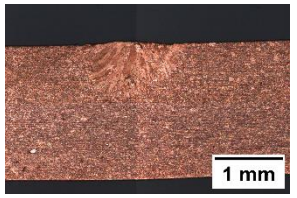	

Table 4.5- Top view and cross section obtained with different rotation diameters (laser power = 4000 W, welding speed = 4.0 m/min, focal point position = 0, rotation frequency = 100 Hz, beam trajectory = circular).

Rotation diameter (mm)	0 (Without scanning)	0.6	0.8	1.0	1.2	1.4
Top view	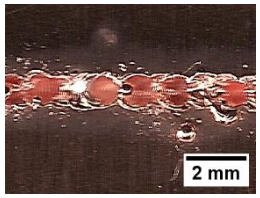	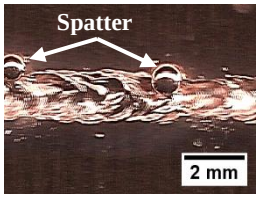	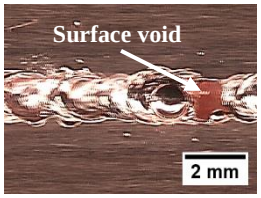	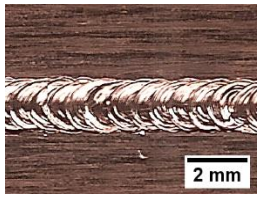	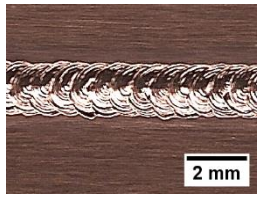	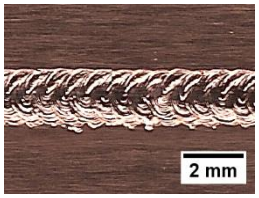
Cross section	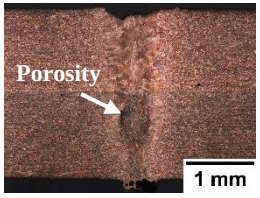	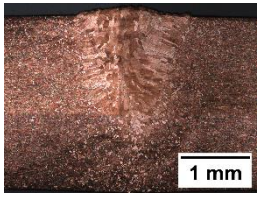	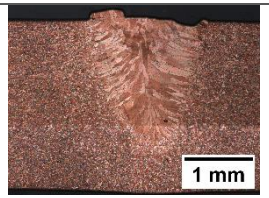	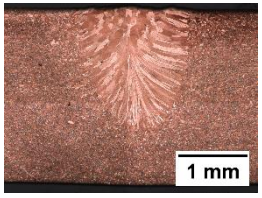	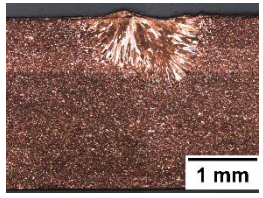	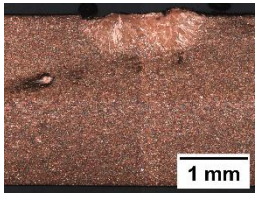

Table 4.6 - Top view and cross section obtained with different rotation diameters (laser power = 4000 W, welding speed = 3.0 m/min, focal point position = 0, rotation frequency = 100 Hz, beam trajectory = circular).

Rotation diameter (mm)	0.6	0.8	1.0	1.2
Top view	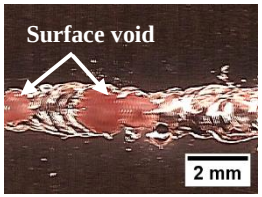	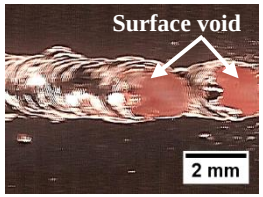	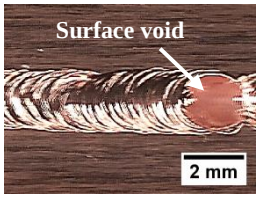	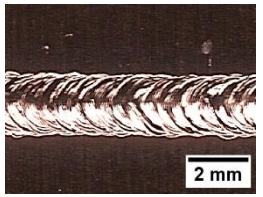
Cross section	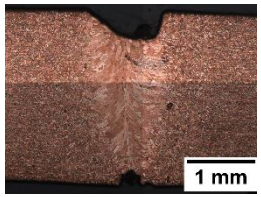	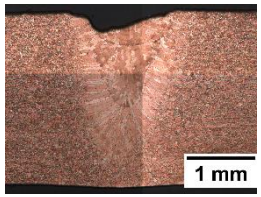	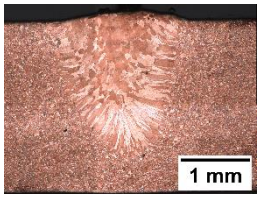	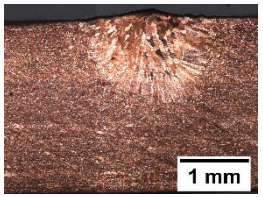

Table 4.7 - Top view and cross section obtained with different rotation frequencies (laser power = 4000 W, welding speed = 4.0 m/min, focal point position = 0, rotation diameter = 1.0 mm, beam trajectory = circular).

Rotation frequency (Hz)	100	180	240	300	360
Top view	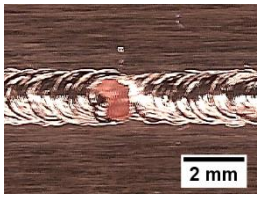	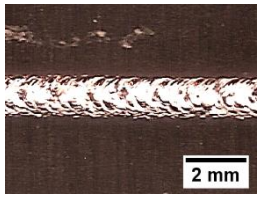	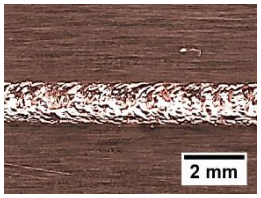	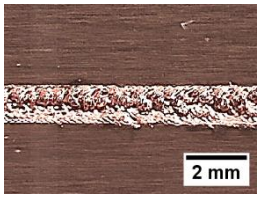	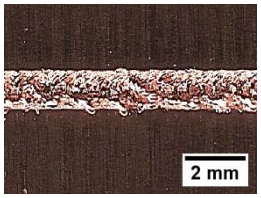
Cross section	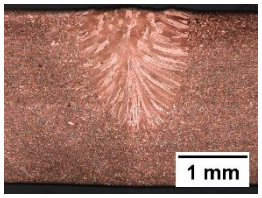	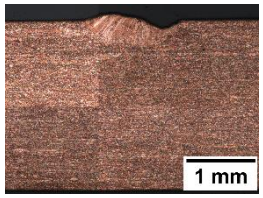	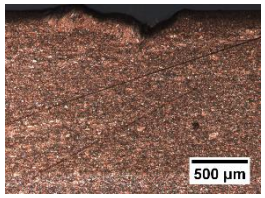	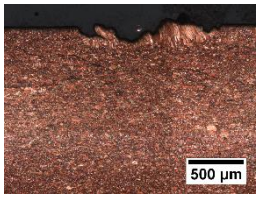	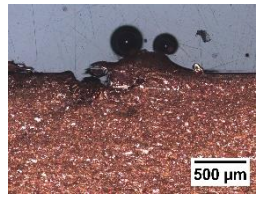

Table 4.8 - Top view and cross section obtained with different rotation frequencies (laser power = 4000 W, welding speed = 5.0 m/min, focal point position = 0, rotation diameter = 1.0 mm, beam trajectory = circular).

Rotation frequency (Hz)	100	180	240	300	360
Top view	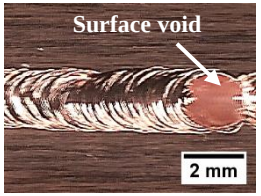	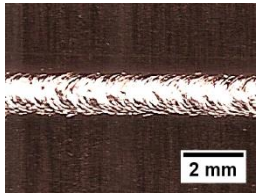	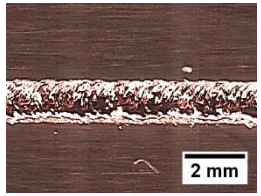	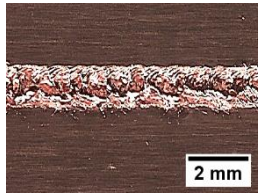	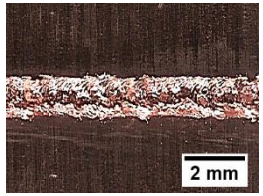
Cross section	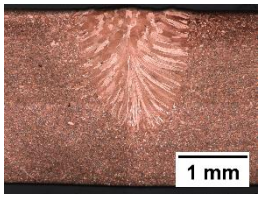	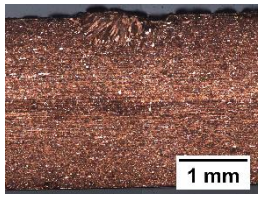	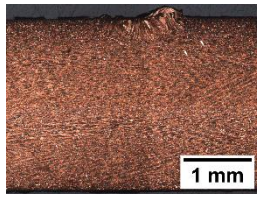	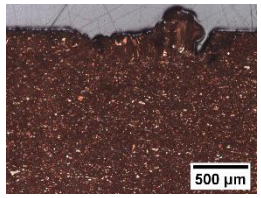	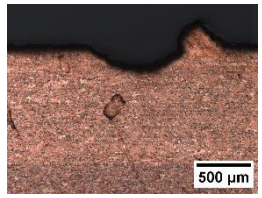

Table 4.9 - Top view and cross section obtained with different beam trajectories (laser power = 4000 W, welding speed = 4.0 m/min, focal point position = 0, rotation diameter = 1.0 mm).

Beam trajectory	Circular, O (f=100 Hz)	Linear, I (f=100 Hz)	Infinity, ∞ (f=100 Hz)	Infinity, 8 (f=100 Hz)	Infinity, ∞ (f=200 Hz)	Infinity, 8 (f=200 Hz)
Top view	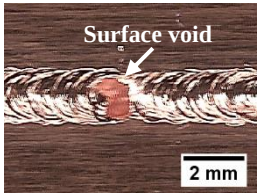	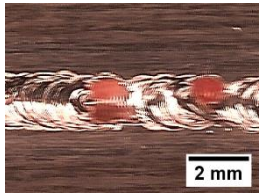	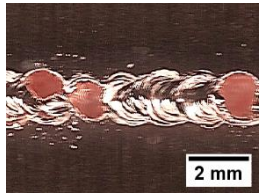	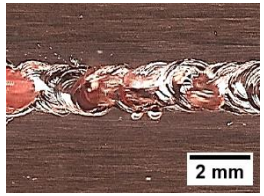	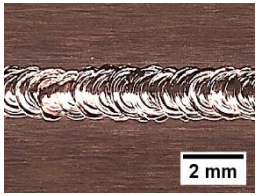	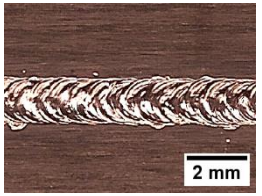
Cross section	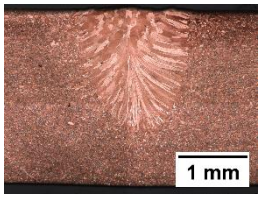	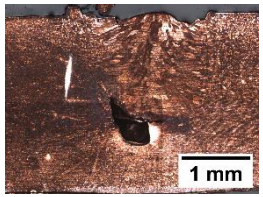	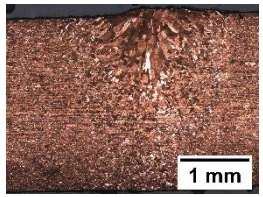	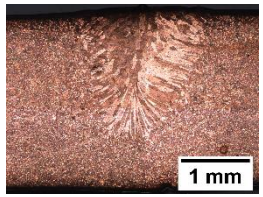	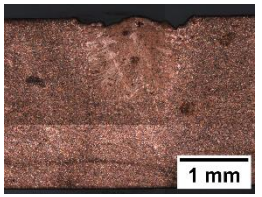	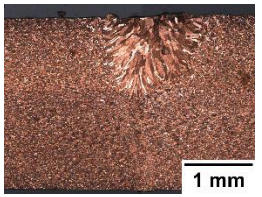

The appearance and cross section of the samples obtained with different focal point positions are shown in Table 4.4. At negative focal point position, a full weld penetration can be identified. These samples also present a large amount of welding defects such as surface voids and spatter.

Tables 4.5 and 4.6 show the influence of different rotation diameters in LBW of pure copper. Two different values of welding speed (3 and 4 m/min) were tested and compared. To evaluate the influence of the wobbling movement in the LBW process, a rotation diameter equals 0 mm was also analysed. When the rotation diameter was nihil, the path described by the laser is equivalent to the path of a laser beam without scanning. In this case, the sample exhibits a large amount of surface voids, spatters and small pores. According to Heider et al. [36], these welding defects result from the oscillation of the keyhole as a consequence of its instability with eventual collapse.

Figure 4.5 shows the trend of surface void formation at different rotation diameters. The surface voids decreased as the rotation diameter increased for two of the welding speeds tested. Also, at a welding speed of 3 m/min the formation of surface defects is more evident than at 4 m/min which confirms the previously obtained results.

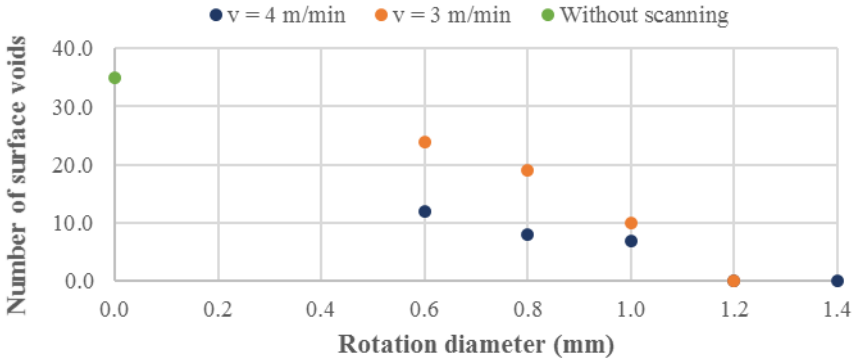

Figure 4.5 - Surface void formation tendency at different rotation diameters.

Tables 4.7 and 4.8 show the top view and the cross section of the samples obtained with 4 m/min and 3 m/min welding speed, respectively, with different rotation frequencies. For both cases, at rotation frequencies greater than 100 Hz it is not possible to weld properly copper with the present set-up. When the rotation frequency is high, the interaction time is very short, and so the deposition of energy into the material is not achieved, which hinders the melting of the material. For high rotation frequencies, the weld seam is also irregular and the weld depth is very small. However, in these samples the weld has no spatter or surface voids.

Table 4.9 shows the influence of beam trajectory on the top view and the cross section of the samples obtained with rotation frequencies of 100 and 200 Hz. At a rotation frequency of 100 Hz, all the beam trajectories tested produced welds with a large number of surface defects, especially the infinity shape

trajectories. However, at a rotation frequency of 200 Hz, in the infinity shape trajectories all the spatter and surface voids were supressed, as it can be seen in Figure 4.6.

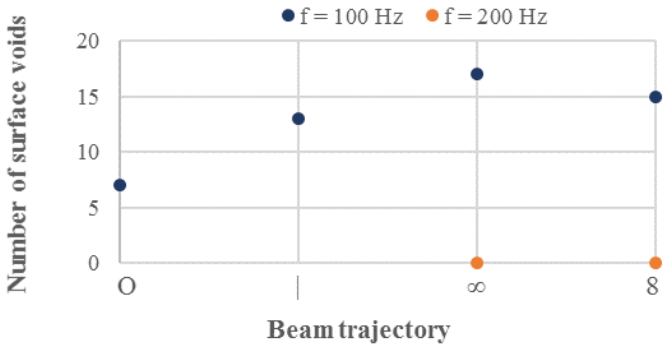

Figure 4.6 - Surface void formation tendency at different beam trajectories.

4.2.1.1. Effect of process parameters on the weld geometry

From the tests conducted, the penetration depth and bead width increased with laser power as expected [41]. At a laser power of 3000 W the laser welding penetration depth observed was lower than 1 mm while it increased to 2.5 mm at 5000 W. Figure 4.7 shows the relationship between laser power and weld depth and bead width.

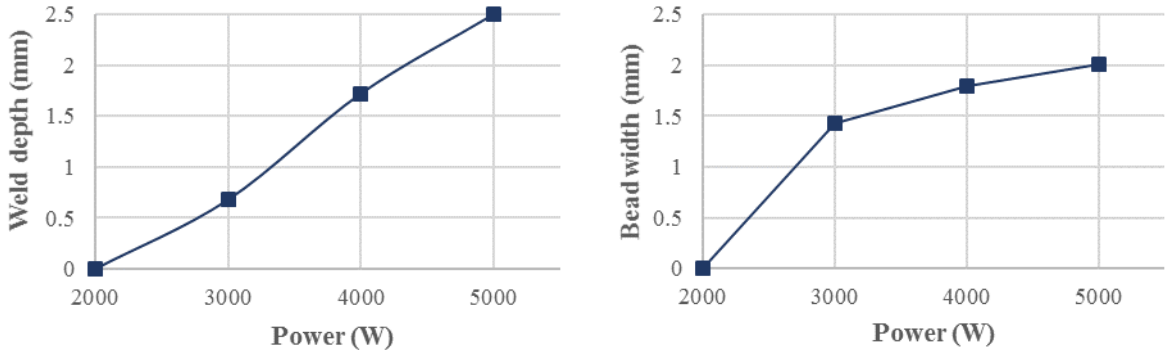

Figure 4.7 – Variation of weld geometry with beam power (welding speed = 4.0 m/min, focal point position = 0, rotation diameter = 1.0 mm, rotation frequency = 100 Hz, beam trajectory = circular).

Figure 4.8 shows the influence of welding speed on the same geometrical characteristics of the weld and it can be seen that both the weld depth and the bead width decreased as the welding speed increased. At a welding speed of 2 m/min, there is full penetration and the welding mode was keyhole as seen in Table 4.3. When the welding speed increases, the welding mode shifted to conduction. At a welding speed of 5 m/min, the laser welding penetration depth was about 1.5 mm which correspond to the penetration requirement for the industrial application.

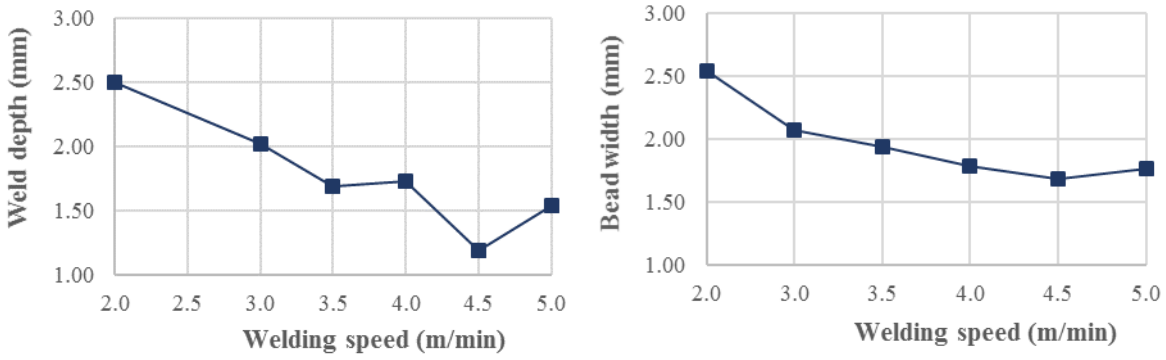

Figure 4.8 – Variation of weld geometry with different welding speeds (laser power = 4000 W, focal point position = 0 mm, rotation diameter = 1.0 mm, rotation frequency = 100 Hz, beam trajectory = circular).

Figure 4.9 shows the relationship between focal point position and welding geometry. The weld depth and the bead width decrease as the focal point position increases. At a focal point position of 2 mm, copper could not melt due to the low power density insufficiency to overcome Cu high thermal conductivity and high reflectivity. With positive focal point position, the penetration depth is drastically reduced.

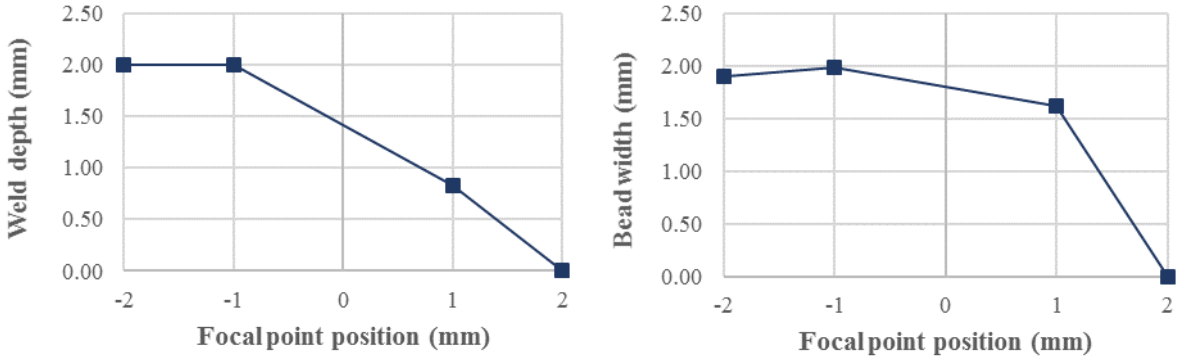

Figure 4.9 - Weld geometry with different focal point position (laser power = 4000 W, welding speed = 4 m/min, rotation diameter = 1.0 mm, rotation frequency = 100 Hz, beam trajectory = circular).

Figure 4.10 shows the relation between weld depth and bead width with rotation diameters. Weld penetration decreases as rotation diameter increases [42]. At a welding speed of 3 m/min, the influence of rotation diameter in weld penetration is more evident than at 4 m/min. For rotation diameters higher than 1.0 mm, it was noted a sharp decrease in penetration. The width of the weld bead was almost constant at a welding speed of 4 m/min. However, at a welding speed of 3 m/min, the bead width increased as the rotation diameter increased.

As previously mentioned, low rotation diameters lead to the formation of the keyhole while high rotation diameters lead to a conduction welding mode. However, when the rotation diameter is too high, the heat

flow behaves as if two heat sources were used with two hot spots as it can be seen at rotation diameters of 1.2 and 1.4 mm. this will be discussed later in this thesis.

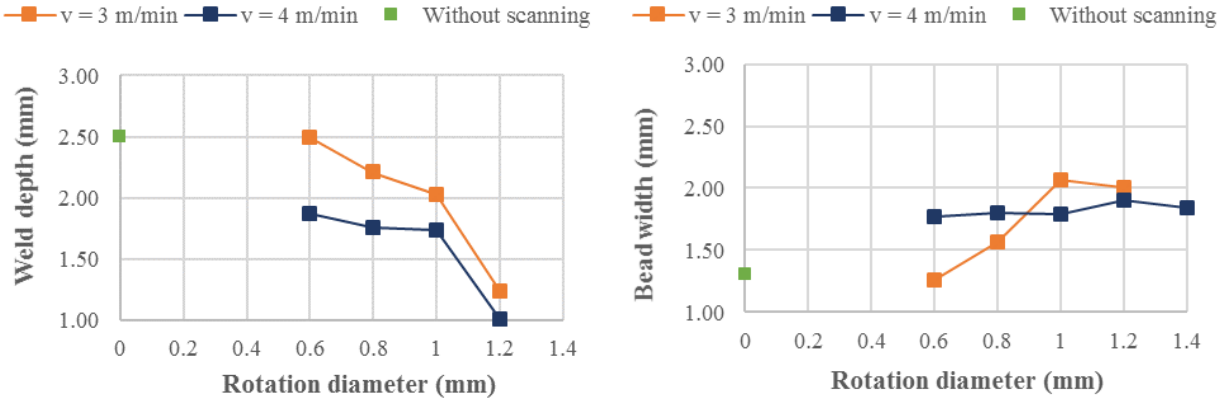

Figure 4.10 - Weld geometry with different rotation diameters at a welding speed of 3 m/min and 4 m/min (laser power = 4000 W, focal point position = 0, rotation frequency = 100 Hz, beam trajectory = circular).

Figure 4.11 shows that for rotation frequencies higher than 100 Hz, the penetration depth is below 0.5 mm. High rotation frequencies cause an insufficient weld penetration due to low interaction times combined with the low power density of the multimode fiber used.

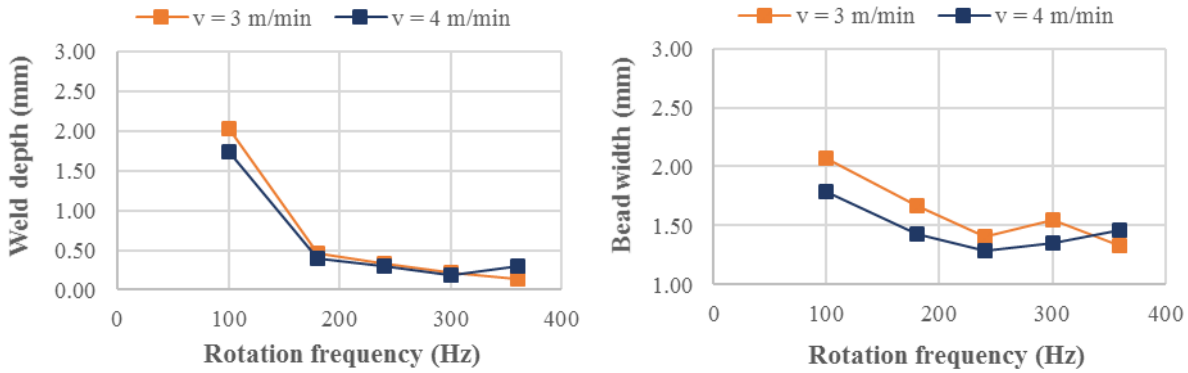

Figure 4.11 - Weld geometry with different rotation frequencies at a welding speed of 3 m/min and 4 m/min (laser power = 4000 W, focal point position = 0, rotation diameter = 1.0 mm, beam trajectory = O).

In the vertical infinity trajectory, increasing the frequency lead to a decreasing of weld depth (Figure 4.12). This result is similar to th previously discussed for the circular shape. However, the horizontal infinity trajectory exhibits an inverse relationship between frequency and weld depth. Additionally, the weld produced with the infinity shape at 200 Hz presented undercuts in the full weld length.

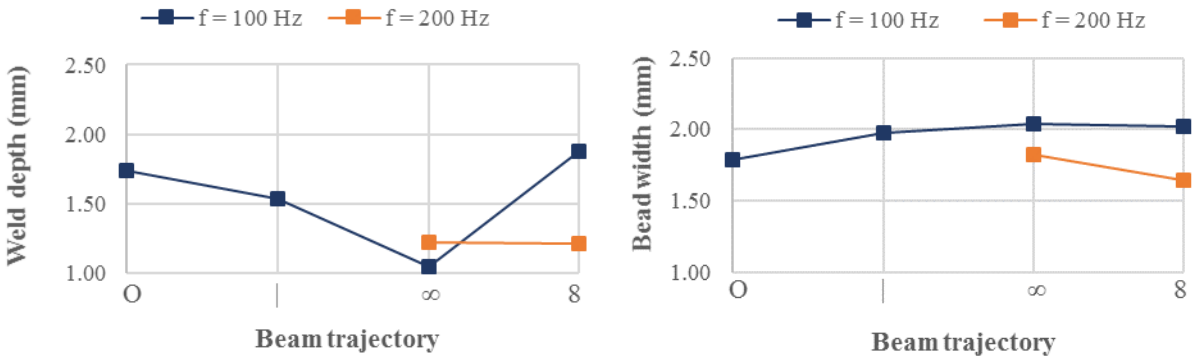

Figure 4.12 - Weld geometry with different beam shapes (laser power = 4000 W, welding speed = 4 m/min, focal point position = 0, rotation diameter = 1 mm, rotation frequency = 100 Hz).

4.2.2. Single-mode fiber

Table 4.10 shows the influence of rotation frequencies at two different laser powers (2500 and 2700 W). There seems to be a tendency to reduce the weld defects as the rotation frequency increase. At 200 Hz of rotation frequency, both welds show a large amount of spatter and surface voids. These defects are completely supressed at higher rotation frequencies, except for a rotation frequency of 500 Hz with a laser power of 2700 W.

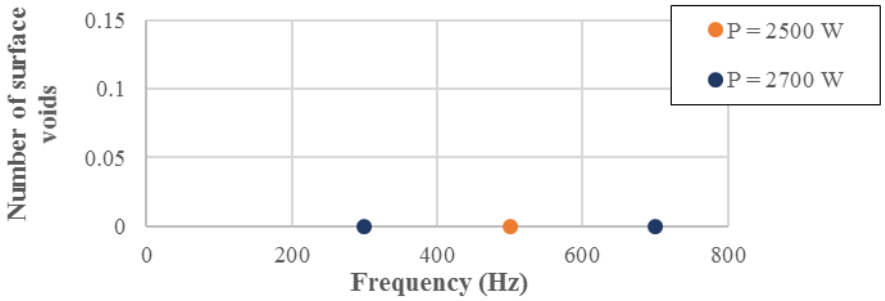

Figure 4.13 - Surface void formation tendency at different rotation frequencies and laser powers.

Table 4.11 illustrate the influence of rotation diameter. At a rotation diameter of 0.5 mm, a keyhole was formed with a few surface defects. At a rotation diameter of 0.9 mm, a conduction mode weld was produced without defects. As the rotation diameter increased, the weld defects, weld depth and bead width decreased. It is possible to conclude that conduction provide a greater stability to the weld process of pure copper.

4.2.2.1. Effect of process parameters on the weld geometry

The weld depth and bead width decreased as the rotation frequency increased for both laser powers (Figure 4.14). A good weld (without defects and with a good weld geometry) was obtained at a rotation frequency of 300 Hz, the weld depth and a bead width were 1.49 and 1.85 mm, respectively. It is important to note that these welds were made in 2 mm thick plates.

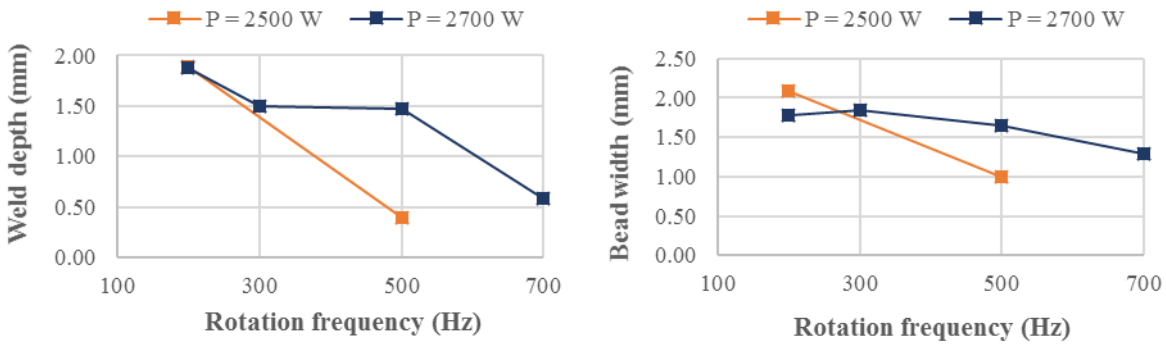

Figure 4.14 - Weld geometry with different rotation frequencies and laser powers (welding speed = 2 m/min, focal point position = 0, rotation diameter = 0.7 mm, beam trajectory = circular).

Similar results are verified with multimode fiber laser, that is, single-mode fiber laser can weld copper at lower laser powers, lower rotation diameters and higher rotation frequencies but at low welding speeds. Additionally, low rotation diameters lead to small bead width and higher rotation frequencies supress weld defects. As mentioned in chapter 2, a small fiber diameter leads to a narrow beam with great power intensity. These characteristics are especially important to weld copper because of its high thermal conductivity and low absorptivity. So, using single mode laser could be effective to produce 1.5 mm weld depth but the welding speed must be low.

Table 4.10 – Top view and cross section obtain with different rotation frequencies and laser powers (welding speed = 2.0 m/min, focal point position = 0 mm, rotation diameter = 0.7 mm, beam trajectory = circular).

Rotation frequency (Hz)	200 (P=2500 W)	500 (P=2500 W)	200 (P=2700 W)	300 (P=2700 W)	500 (P=2700 W)	700 (P=2700 W)
Appearance	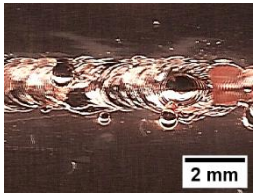	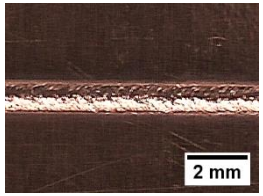	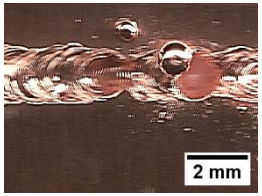	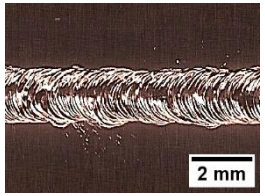	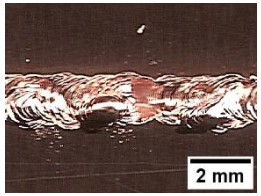	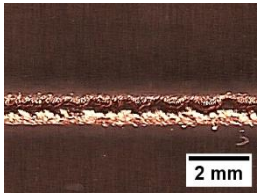
Cross section	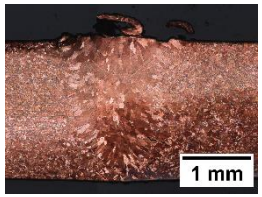	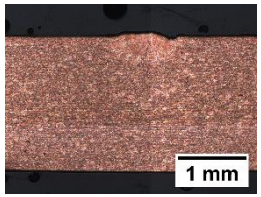	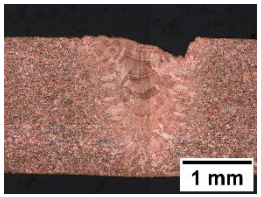	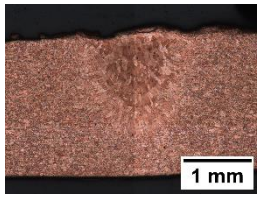	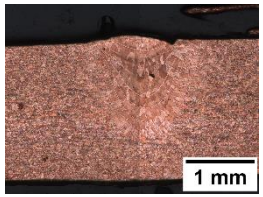	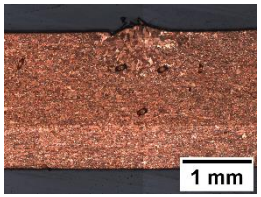

Table 4.11 – Top view and cross section obtain with different rotation diameters and frequencies (laser power = 3100 W, welding speed = 2.5 m/min, focal point position = 0, beam trajectory = circular).

Rotation diameter (mm)	0.5 (*f* = 500 Hz)	0.9 (*f* = 500 Hz)	0.7 (*f* = 300 Hz)	0.7 (*f* = 700 Hz)
Appearance	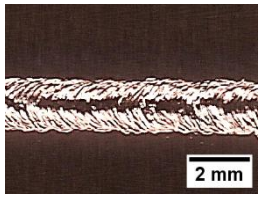	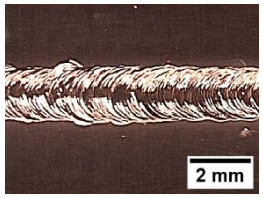	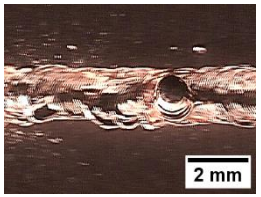	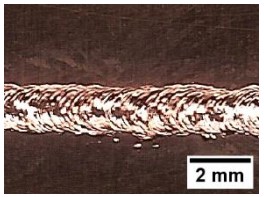
Cross section	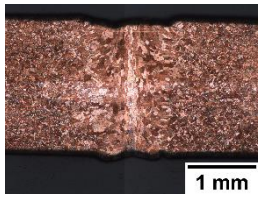	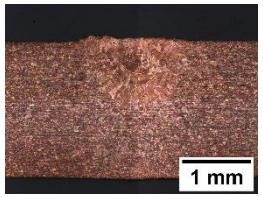	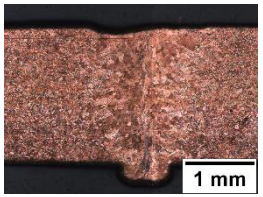	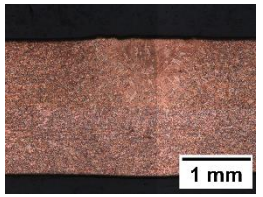

4.3. Wobbling effect on the weld depth

In order to understand the effect of overlap caused by the wobbling movement on the weld depth, modelling of the laser beam path in both X and Y directions was performed considering equations 4 and 5 developed by [31,42]. A mathematical model was developed in MatLab to reproduce the beam trajectories on a plate surface varying the beam rotation diameter and frequency.

The wobbling movement is the result of an imposed oscillation movement superposed to the travel direction and the welding speed. The oscillation movement is a consequence of rotation diameter combined with rotation frequency. Thus, the three parameters determine overlap of the path described superposing circular oscillations. The beam trajectory and overlap can be achieved using the equation 4 and 5, respectively.

Figure 4.15 shows the modulated beam paths for rotation diameters of 0.6 and 1.4 mm. At a welding speed of 4 m/min and the rotation frequency of 100 Hz, the path described exhibits an overlap of 25% for 0.6 mm and an overlap of 74% for 1.4 mm.

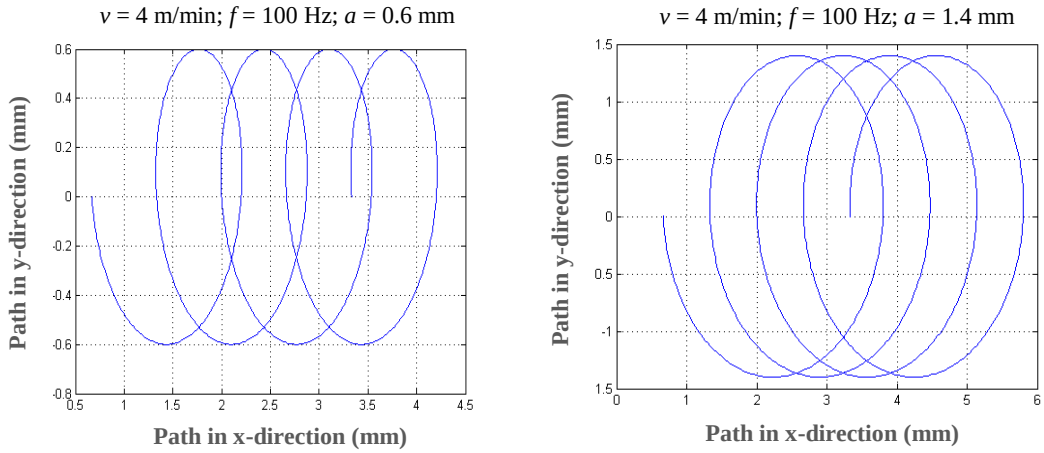

Figure 4.15 – Oscillation function dependent of the rotation diameter.

Figure 4.16 shows the relationship between overlap and rotation diameter and the influence of overlap in weld depth. As the rotation diameter decreased the overlap decreased [43] and the weld penetration increased. This is confirmed by the presence of a keyhole in the welds produced without scanning and with the rotation diameter of 0.6 mm, at a welding speed of 3 m/min. Increasing the overlap, the weld mode observed is mostly conduction.

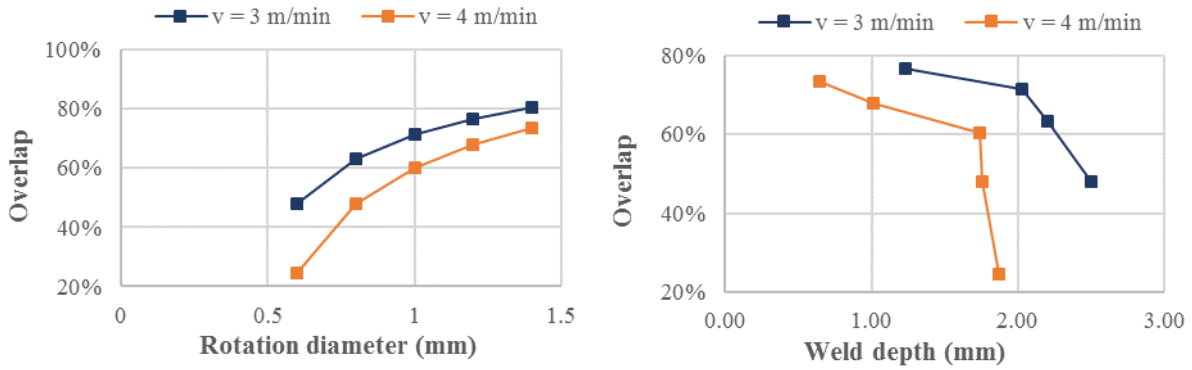

Figure 4.16 – Relation between rotation diameter and overlap and influence of overlap in weld depth (laser power = 4000 W, focal point position = 0, rotation frequency = 100 Hz, beam trajectory = circular).

At a welding speed of 4 m/min and a rotation diameter of 1.0 mm, the path described in Figure 4.17 exhibit an overlap of 60 % for 100 Hz and an overlap of 90% for 360 Hz. The overlap increases as the rotation frequency increases.

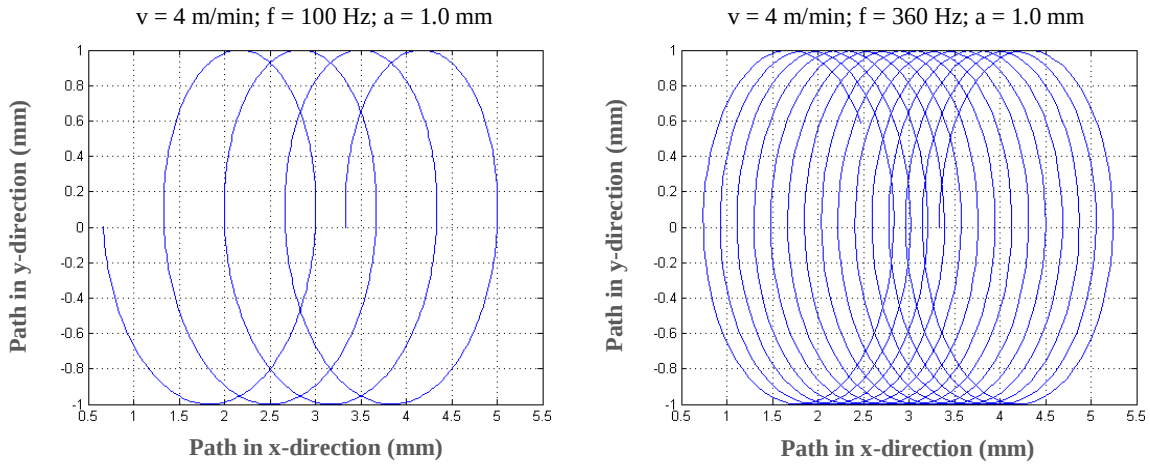

Figure 4.17 - Oscillation function dependent of the rotation diameter.

The range of rotation frequencies tested produced higher overlapping than the obtained varying the diameter, as it can be seen in Figure 4.18. These high overlaps seem to be the cause of the very low weld depths obtained. It is possible to conclude that overlap should not exceed 80%.

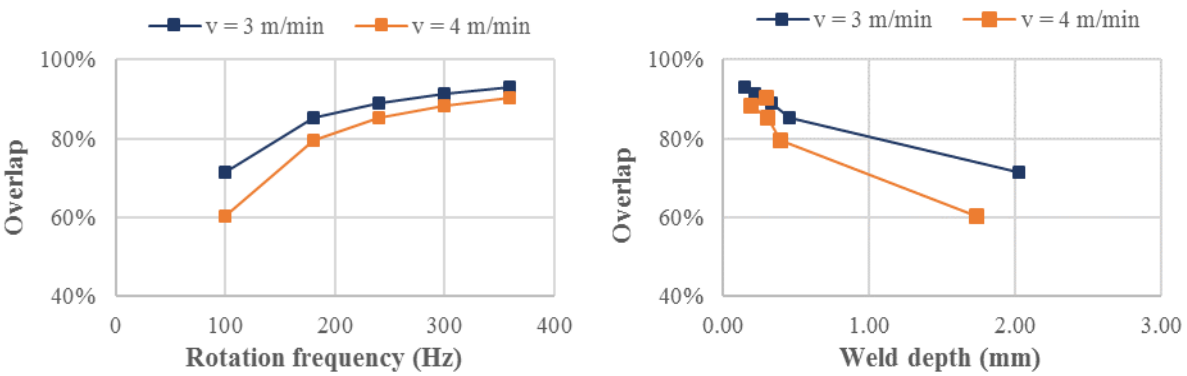

Figure 4.18 - Relationship between rotation frequency and overlap and influence of overlap in weld depth (laser power = 4000 W, focal point position = 0, rotation diameter = 1.0 mm, beam trajectory = circular)

Another important observation in the present results is that the welding speed influences the overlap. As expected, higher welding speeds produce lower overlaps.

Heat input in wobbling LBW is not constant, i.e. it changes in time. Overlap seems to influence energy transference to the workpiece because of the relation between overlap and weld depth. However, overlap cannot be directly related to heat input, especially in copper. Firstly, same overlap can be obtained with different parameters. For example, similar overlaps can be obtained with different rotation diameters once overlap also depends on the welding speed and rotation frequency. However, smaller rotation diameters imply a small area of laser radiation which conduce to a greater heat accumulation. This example applies to the 3 parameters.

Another parameter to consider is the absorptivity which depends on the temperature. Higher feed rates, i.e., higher welding speeds or/and higher rotation diameter or/and higher rotation frequencies, lead to a lower interaction time in each point of the weld seam. These results in a lower energy transferred to the sample, so the temperature is low and the absorptivity is limited or reduced.

Summarizing, overlap can be related to welding speed, rotation diameter and rotation frequency to provide a tendency of weld depth variation but cannot be used to stablish an accurate relationship with the heat input.

4.4. Metallographic analysis

The material microstructure is shown in Figure 4.19. It is a fine grain structure with many twin crystals which suggests that the material has been previously cold worked (cold rolled) generating a high dislocations density [12].

The typical weld bead surface produced with wobbling LBW is depicted in Figure 4.20 a). The weld bead surface reveals the rotation pattern and the overlaps described by the laser beam and shows no welding defects like surface voids, spatter, cracks or undercuts. The centre of the weld is slightly misaligned due to the asymmetric energy input as a result of the different energy input per length. The vectors of welding speed and rotation are in opposite directions for the left side of the welding seam (lower energy input) and in the same direction for the right side (higher energy input), as it can be observed in Figure 4.20 b).

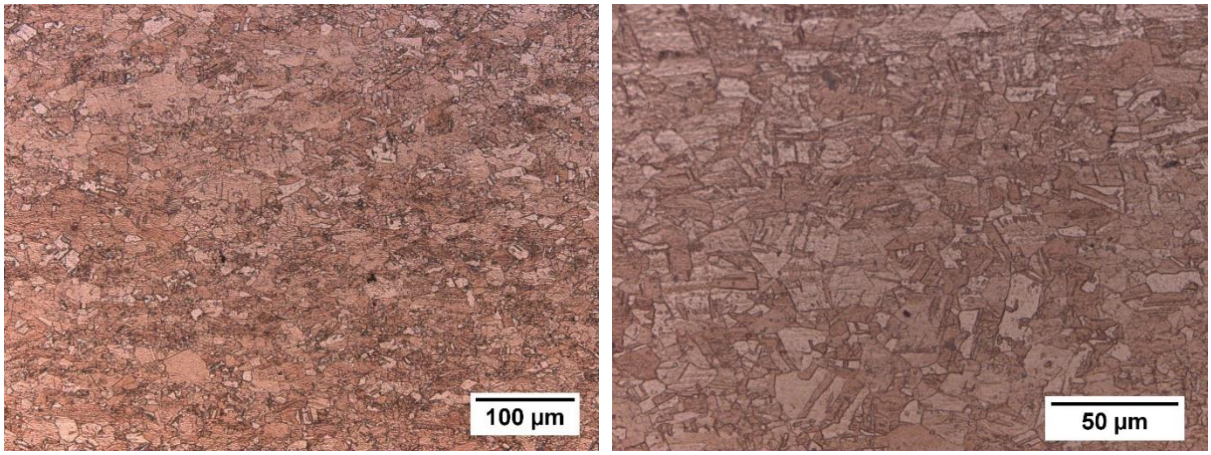

Figure 4.19 – Macrograph of base material.

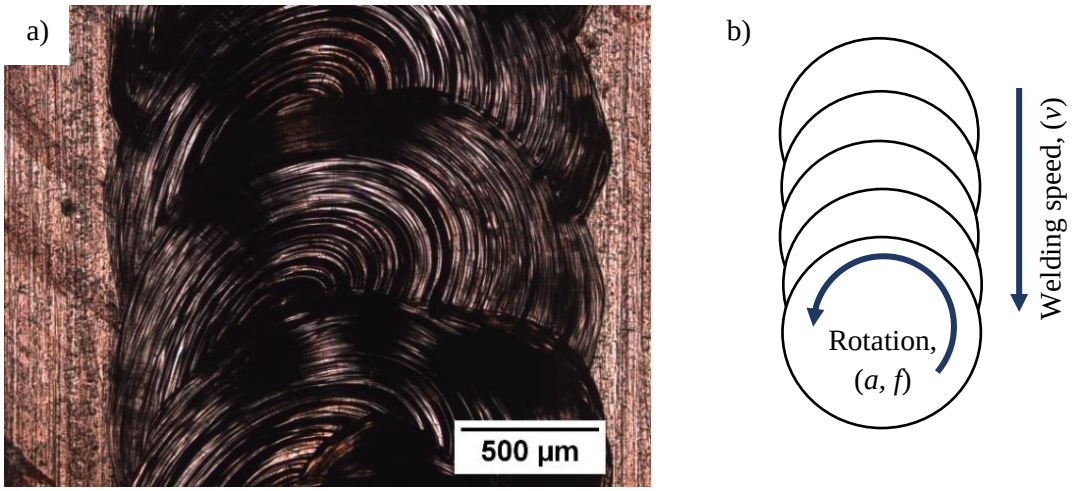

Figure 4. 20 – Weld bead surface a) of sample 6D (laser power = 4000 W, welding speed = 4 m/min, focal point position = 0, rotation amplitude = 1.2 mm, rotation frequency = 100 Hz, beam trajectory = circular) and its b) vectorial scheme.

Macrographs of most significant welds are shown in Figure 4.21 to 4.28, as well as micrographs of identified zones in the welds.

From the macro- and micrographs of the weld bead cross section, it is possible to identify the three different zones characteristic of laser beam welding process: the fusion zone (FZ), the heat affected zone (HAZ) and the unaffected base material (BM). The different colours observed in these three zones are related to differences in grain orientation under optical microscopy.

The fusion zone is constituted by columnar (near the HAZ) and equiaxed grains (in the centre of FZ). This zone is formed during solidification by epitaxial crystal growth on non-melted grains of transition solid/liquid zone. The direction of maximum heat flow is perpendicular to the fusion boundary, so grains tend to grow faster in that direction, which results in curved columnar grains in the fusion zone. Under certain solidification conditions the curved columnar grains may transit to equiaxed grains at the centre region of the weld during their growth process. This transition takes place when nucleation of equiaxed grains occurs in the liquid ahead of the columnar zone.

The grain structure observed in the heat affected zone was identical to the one found in the base material but with a larger grain size. In HAZ, the maximum temperature is below the melting temperature but it is high enough to modify the microstructure. In this zone, recrystallization and grain growth drastically reduce the mechanical properties of the material.

In most of the welds, cold bands were identified as reported by [45]. These bands cross the grains and are present in the fusion zone. Cold bands seem to be related with the grain orientation since they are more evident in certain grains, as it can be seen in Figure 4.28. The grains marked with G_1, G_2 and G_3 show no evidence of cold bands unlike the adjacent grains. It is assumed henceforth that these grains have the same orientation because of their colour and internal morphology. Furthermore, these bands also appear to be related with heat input, as they are mostly observed in welds produced with high heat input. In welds produced with a single-mode fiber, cold bands are more perceptible than in welds produced with multimode fiber.

Fine cell-type substructures inside the grains were identified, indicating that the etchant has attacked high-energy boundaries (areas) revealing substructures in the fusion zone. Some grains present oriented features while the others have a random substructure. The substructure and its morphology can be related with the crystallographic plane of grain growth and the dislocation networks. These cell substructures are present in all the samples produced but are more evident in high heat input welds. These substructures will be discussed in detail later.

In addition to the surface defects previously analysed, it is also worth to mention the defects inside the weld seam. Porosity is the most common defects found in copper welding. Several pores with small dimensions (2 to 16 μm) were identified in the samples produced. Because of their dimensions, these

pores were not detected in radiography and may be considered irrelevant. The inclusions observed in Figure 4.24 A_3) were caused by partial melting of the jig substrate material.

Other defects observed in several welds were undercuts. These undercuts are possibly a consequence of the high welding speed combined with the wobbling movement (welding speed, rotation diameter and rotation frequency) which causes a surface tension distribution larger in the middle and smaller close to the weld edges, leading to molten metal flow from the edge to the bead centre.

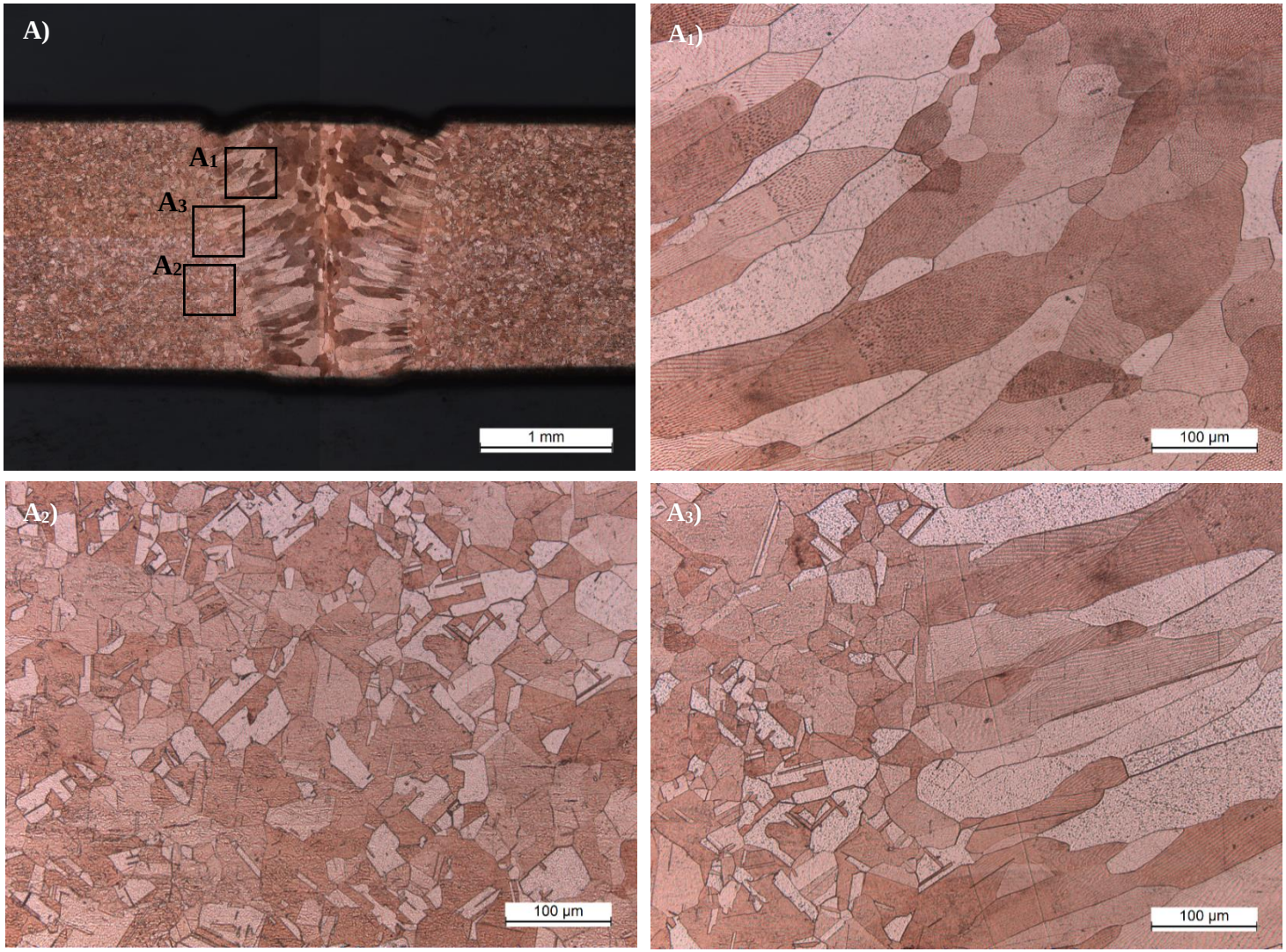

Figure 4.21 - Cross section macrograph of sample 3B (laser power = 5000 W, welding speed = 4 m/min, focal point position = 0, rotation diameter = 1.0 mm, rotation frequency = 100 Hz, beam trajectory = circular) with detailed micrograph.

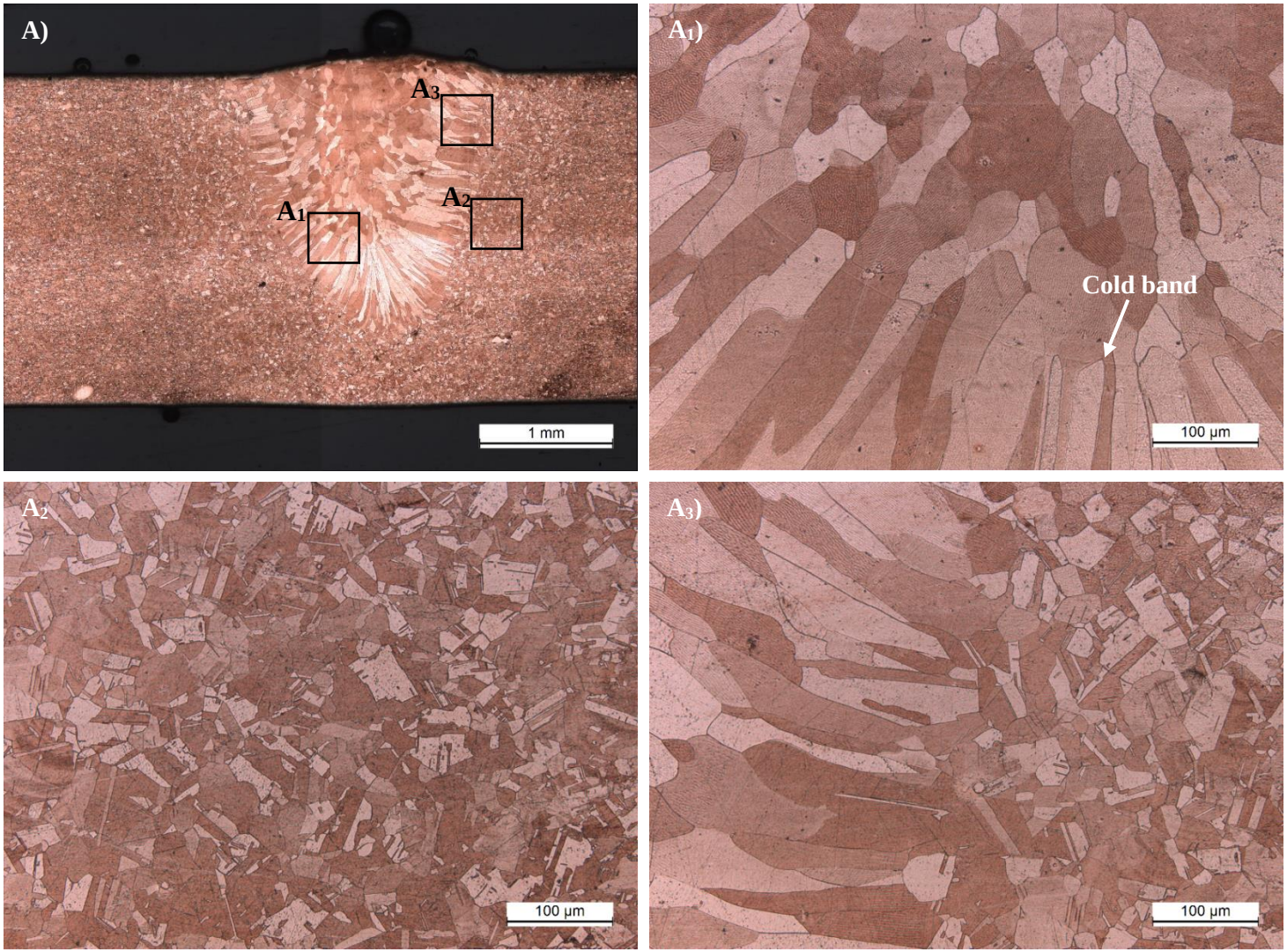

Figure 4.22 - Cross section macrograph of sample 4B (laser power = 4000 W, welding speed = 3 m/min, focal point position = 0, rotation diameter = 1.0 mm, rotation frequency = 100 Hz, beam trajectory = circular) with detailed micrograph.

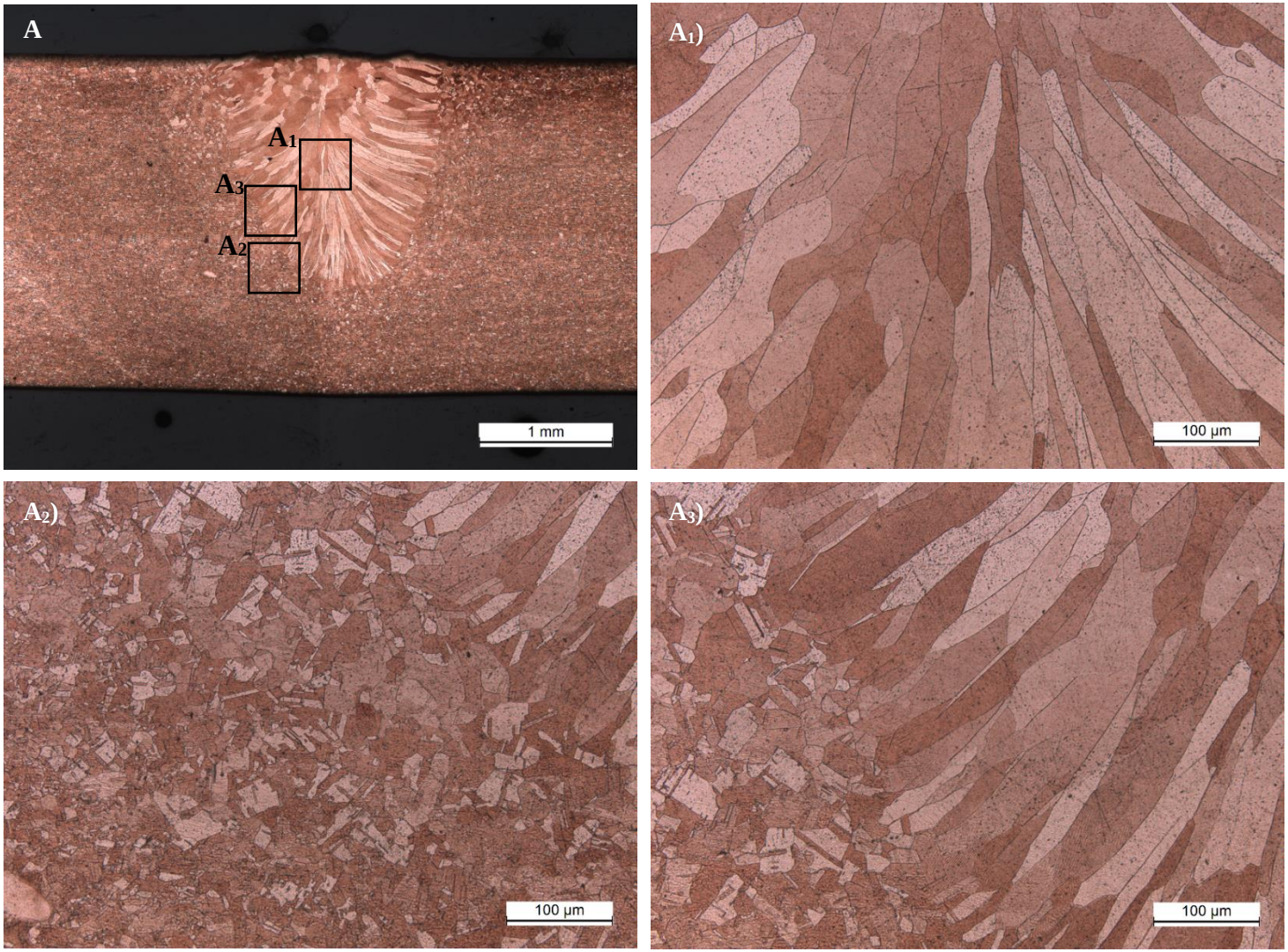

Figure 4. 23 - Cross section macrograph of sample 4C (laser power = 4000 W, welding speed = 4 m/min, focal point position = 0, rotation diameter = 1.0 mm, rotation frequency = 100 Hz, beam trajectory = circular) with detailed micrograph.

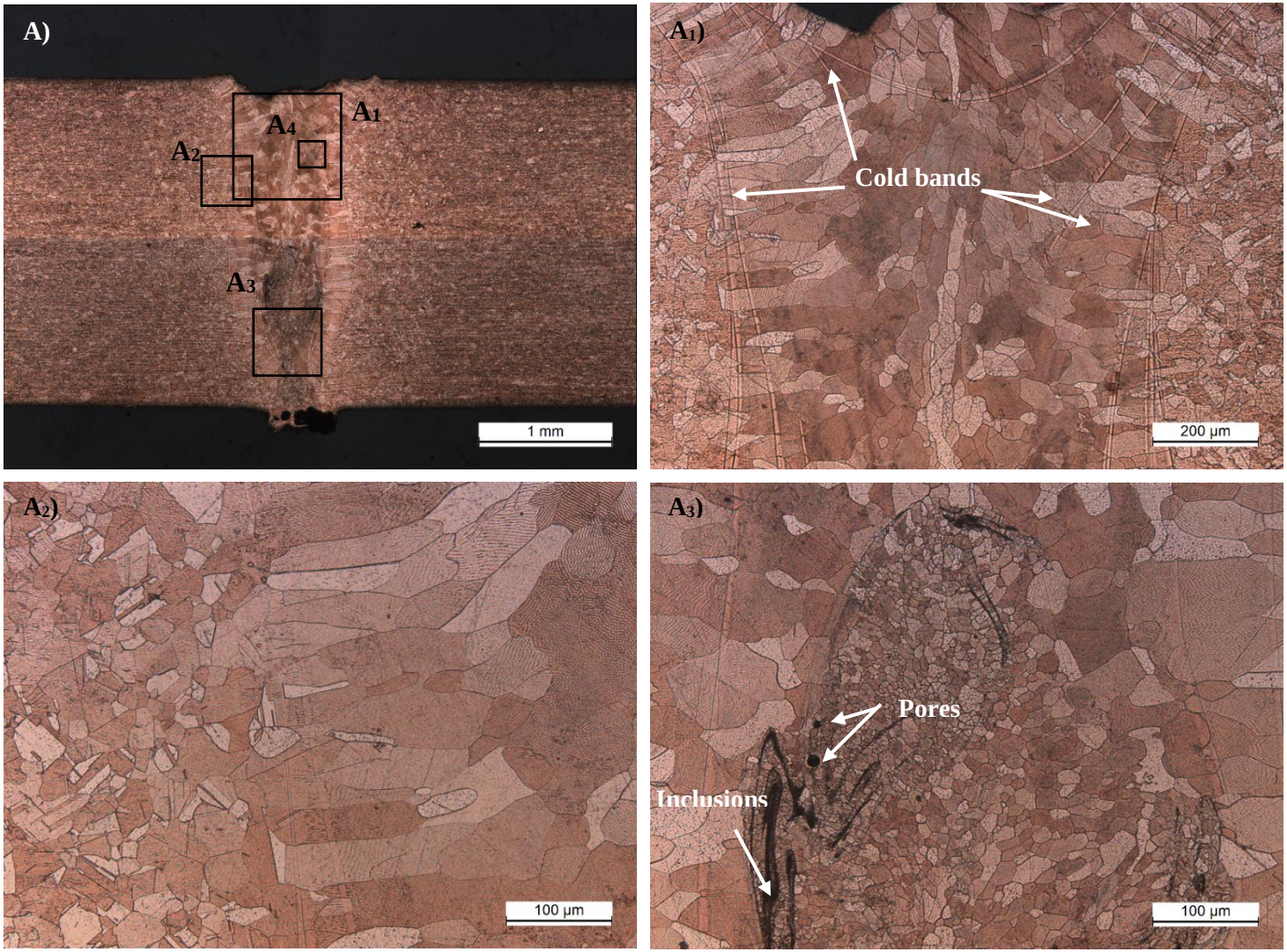

Figure 4.24 - Cross section macrograph of sample 6A (laser power = 4000 W, welding speed = 4 m/min, focal point position = 0, rotation diameter = 0, rotation frequency = 100 Hz, beam trajectory = circular) with detailed micrograph.

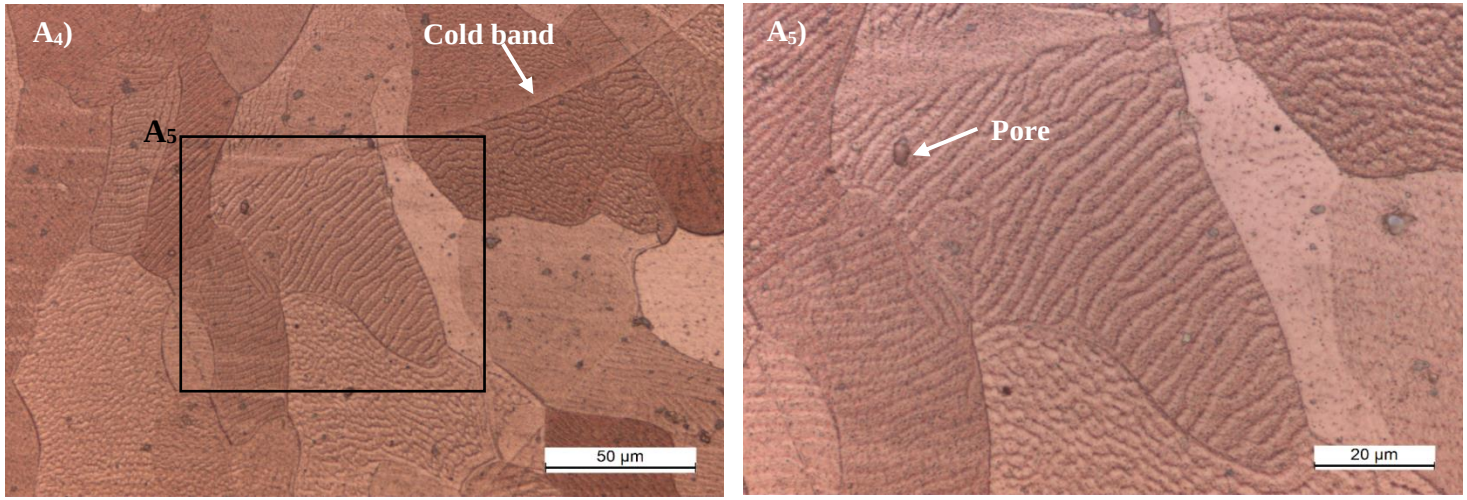

Figure 4.25 - Detailed micrograph of sample 6A (continuation of Figure 4.24).

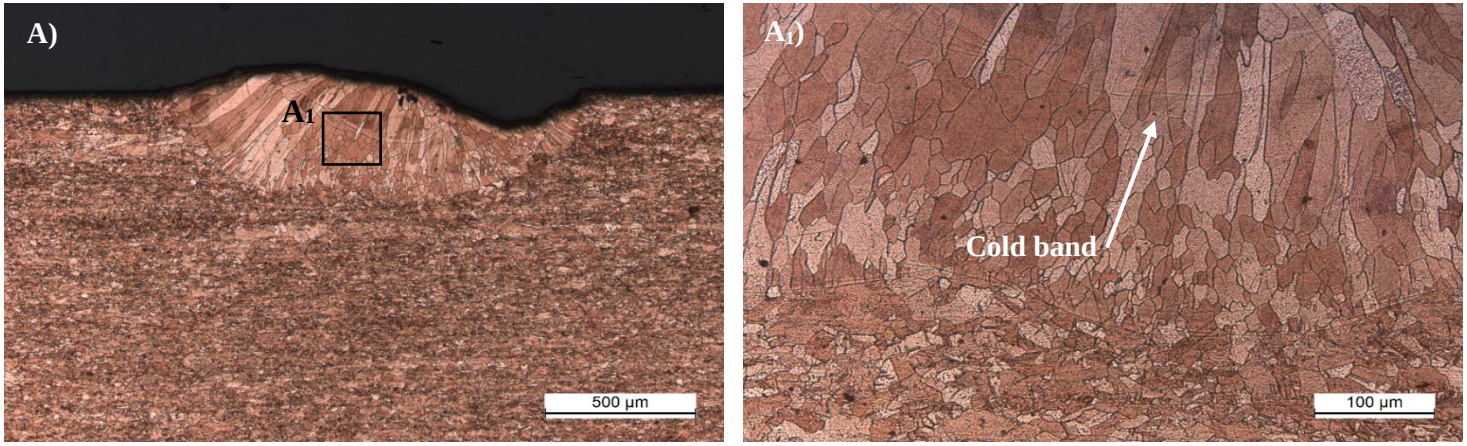

Figure 4.26 – Cross section macrograph of sample 7A (laser power = 4000 W, welding speed = 4 m/min, focal point position = 0, rotation diameter = 1.0 mm, rotation frequency = 180 Hz, beam trajectory = circular) with detailed micrograph.

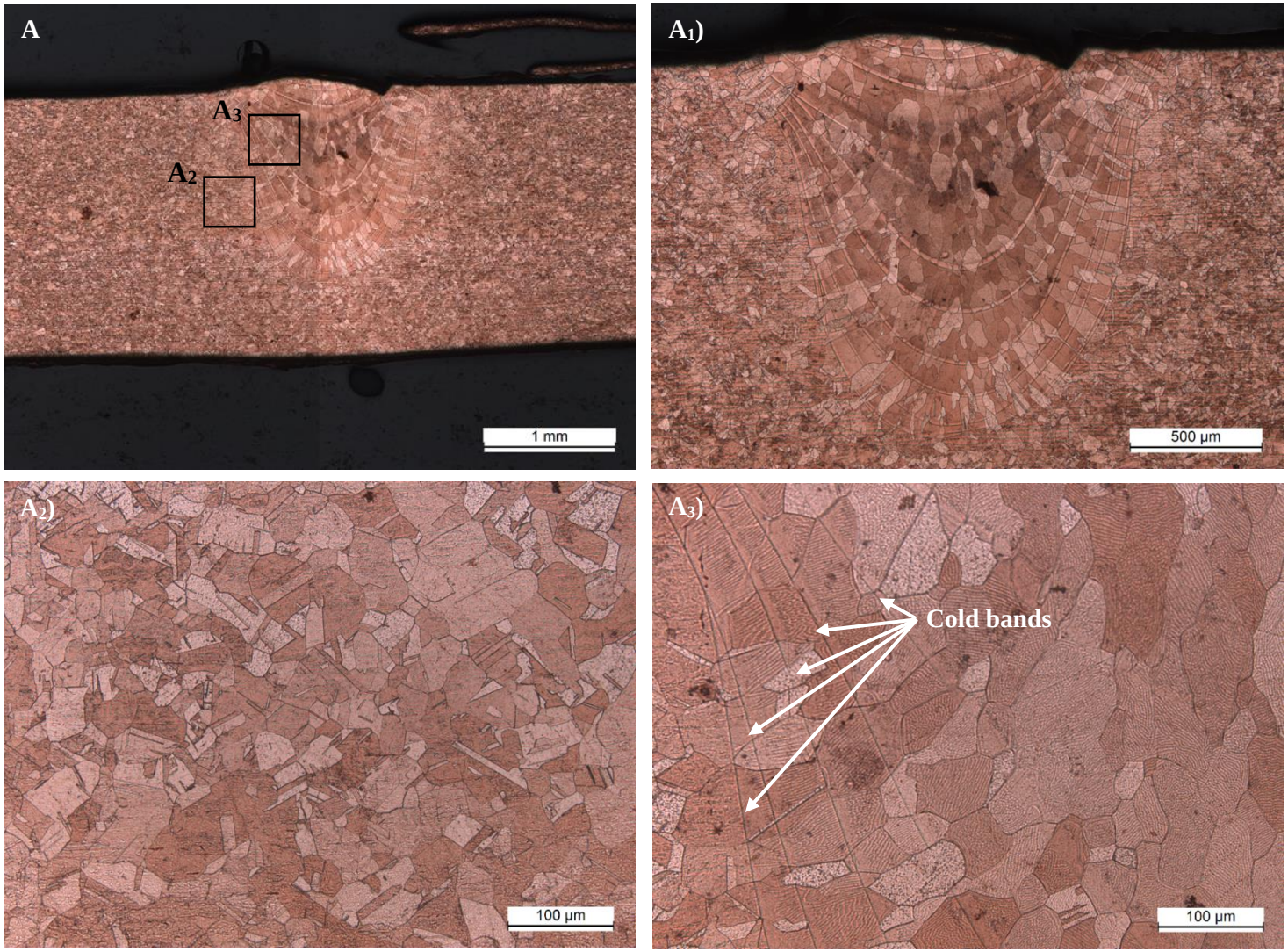

Figure 4.27 - Cross section macrograph of sample 10D (laser power = 2700 W, welding speed = 2 m/min, focal point position = 0, rotation diameter = 0.7 mm, rotation frequency = 300 Hz, beam trajectory = circular) with detailed micrograph.

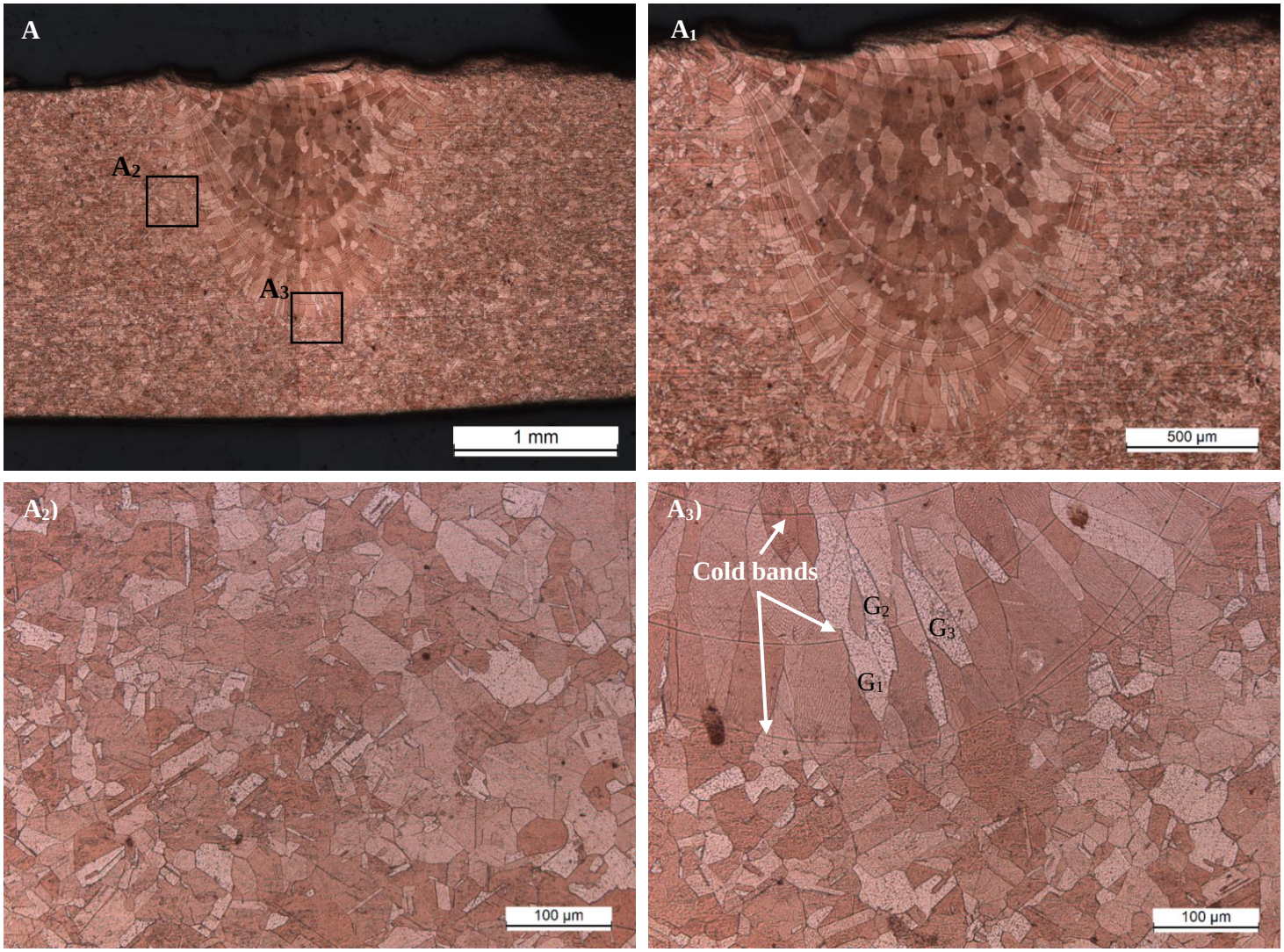

Figure 4. 28 - Cross section macrograph of sample 10A (laser power = 2700 W, welding speed = 2 m/min, focal point position = 0, rotation diameter = 0.7 mm, rotation frequency = 500 Hz, beam trajectory = circular) with detailed micrograph.

4.5. SEM/ EDS analysis

In order to study in detail the grain internal microstructure and the material composition, SEM with EDS analysis were performed.

In the base material, twinning was observed, as already identified by optical microscopy. Figure 4.29 b) shows that each grain is subdivided into segments of deformed substructures comparable to cells. The grains G_1 and G_2 show different substructures which may be related with the crystallographic orientation. Similar deformation microstructures in polycrystalline copper during cold rolling have been reported [48]. The existence of twinning and deformation microstructures confirm that the material had been deformed in the plastic regime.

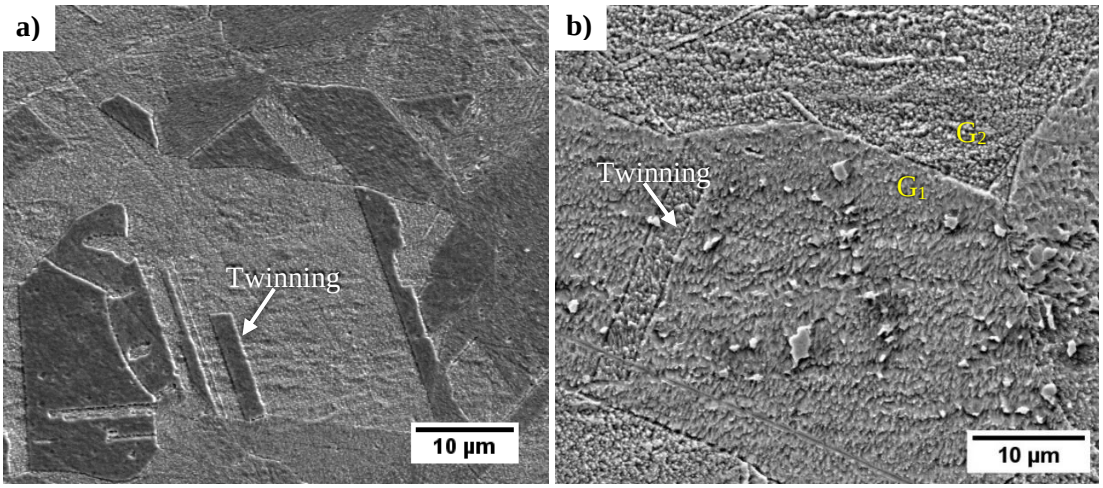

Figure 4.29 - Base material analysis showing twin structures.

Similar microstructures were found in the fusion zone. In Figure 4.30 a), double grain boundaries were identified between grains with different and similar crystallographic orientations. The grain orientation can be distinguished by the different colours detected. Double grain boundaries were occasionally observed. In Figure 4.30 b), the microstructures of the grain can be observed in greater detail.

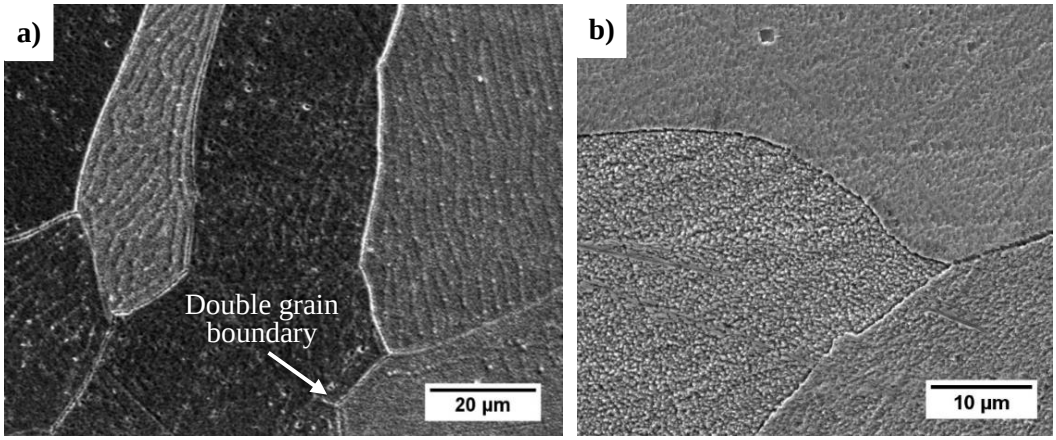

Figure 4. 30 – SEM analysis in fusion zone from sample a) 6A and b) 4B.

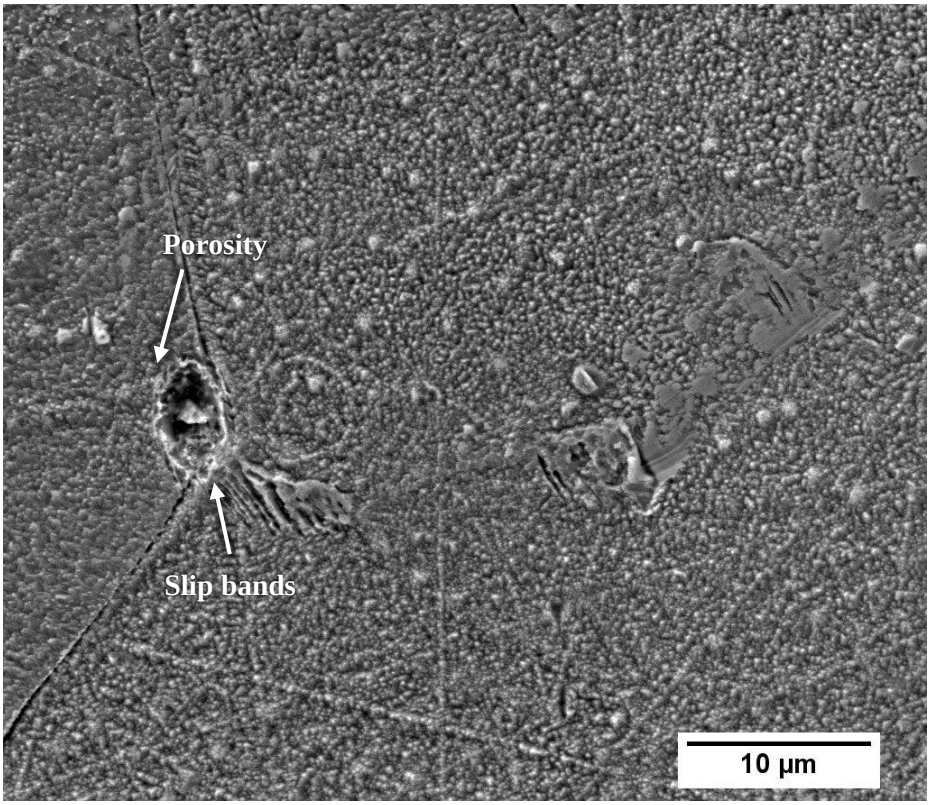

Figure 4.31 – SEM analysis of the fusion zone from sample 4B.

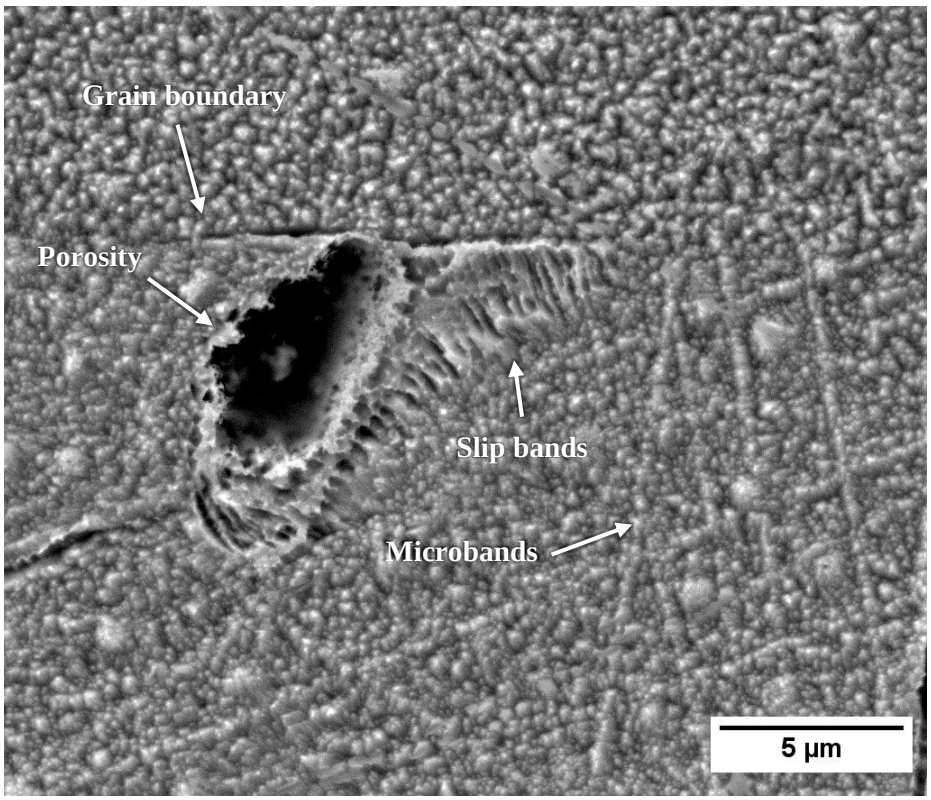

Figure 4.32 - SEM analysis of the fusion zone from sample 4B. Identification of the grains substructures.

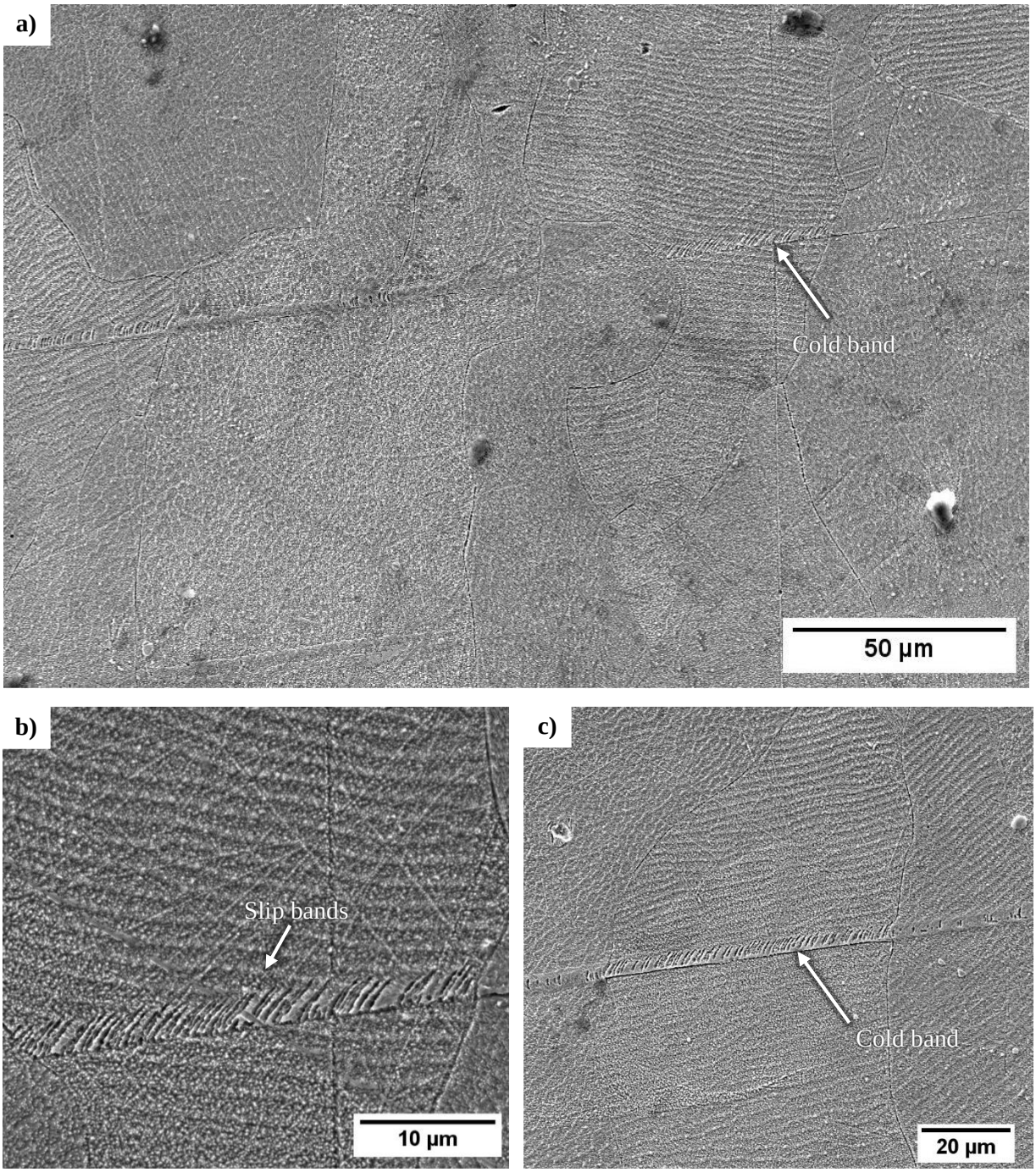

Figure 4.33 – SEM analysis of the fusion zone from sample 4B. Identification of cold and slip bands.

Figure 4.31 shows a porosity found in the fusion zone of sample 4B. This porosity is approximately 7 µm and was located near a grain boundary. An EDS analysis, shown in Figure 4.34, was performed to inspect its chemical composition. The analysis revealed a high content of oxygen which resulted from Cu_2O particles dissociation during melting. The absence of hydrogen indicates that the shielding gas was sufficient to protect the sample from atmospheric gases. The analysis also revealed a small amount of carbon due to the coating used during sample preparation.

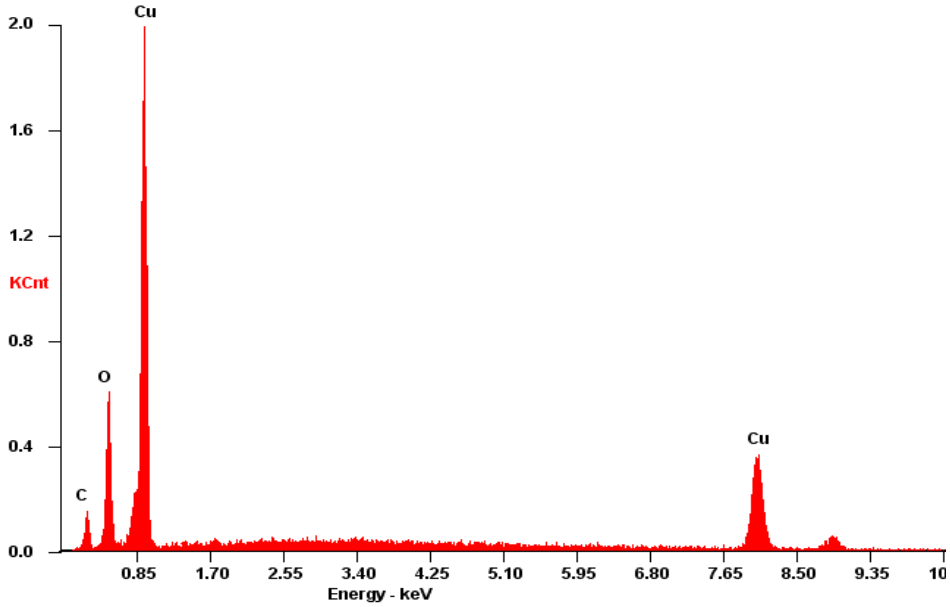

Figure 4. 34 –EDS analysis from a porosity founded in sample 4B.

The grain microstructure is organized in cells and band structures. Figure 4.32 shows several microbands which are defined by narrow zones formed in the material to accommodate local shear tensions. These microband walls were not always defined, although some were very distinct. According to [48] dislocation walls and microbands are responsible for grains subdivision. Meyers et al. [49] studied cold and hot deformation in polycrystalline FCC metals and reported that deformation structures generally consist of groups of cells.

Slip bands were also observed within the grains in the fusion zone. These slip bands are caused by deformation of copper crystals at high temperatures [50]. Figure 4.31 and Figure 4.32 show slip bands near a porosity. However, it is also possible to observe slip bands crossing grains in the samples analysed. It seems that cold bands, previously observed in the micrographs, are probably formed by a group of slip bands, as it can be seen in Figure 4.33. The orientation of the slip bands differs from grain to grain which could be attributed to the crystallographic planes of orientation.

The grains from the fusion zone and the base material also show substructures. In the base material, it is assumed that cold rolling caused a plastic deformation that lead to a creation of cells and band structures. In the fusion zone, as a result of nucleation and grain growth, these deformations are lost. However, the existence of grain substructures and slip bands suggest that the oscillation of the laser beam introduced residual stress during solidification and then, deformation. This could be associated to the high cooling rate obtained with an oscillated beam. The beam's high velocity caused by the wobbling movement, increased the cooling rate [10]. Nevertheless, a deeper study on these features is out of the scope of this thesis.

4.6. XRD analysis

To evaluate the microstructural modifications during the LBW process, X-ray diffraction (XRD) analysis were performed on some welds. The 3D XRD graphs obtained are presented in Figures 4.35 to 4.37.

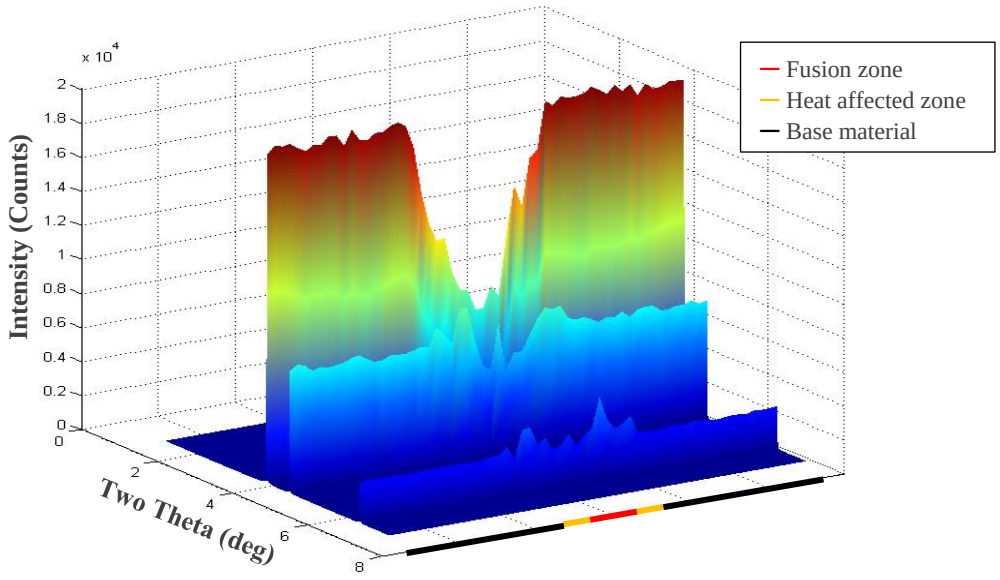

Figure 4.35 – XRD patterns along sample 4B (synchrotron radiation, 0.1430 Å wavelength).

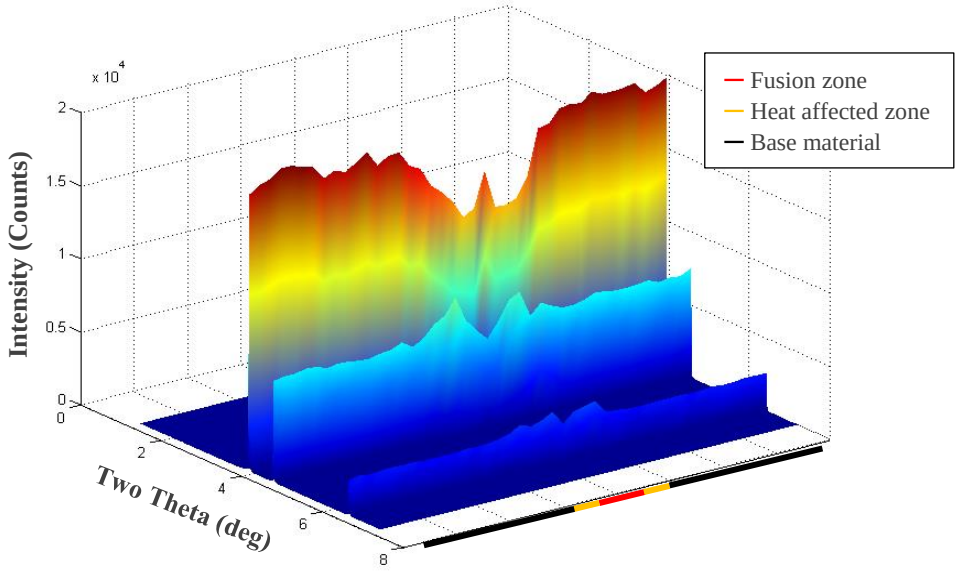

Figure 4.36 - XRD patterns along sample 6A (synchrotron radiation, 0.1430 Å wavelength).

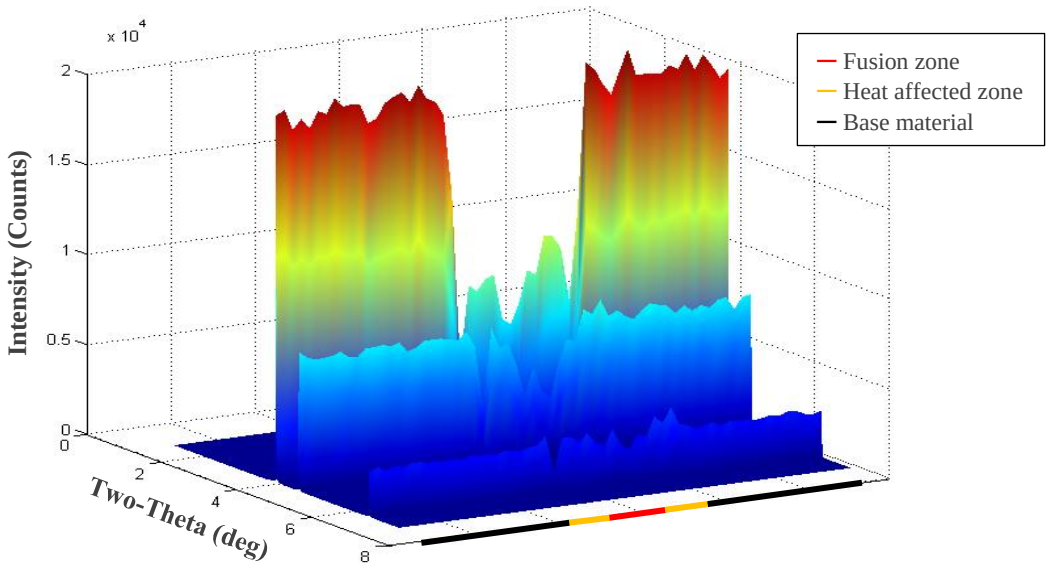

Figure 4.37 - XRD patterns along sample 10D (synchrotron radiation, 0.1430 Å wavelength).

In all the XRD analysis, it is possible to identify the peaks in the base material. These peaks are caused by the polycrystalline structure of copper. Each grain in a polycrystalline aggregate normally has a crystallographic orientation different from that of its neighbours [51]. The different orientation of Cu grains produces sharp peaks with different intensities in the X-ray diffractogram.

In the fusion zone, there is a decrease of the peaks intensity compared to the base material. This difference is associated with the microstructural changes occurred during the weld process and suggests that the grains of the fusion zone are larger and randomly oriented. This modification in the texture intensity could be also related with residual stress.

4.7. Hardness measurement

Vickers hardness measurements were performed in all the samples to evaluate the relative mechanical resistance along the cross section of each weld. The hardness profile obtained of some relevant welds are presented in Figures 4.38 to 4.45.

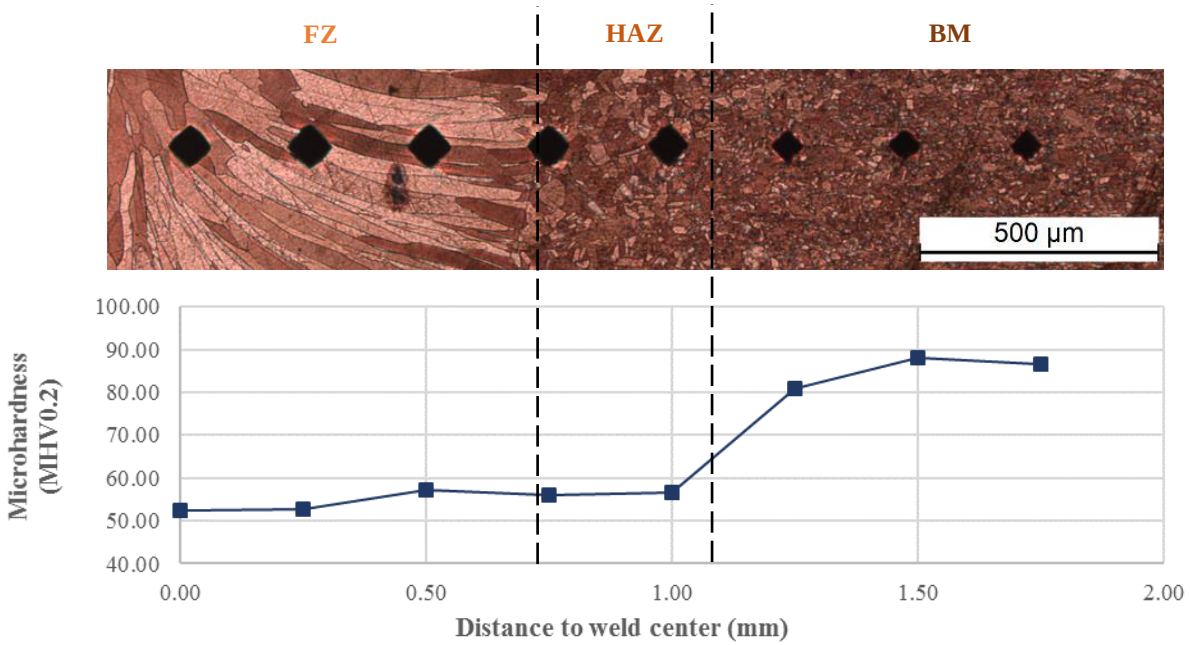

Figure 4.38 - Hardness profile of the sample 4C (laser power = 4000 W, welding speed = 4.0 m/min, focal point position = 0, rotation diameter = 1.0 mm, rotation frequency = 100 Hz, beam trajectory = circular).

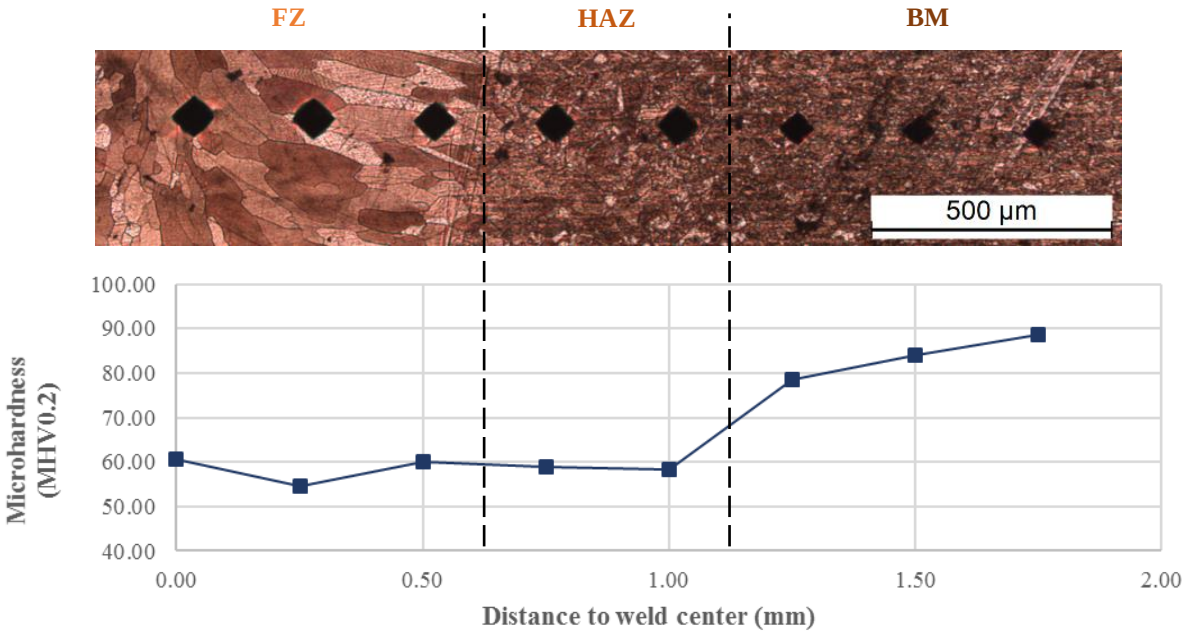

Figure 4.39 - Hardness profile of the sample 6B (laser power = 4000 W, welding speed = 4.0 m/min, focal point position = 0, rotation diameter = 0.6 mm, rotation frequency = 100 Hz, beam trajectory = circular).

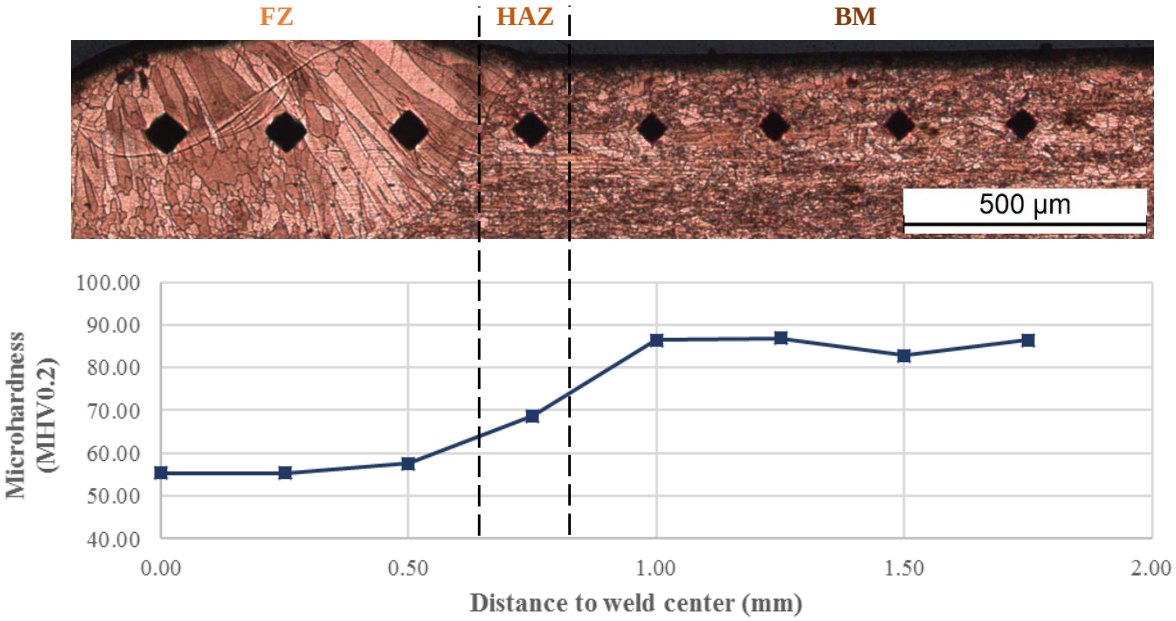

Figure 4.40 - Hardness profile of the sample 7A (laser power = 4000 W, welding speed = 4.0 m/min, focal point position = 0, rotation diameter = 1.0 mm, rotation frequency = 180 Hz, beam trajectory = circular).

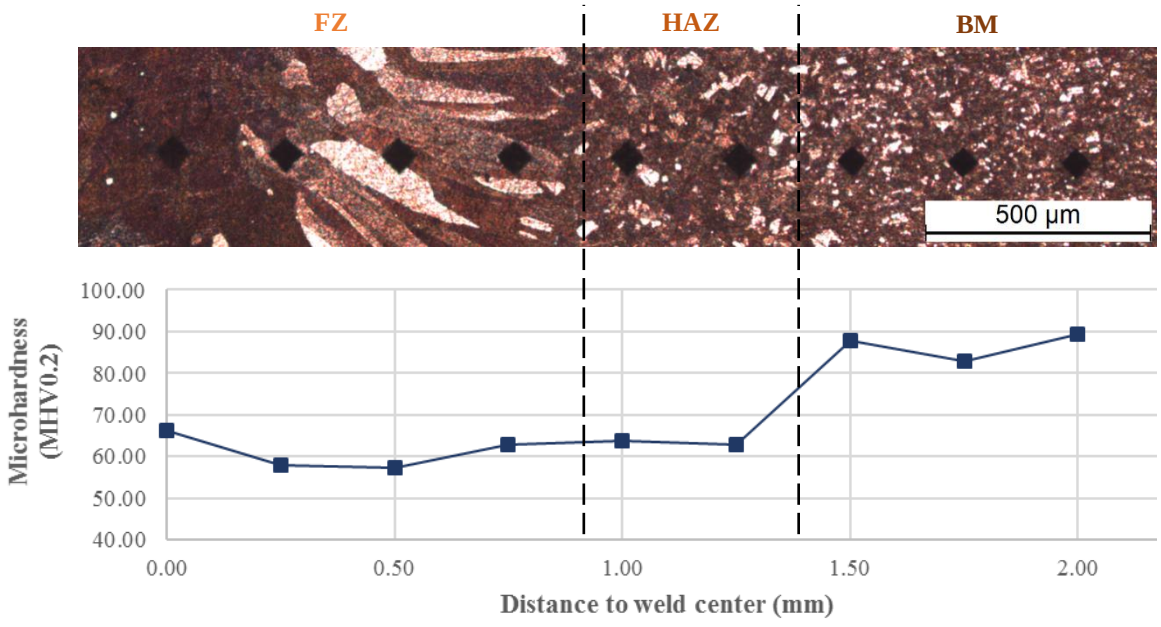

Figure 4.41 - Hardness profile of the sample 8A (laser power = 4000 W, welding speed = 4.0 m/min, focal point position = 0, rotation diameter = 1.0 mm, rotation frequency = 100 Hz, beam trajectory = linear).

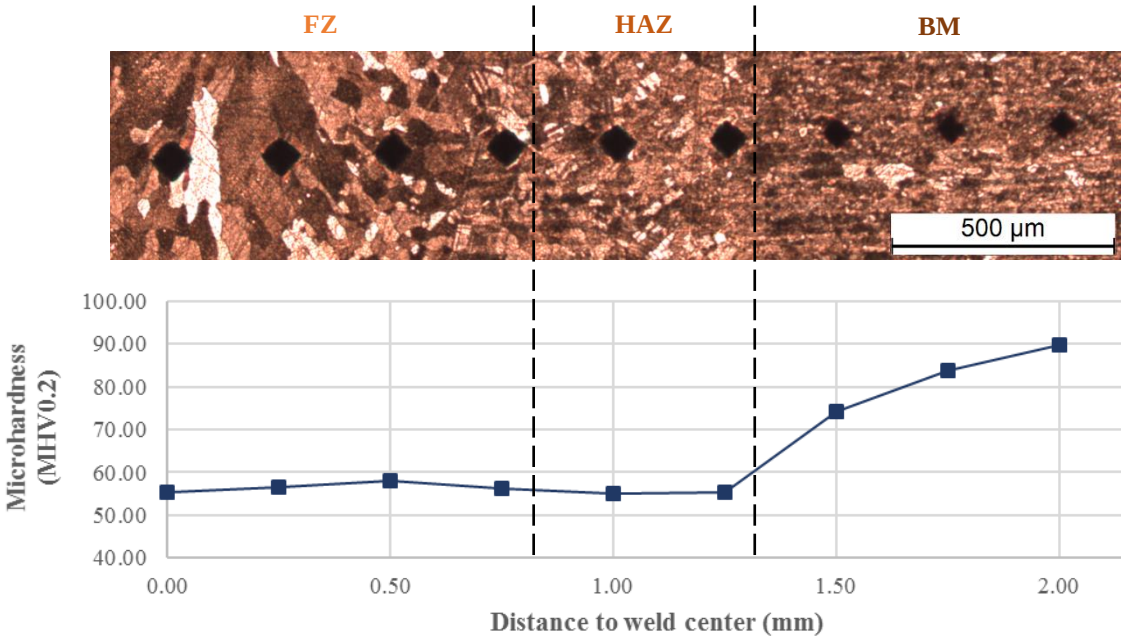

Figure 4.42 - Hardness profile of the sample 8B (laser power = 4000 W, welding speed = 4.0 m/min, focal point position = 0, rotation diameter = 1.0 mm, rotation frequency = 100 Hz, beam trajectory = horizontal infinity).

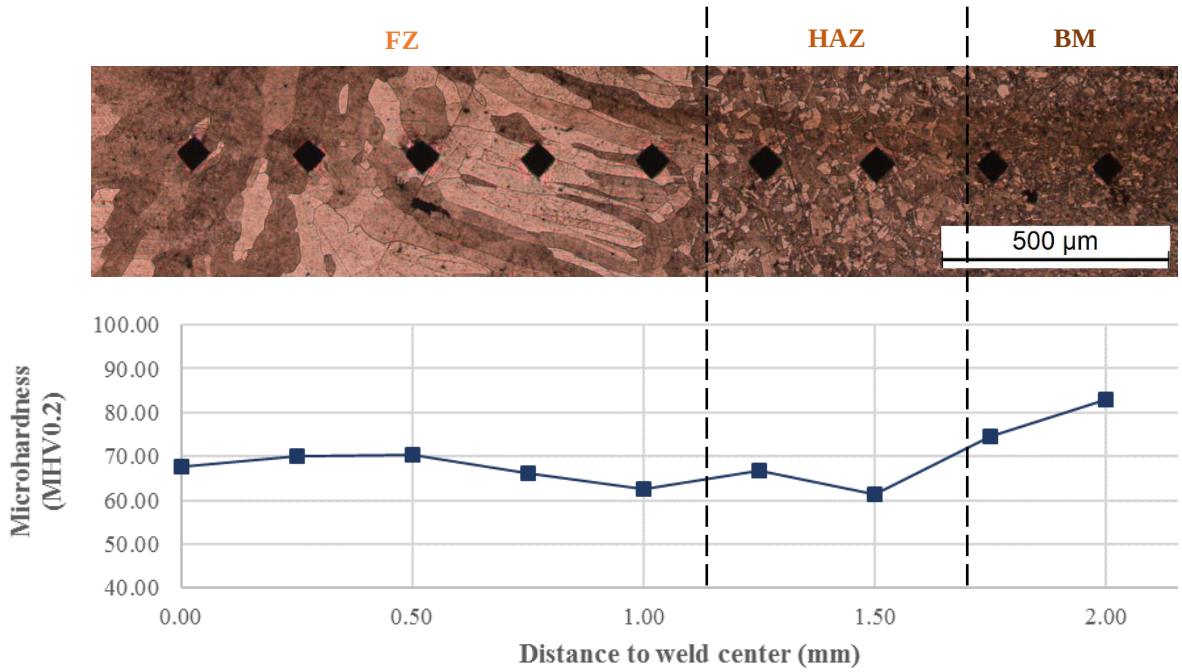

Figure 4.43 - Hardness profile of the sample 8C (laser power = 4000 W, welding speed = 4.0 m/min, focal point position = 0, rotation diameter = 1.0 mm, rotation frequency = 100 Hz, beam trajectory = vertical infinity).

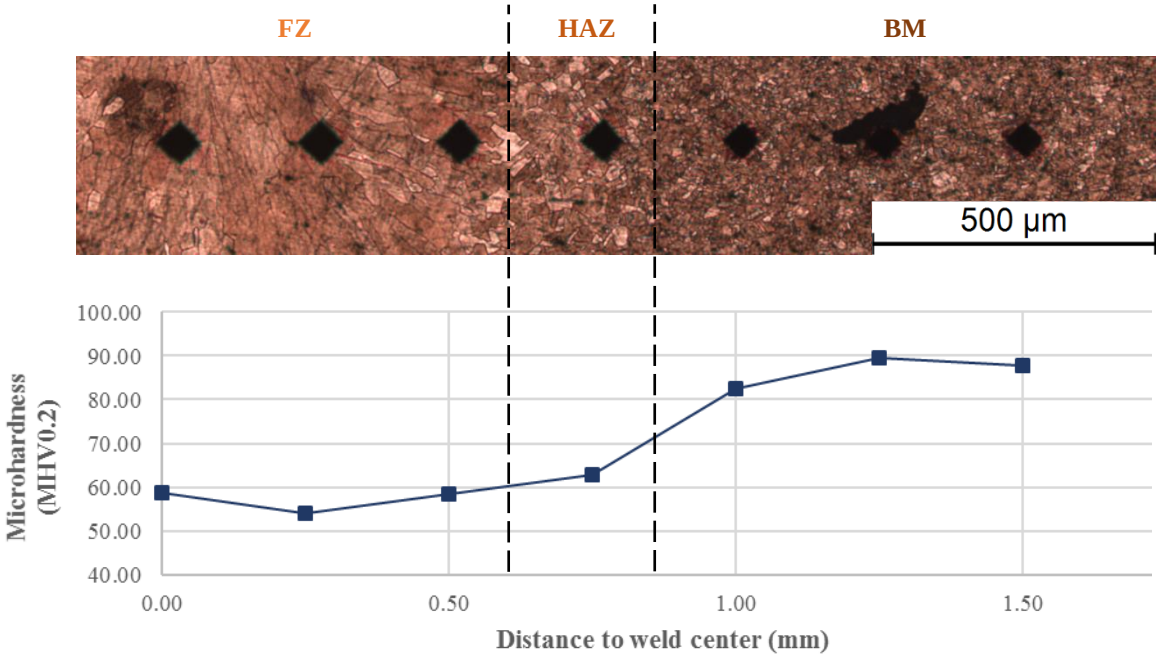

Figure 4.44 - Hardness profile of the sample 8D (laser power = 4000 W, welding speed = 4.0 m/min, focal point position = 0, rotation diameter = 1.0 mm, rotation frequency = 200 Hz, beam trajectory = horizontal infinity).

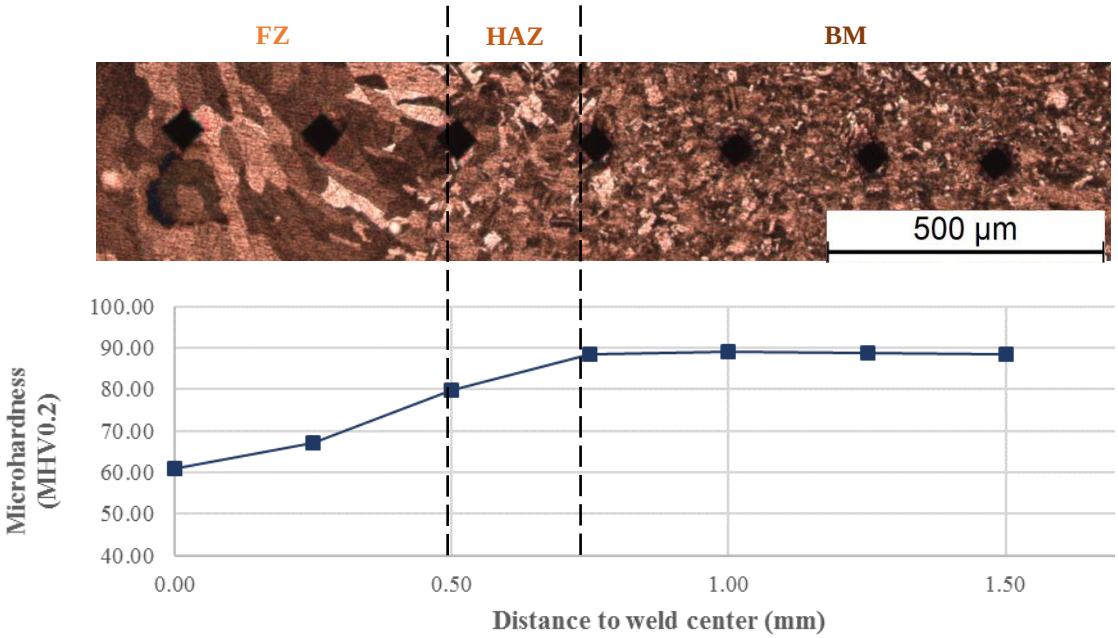

Figure 4.45 - Hardness profile of the sample 8E (laser power = 4000 W, welding speed = 4.0 m/min, focal point position = 0, rotation diameter = 1.0 mm, rotation frequency = 200 Hz, beam trajectory = vertical infinity).

The hardness values measured are consistent with what was expected for LBW. All the samples show the same evolution: there is an almost continuous increase of hardness from the fusion zone to the base material. The fusion zone, which is the most affected by the heat, presents a lower hardness with values between 56 and 67% of the parent material. In the heat affected zone the grain size is strongly reduced, increasing the grain boundaries density and thus the hardness. The hardness of the base material was in the 85-90 HV. These values are consistent with a previous cold rolled Cu [7].

It is possible to observe a slight difference between the hardness values of the fusion zone in Figure 4.39. The sample 6B has the same parameters than 4C except for the rotation diameter which is lower. As explain before, a lower rotation diameter leads to a higher energy transference. Therefore, the weld mode on 4C is conduction while in 6B is a transition mode from keyhole to conduction. This results in a small grain size in the centre of the weld which increase the hardness.

These results verified that the hardness increases as the grain size decreases [49] due to an increasing difficulty of dislocations to overcome obstacles. The increase in the grain boundary concentration would hinder the dislocation mobility, and thus enhance the strength or hardness of materials in macroscopic manifestations [53].

Figure 4.41 to Figure 4.45, show the hardness profiles with different beam trajectories. These show a tendency to increase the hardness from the FZ into the BM. The hardness values obtained with the linear and infinity shape are similar to the profiles obtained with the circular shape. However, the hardness profile of the eight shape shows a slight increasing of the hardness in the fusion zone. This increase of hardness does not seem to be related with the grain size.

4.8. Electrical conductivity testing

Since one of the major concerns of this investigations was to obtain welds with the same electrical conductivity as the base material, electrical conductivity tests were performed in selected samples to compare welds produced with and without scanning, with different beam intensities and in multi- and single-mode. Figure 4.46 to 4.50 depict the measured values.

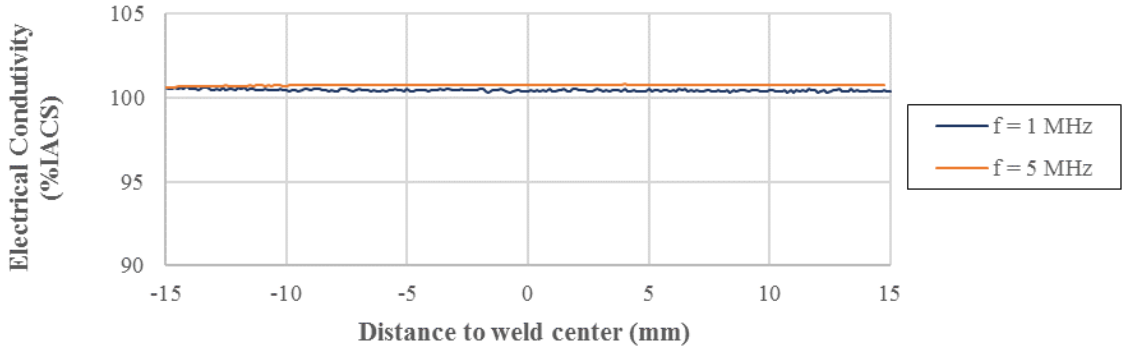

Figure 4.46 – Electrical conductivity profile of the sample 4B (laser power = 4000 W, welding speed = 3.5 m/min, focal point position = 0, rotation diameter = 1.0 mm, rotation frequency = 100 Hz, beam trajectory = circular).

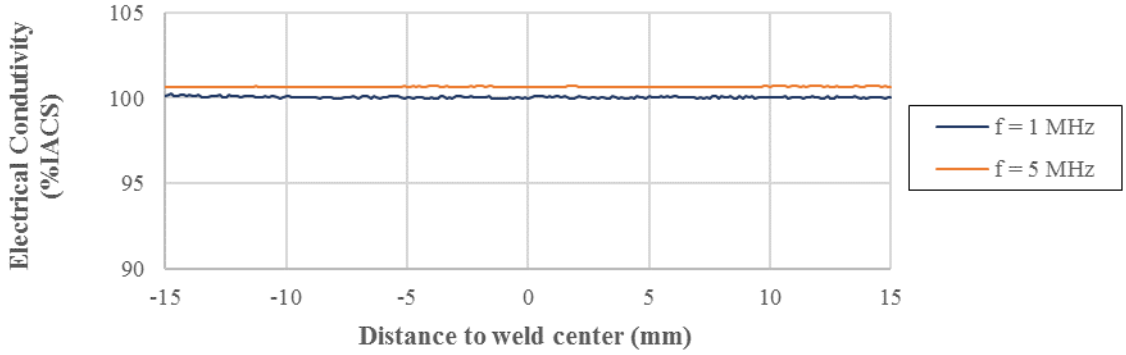

Figure 4.47 - Electrical conductivity profile of the sample 4E (laser power = 4000 W, welding speed = 4.5 m/min, focal point position = 0, rotation diameter = 1.0 mm, rotation frequency = 100 Hz, beam trajectory = circular).

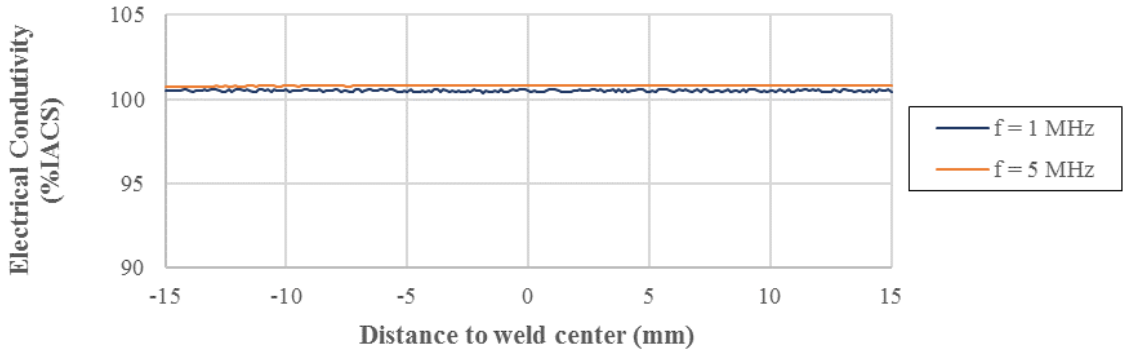

Figure 4.48 - Electrical conductivity profile of the sample 6E (laser power = 4000 W, welding speed = 4.0 m/min, focal point position = 0, rotation diameter = 1.4 mm, rotation frequency = 100 Hz, beam trajectory = circular).

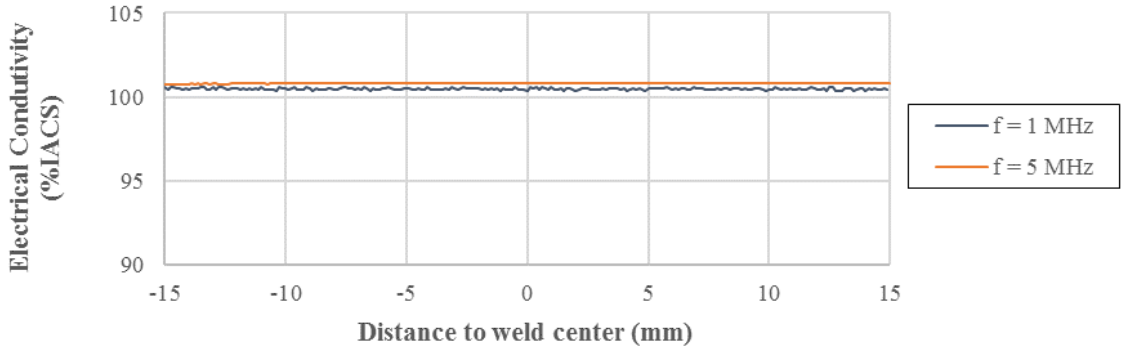

Figure 4.49 - Electrical conductivity profile of the sample 10D (laser power = 2700 W, welding speed = 2.0 m/min, focal point position = 0, rotation diameter = 0.7 mm, rotation frequency = 200 Hz, beam trajectory = circular).

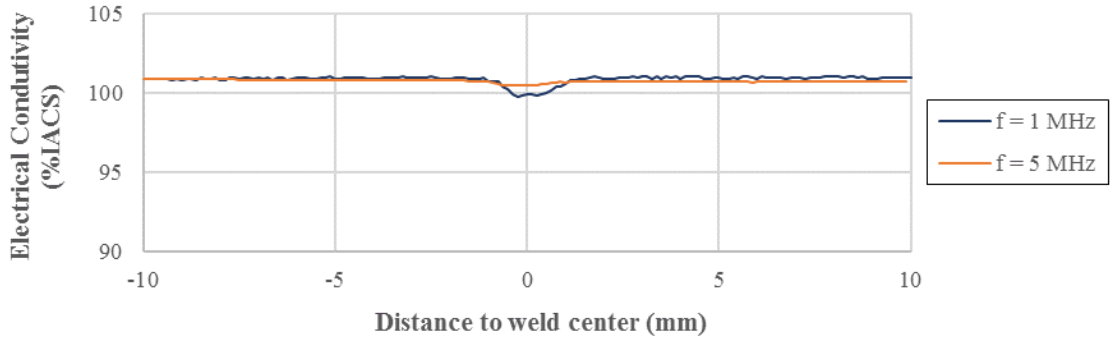

Figure 4.50 - Electrical conductivity profile of the sample 6A (laser power = 4000 W, welding speed = 4.0 m/min, focal point position = 0, rotation diameter = 0, rotation frequency = 100 Hz, beam trajectory = circular).

In all welds analysed, the electrical conductivity shows no variation from the base material to the welded zone. This allows to conclude that, since copper is a highly conductive material, the changes in the microstructure due to processing are not relevant to affect conductivity. This result is in close agreement with [52] which reported that electrical properties of pure cooper are just affected when impurities exist in the welds.

Sample 6A shows a decrease of 2% of electrical conductivity in the weld region due to the presence of several defects such as material loss at the surface, spatter and inclusions as shown in the macrograph depicted in Figure 4.50.

CHAPTER 5

CONCLUSIONS AND FUTURE WORK

The present work contributed to a deeper understanding of the effect of wobbling laser beam welding of pure copper. Based on the results achieved the following can be concluded:

- A good control of the wobbling parameters is extremely important to reduce weld defects;
- From the different beam trajectories tested the circular ones produced less melt ejections;
- The beam oscillation had a positive impact on the welding process since the welding mode shifted from keyhole to conduction. Without oscillation, the sample exhibit a large amount of surface voids, spatters and small pores caused by the keyhole instability;
- High rotation diameters and rotation frequencies increased the weld overlap leading to a short interaction time and, thus, the weld penetration decreases. However, the weld surfaces aspect shows less defects (spatter and surface voids). Since the process is not symmetric due to the beam rotation, undercuts are for high rotation frequencies;
- At higher welding speeds, although the surface voids and spatter are reduced, the weld depth drastically decrease;
- Internal porosities were seen in most of the welds with very small dimensions (2 to 16 µm) and, thus, were considered irrelevant;
- Welds free of defects with 1.5 mm depth, could be produced at a multimode beam power above 4 kW, welding speed between 3.5 and 4 m/min with a circular spatial modulation with a beam rotation of 0.6 to 1 mm diameter at 100 Hz frequency;
- Though some authors reported that Cu can be effectively welded without shielding gas, argon was seen to supress melt ejections, resulting in a better weld surface aspect;

- Multimode and single-mode fiber laser show similar behaviours in what concerns weld bead and weld depth. However, single-mode fiber laser could be used lower laser powers, lower rotation diameters and higher rotation frequencies, since they have a more intense energy distribution;
- Since copper is a highly conductive material, wobbling laser beam welding did not affected the electrical conductivity of Cu which remains constant;
- In copper microstructure, cell-type substructures and bands within the grains were identified in the fusion zone, heat affected zone and base material. These substructures had different orientations between grains;
- The microstructure of most welds showed cold bands. These bands crossed the grains, were present in the fusion zone, were more evident in certain grain orientations and were easily identified in welds with a high heat input. SEM analysis suggested that cold bands were probably formed by a group of slip bands;
- XRD analysis showed that in the fusion zone the grain size increased and the grains are randomly oriented, as excepted;
- In all samples, the hardness increased from the fusion zone to the base material. It was verified that a decrease of grain size leaded to an increase of hardness due to an increasing difficulty of dislocations to overcome obstacles. Furthermore, the hardness profile of the vertical infinity trajectory showed a slight increasing of the hardness values in the fusion zone.

Although the main objectives of this work were achieved, opportunities for further investigation were identified, namely:

- Apply the procedure developed to both butt and lap welding;
- Develop a numerical model that predicts the heat flow caused by a wobbling moving heat source. This model could give a deeper understanding of the process mechanisms;
- Study the substructures within the grains observed in the fusion zone with more advanced techniques.

REFERENCES

[1] Davis, J. R. (2001). *Copper and copper alloys.* (1ª *ed.*) United States of America: ASM International

[2] Voort, George F. V. (2004). *Metallography and microstructures* (Vol. 9). United States of America: ASM Handbook Committee.

[3] Caron, R., Barth, R., Tyler, D. (2004). Metallography and Microstructures of Copper and Its Alloys. *ASM Handbook: Metallography and Microstructures*, 9, 775–788.

[4] *Welding of copper and its alloys.* Available from: <http://www.twi-global.com>

[5] Deininger, Christoph. (2011). Copper machining with lasers. *Laser Journal*, 3, 28-31.

[6] Blom, A., Dunias, P., Engen, P., Hoving, W. (2003). Process spread reduction of laser micro-spot welding of thin copper parts using real-time control. *SPIE*, 4977, 493-500.

[7] Chapman, David. (2016). High Conductivity Copper for Electrical Engineering. *Copper Development Association*, 122.

[8] Steen, W., Mazumber, J. (2010). *Laser material processing*. (4ª *ed*.) London: Springer. TROCAR E ACRESCENTAR

[9] Majumdar, J., Manna, I. (2003). Laser processing of materials. *Sadhana*, 28, 495-562.

[10] Kou, Sindo. (2003). *Welding metallurgy*. (2ª *ed.*) New Jersey: John Wiley & Sons, Inc.

[11] Quintino, L., Costa, A., Miranda, R., Yapp, D., Kumar, V., Kong, C. (2007). Welding with high power fiber laser – A preliminary study. *Materials and Design*, 28, 1231-1237.

[12] Ikeagu, Chukwugozie. (2007). *Evaluating the effect of different welding processes on the distortion of 4 mm thick DH36 ship panels*, Msc Thesis. Cranfield University, School of Applied Sciences.

[13] Liptak, B. (2002). *Instrument Engineers' Handbook*. (3ª ed.), USA: CRC Press.

[14] Shannon, Geoff. (2015). *Single mode fiber laser markers offer processing advantages.* Amada Miyachi America, Inc.

[15] Alda, Javier. (2003). *Laser and Gaussian Beam Propagation and Transformation. Encyclopaedia of Optical Engineering.* New York: Marcel Dekker, Inc.

[16] Suder, Wojciech. (2012). *Study of fundamental parameters in hybrid laser welding*, PhD Thesis. Cranfield University, Scholl of Applied Sciences.

[17] Assunção, E., Williams, S. (2013). Comparison of continuous wave and pulsed wave laser welding effects. *Optics and lasers in Engineering*, 51, 674-680.

[18] Zhou, J., Tsai, H., Wang, P. (2005). Transport phenomena and keyhole dynamics during pulsed laser welding. *Journal of Heat Transfer*, 128, 680-690.

[19] Schultz, H. (1989). *Electron beam welding*. Germany: Woodhead Publishing.

[20] Hansen, K., Kristiansen, M., Olsen, F. (2014). Beam trajectory to control of weld pool size in width and depth. *Physics Procedia*, 56, 467-476.

[21] Miyamoto, I., Kosumi, T., Seo-jeong, P., Huragishi, H., Watanabe, K., Ooie, T. (2004). Applications of single mode fiber lasers to novel micromachining. Proceedings of LMP 2004, Osaka.

[22] Abt, F., Boley, M., Weber, R., Graf, T. (2011) Ray videography for investigation of capillary and melt pool dynamics, Proceedings in ICALEO, Orlando, USA.

[23] Fujinga, S., Takenaka, H.; Narikiyo, T.; Katayama, S.; Matsunawa, A. (2000) Direct observation of keyhole behaviour during pulse modulation high-power Nd:YAG laser irradiation. *Journal of Physics D: Applied* Physics, 33, 492–497.

[24] Laslau, R., Boboescu, R. (2011). Laser beam focal point positioning effects on laser welds surfaces. *International Conference of Scientific Paper*, AFASES 2011.

[25] Haran, F., Hand, D., Peters, C., Jones, J. (1997). Focus control system for laser welding. *Applied optics*, 36, 5246-5251.

[26] M. Pastor, M., Zhao, H., Martukanitz, R., Debroy, T. (1999). Porosity, Underfill and Magnesium Loss during Continuous Wave Nd:YAG Laser Welding of Thin Plates of Aluminum Alloys 5182 and 5754. *Welding Journal*, 207-216.

[27] Olson, D., Siewert, T., Liu, Stephen, Edwards, G. (2004). *Welding, brazing and soldering* (Vol. 6). United States of America: ASM Handbook Committee.

[28] *Wobble welding method*. Available from: <http://www.spilasers.com>

[29] Kratzsch, M., Standfuss, J., Klotzbach, A., Kaspar, J., Brenner, B., Beyer, E. (2011). Laser Beam Welding with High-Frequency Beam Oscillation: Welding of Dissimilar Materials with Brilliant Fiber Lasers. *Physics procedia*, 12, 142-149.

[30] Gedicke, J., Olowinsky, A., Artal, J., Gillner, A. (2007). Influence of temporal and spatial laser power modulation on melt pool dynamics. *Laser Materials Processing Conference*, Proc. Of ICALEO 2007, 816-822.

[31] Haeusler, A., Schurmann, A., Scholer, C., Olowinsky, A., Gilner, A., Poprawe, R. (2017). Quality improvement of copper welds by laser microwelding with the usage of special power modulation. *Journal of Laser Applications*, 29, doi: 10.2351/1.4983505.

[32] Sundqvist, J., Kaplan, A., Shachaf, L., Kong, C. (2017). Analytical heat conduction modelling for shaped laser beams. *Journal of Materials Processing Tech*., 247, 48-54.

[33] *Fiber laser welding technique joins challenging metals.* Available from: <http://www.industrial-lasers.com>

[34] Safdar, S., Li, L., Sheikh, M. (2007). Numerical analysis of the effects of non-conventional laser beam geometries during melting of metallic materials. *Journal of Physics D: Applied Physics*, 40, 593-603.

[35] Petring, D., Goneghany, V. (2011). Parameter dependencies of copper welding with multi-kw lasers at 1 micron wavelength. *Physics Procedia*, 12, 95-104.

[36] Heider, A., Stritt, P., Hess, A., Weber, R., Graf, T. (2011). Process stabilization at welding copper by laser power modulation. *Physics Procedia*, 12, 81-87.

[37] Hess, A., Schuster, R., Heider, A., Weber, R., Graf, T. (2011). Continuous wave laser welding of copper with combined beams at wavelengths of 1030 nm and 515 nm. *Physics procedia*, 12, 88-94.

[38] Kraetzsch, M., Standfuss, J., Klotzbach, A., Kaspar, J., Brenner, B., Beyer, E. (2011). Laser beam welding with high-frequency beam oscillation: welding of dissimilar materials with brilliant fiber lasers. *Physics Procedia*, 12, 142-149.

[39] Heider, A., Sollinger, J., Abt, F., Boley, R., Weber, R., Graf, T. (2013). High-speed X-ray analysis of spatter formation in laser welding of copper. *Physics Procedia*, 41, 112-118.

[40] Liebl, S., Wiedenmann, R., Ganser, A, Schmitz, P., Zaech, M. (2014). Laser welding of copper using multi-mode fiber lasers at near infrared wavelength. *Physics Procedia*, 56, 591-600.

[41] Miyagi, M., Zhang, X. (2015). Investigation of laser welding phenomena of pure copper by X-ray observation system. *Journal of Laser Applications*, 27, doi: 10.2351/1.4927609.

[42] Miyagi, M., Zhang, X., Kawahito, Y., Katayama, S. (2017). Surface void suppression for pure copper by high-speed laser scanner welding. *Journal of Materials Processing*, 240, 52-59.

[43] Schmitt, F., Mehlmann, B., Gedicke, J., Olowinsky, A., Gillner, A., Poprawe, R. (2010). Laser beam micro welding with high brilliant fiber lasers. *Journal of Laser Micro/Nanoengineering*, 5, 1997-203.

[44] Reisgen, U., Olschock, S., Jakobs, S., Turner, C. (2016). Sound welding of copper: laser beam welding in vaccum. *Physics Procedia*, 83, 447-454.

[45] Biro, E., Weckman, D., Zhou, Y. (2002). Pulsed Nd:YAG Laser Welding of Copper Using Oxygenated Assist Gases. *Metallurgical and Materials Transactions*, 33A, 2002-2009.

[46] Klages, K. Gedicke, J., Olowinsky, A. (2005). Pulse forming at laser beam micro welding. Laser Materials Processing Conference: Proc. Of ICALEO 2005.

[47] Heider, A., Weber, R., Graf, T. (2012). High-Quality Laser Welding of Copper Using Appropriate Power Modulation. *Proceedings*, ICALEO 2012, 31, 531-538.

[48] Ananthan, V., Leffers, T., Hansen, N. (1991). Cell and band structures in cold rolled polycrystalline copper. *Materials Science and Technology*, 7, 1069-1075.

[49] Meyers, M., Andrade, U., Choksi, A. (1995). The effect of grain size on the high-strain, high-strain-rate behavior of copper. *Metallurgical and Materials Transactions*, 26 A, 2881-2890.

[50] Murali, S., Srikanth, N., Vath III, C. (2003). Grains, deformation substructures, and slip bands observed in thermosonic copper ball bonding. *Materials Characterization*, 50, 39-50.

[51] Cullity, B. D. (1956). *Elements of X-Ray Diffraction*. (1ª *ed.*) United States of America: Addison-Wesley Publishing Company, Inc.

[52] Chen, H., Bi, G., Nai, M., Wei, J. (2015). Enhanced welding efficiency in laser welding of highly reflective pure copper. *Journal of Materials Processing Technology*, 216, 287-293.

[53] Wang, Y., Zhang, J., Wei, Q., Zhao, Y. (2013). Grain size effects on the compressibility and yield strength of copper. *Journal of Physics and Chemistry of Solids*, 74, 75-79.

[54] Matweb website last visited in August 2017:

http://www.matweb.com/search/datasheet.aspx?matguid=3c78d450e90f48c48d68e2d17a8e51f7&ckck=1

[55] *IPG Photonics' wobble heads*. Available from: <http:// www.ipgphotonics.com>

ANNEXES

A1. Chemical analysis report

NDT Services Ltd
99 Victory Road,
Derby, DE24 8EL

Telephone: +44 0 1332 275820
Facsimile: +44 0 1332 275817
www.intertek.com

CHEMICAL ANALYSIS REPORT

Report No: V111710E1/17
Issue No: 1
Date received: 16-Mar-17
Date of test: 17-Mar-17
Date of issue: 17-Mar-17

Client: CARRS WELDING PRODUCTS LTD
Unit 8 Henson Way
Telford Way Industrial Estate
Kettering
Northants
NN16 8PZ

Order No : 26354

FAO: Alison Holland

Description : Chemical Analysis of sheet sample
Identification : N/A
Material: Copper C101

Quantity: 1

Basis of test : Spectrographic analysis was carried out to MCP52 issue 6, the results are as follows:

RESULTS

	Mean (%)
Copper	99.96
Phosphorous	0.001
Lead	<0.005
Sulphur	<0.001
Iron	<0.005
Nickel	<0.005
Tellurium	<0.005
Arsenic	<0.005
Antimony	<0.005
Silver	<0.005
Selenium	<0.005

For **ndt services limited**

Zahoor Khan .....
Metallurgical Services

NDT ZK 162

NDT 116

Page 1 of 1

B1. Technical drawings of the jig designed

DRAWN	DF	22/02/2017
CHECKED	JS	23/02/2017

CARRS WELDING TECNOLOGIES

SECTION D-D

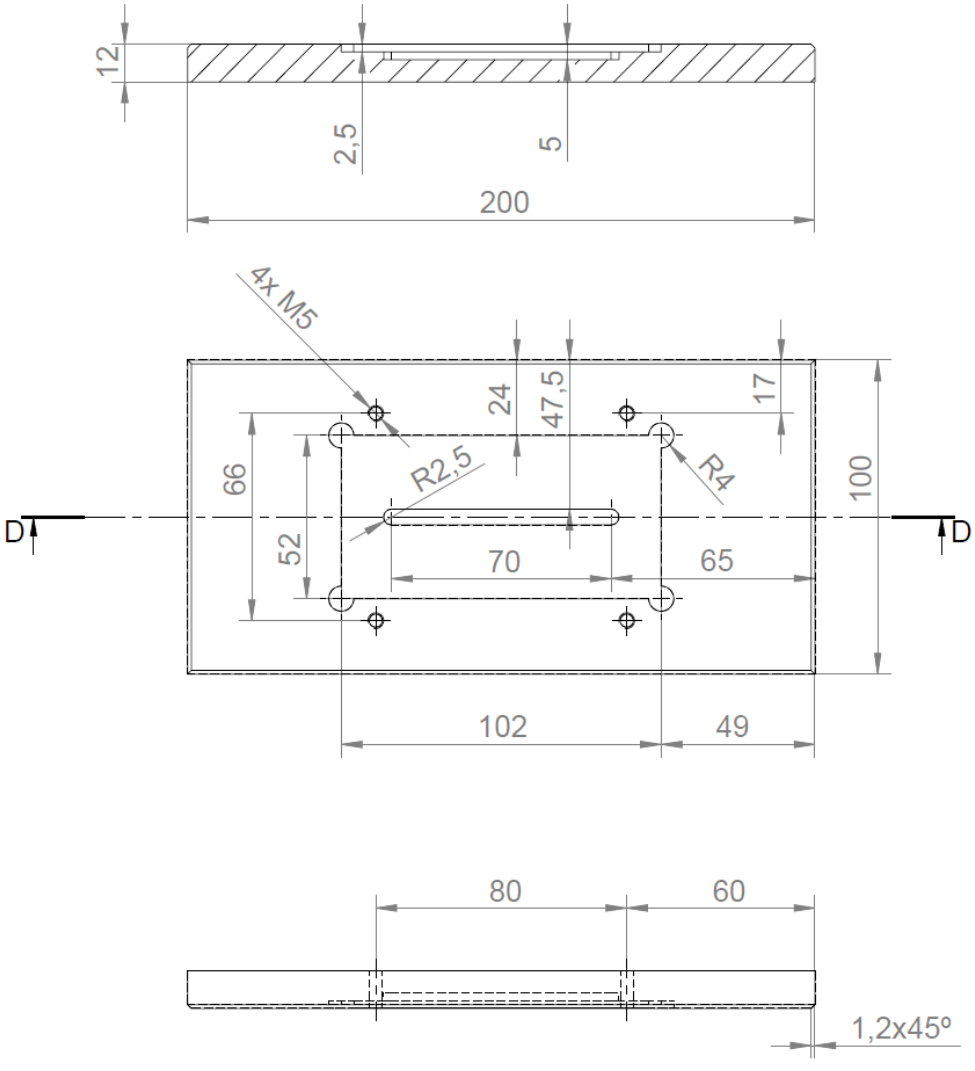

	1:2	PLATE ALIGNER	DWG NO 39615-B2202
	Toleran.		

B2. Technical drawings of the jig designed